

4. SITE 895¹

Shipboard Scientific Party²

HOLE 895A

Date occupied: 30 December 1992
Date departed: 31 December 1992
Time on hole: 1 day, 1 hr, 00 min
Position: 2°16.639'N, 101°26.766'W
Bottom felt (rig floor, m; drill-pipe measurement): 3832.0
Distance between rig floor and sea level (m): 11.3
Water depth (drill-pipe measurement from sea level, m): 3820.7
Total depth (rig floor, m): 3849.2
Penetration (m): 17.2
Number of cores (including cores with no recovery): 2
Total length of cored section (m): 17.2
Total core recovered (m): 2.4
Core recovery (%): 13.8
Oldest sediment cored:
Depth (mbsf): 1.80
Nature: lithic breccia

HOLE 895B

Date occupied: 31 December 1992
Date departed: 1 January 1993
Time on hole: 17 hr, 45 min
Position: 2°16.638'N, 101°26.763'W
Bottom felt (rig floor, m; drill-pipe measurement): 3832.0
Distance between rig floor and sea level (m): 11.3
Water depth (drill-pipe measurement from sea level, m): 3820.7
Total depth (rig floor, m): 3842.3
Penetration (m): 10.3
Number of cores (including cores with no recovery): 1
Total length of cored section (m): 10.3
Total core recovered (m): 1.0
Core recovery (%): 9.9
Igneous section:
Depth top (mbsf): 0.0
Depth bottom (mbsf): 10.3
Nature: serpentized peridotite and gabbroic rocks

HOLE 895C

Date occupied: 1 January 1993

¹ Gillis, K., Mével, C., Allan, J., et al., 1993. *Proc. ODP, Init. Repts.*, 147: College Station, TX (Ocean Drilling Program).

² Shipboard Scientific Party is as given in the list of participants preceding the contents.

Date departed: 1 January 1993
Time on hole: 1 day, 1 hr, 15 min
Position: 2°16.634'N, 101°26.774'W
Bottom felt (rig floor, m; drill-pipe measurement): 3831.0
Distance between rig floor and sea level (m): 11.3
Water depth (drill-pipe measurement from sea level, m): 3819.7
Total depth (rig floor, m): 3868.9
Penetration (m): 37.9
Number of cores (including cores with no recovery): 4
Total length of cored section (m): 37.9
Total core recovered (m): 5.7
Core recovery (%): 15.1
Igneous section:
Depth top (mbsf): 0.0
Depth bottom (mbsf): 37.9
Nature: serpentized peridotite and gabbroic rocks

HOLE 895D

Date occupied: 2 January 1993
Date departed: 8 January 1993
Time on hole: 6 days, 4 hr, 30 min
Position: 2°16.635'N, 101°26.777'W
Bottom felt (rig floor, m; drill-pipe measurement): 3832.0
Distance between rig floor and sea level (m): 11.3
Water depth (drill-pipe measurement from sea level, m): 3820.7
Total depth (rig floor, m): 3925.7
Penetration (m): 93.7
Number of cores (including cores with no recovery): 9
Total length of cored section (m): 93.7
Total core recovered (m): 20.0
Core recovery (%): 21.4
Igneous section:
Depth top (mbsf): 0.0
Depth bottom (mbsf): 93.7
Nature: serpentized peridotite and gabbroic rocks

HOLE 895E

Date occupied: 8 January 1993
Date departed: 12 January 1993
Time on hole: 3 days, 21 hr, 15 min
Position: 2°16.787'N, 101°26.792'W
Bottom felt (rig floor, m; drill-pipe measurement): 3764.0
Distance between rig floor and sea level (m): 11.5

Water depth (drill-pipe measurement from sea level, m): 3752.5

Total depth (rig floor, m): 3851.6

Penetration (m): 87.6

Number of cores (including cores with no recovery): 8

Total length of cored section (m): 87.6

Total core recovered (m): 32.9

Core recovery (%): 37.1

Igneous section:

Depth top (mbsf): 0.0

Depth bottom (mbsf): 93.7

Nature: serpentized peridotite and gabbroic rocks

HOLE 895F

Date occupied: 12 January 1993

Date departed: 13 January 1993

Time on hole: 1 day, 15 hr, 15 min

Position: 2°16.899'N, 101°26.796'W

Bottom felt (rig floor, m; drill-pipe measurement): 3704.0

Distance between rig floor and sea level (m): 11.5

Water depth (drill-pipe measurement from sea level, m): 3692.5

Total depth (rig floor, m): 3730.2

Penetration (m): 26.2

Number of cores (including cores with no recovery): 2

Total length of cored section (m): 26.2

Total core recovered (m): 2.0

Core recovery (%): 7.6

Igneous section:

Depth top (mbsf): 0.0

Depth bottom (mbsf): 26.2

Nature: serpentized peridotite

Principal results: Site 895 is located along the slope south of the intrarift ridge, at the position of 2°16.7'N, 101°26.7'W, in an area where ultramafic rocks were recovered during a *Nautilus* dive program (Francheteau et al., 1990). The aim of drilling at this site was to recover a section of the shallow mantle. Six holes (895A to 895F) penetrated a total of 272.9 m, and 64.56 m was recovered, with an average recovery of 27.5%. Among the six holes, only Holes 895D and 895E had substantial penetration (93.7 and 87.60 m, respectively) and recovery.

The igneous and metamorphic rocks recovered consist predominantly of ultramafic rocks (dunite and harzburgite) and less abundant mafic rocks (gabbro, olivine gabbro, and troctolite). Although all rock types are present in the holes with significant penetration, harzburgites predominate in Hole 895D, whereas dunites and gabbroic rocks are more abundant in Hole 894E. Gradational changes, from dunite to sparsely plagioclase-bearing dunite, to interconnected veins of plagioclase and clinopyroxene separated by patches of dunite, occur in continuous sections of core at Holes 895C and 895E and may suggest that these rocks were formed by melt migration and impregnation.

Despite pervasive serpentinization, harzburgites retain porphyroclastic textures. Spinel shape fabric in both dunites and harzburgites defines a foliation attributed to high-temperature solid-state flow. In Holes 895C, 895D, and 895E, the spinel foliation shows an increasing amount of dip with depth. In dunite and troctolite, traces of plastic deformation of olivine are observed in thin section.

The relatively small amount (less than 2%) of modal clinopyroxene in the ultramafic rocks indicates that they are depleted abyssal peridotites. The dunites are probably the result of melt-wallrock interaction between host harzburgite and invading basaltic melt. It is also possible that the dunites are simple cumulus products of melt crystallization. The associa-

tion harzburgite-dunite-gabbro, as recovered from these holes, is similar to the transition zone in many ophiolite complexes. The relative abundance of dunite suggests that the drilled sections of Site 895 are close to the mantle-crust boundary as recognized in these complexes.

All ultramafic lithologies are affected by extensive alteration, with 50% to 100% of the primary minerals being replaced by secondary phases. Alteration is dominated by serpentine after olivine, with lesser amounts of bastite, talc, magnetite, chlorite, brucite, and trace antigorite. Serpentinization is more intense in dunites than in harzburgites, and in Hole 895E than in Hole 895D. Troctolitic and gabbroic rocks are moderately to pervasively altered and irregularly exhibit a mineral foliation. Secondary minerals include chrysotile, tremolite, magnetite after olivine, and prehnite, chlorite, zeolite, and hydrogrossular after plagioclase. Multiple generations of discrete fracture-filling veins crosscut the pervasive background mesh serpentine texture of the peridotites, and are filled with assemblages of tremolite, chlorite, antigorite(?), magnetite, chrysotile, brucite, clays, zeolites, and aragonite.

The moderate to pervasive metamorphism and associated vein formation in ultramafic and mafic rocks reflects extensive interaction with seawater-derived fluids during successive hydrothermal pulses. In the absence of mineral assemblages defining distinct metamorphic zones, the temperature of interaction is difficult to estimate. Alteration assemblages in the gabbroic rocks suggest incipient interaction at temperatures close to 500°C with extensive reaction under greenschist facies conditions. Serpentinization in the peridotites continued at lower temperatures as evidenced by the presence of zeolites, clays, and brucite. The close association of gabbroic rocks altered to calc-silicate assemblages with the peridotites may reflect migration of calcium-rich fluids under greenschist facies conditions, which were generated during serpentinization of the peridotites.

Paleomagnetic measurements were made on 36 minicores from Holes 895B, 895C, 895D, 895E, and 895F. The magnetization values obtained from 29 peridotite samples range from 0.3 to 25.0 A/m, with an arithmetic mean of 3.8 A/m. This mean is reduced to 3.0 A/m by excluding the highest value of 25.0 A/m, which is anomalous to the sample population. This magnetic intensity suggests that peridotites may be a significant source of marine magnetic anomalies. The average magnetization value for the gabbroic rocks is 0.4 A/m, significantly lower than that of the Hole 894G and Hole 735B gabbros (1–2 A/m). Thermal demagnetization data suggest that relatively pure multidomain magnetites are the dominant magnetic carriers in all rock types.

Stable magnetic inclination values from Hole 895D samples are widely scattered and suggest that drilling may have penetrated several large blocks of crust that experienced different degrees of tectonic rotation. In contrast, the stable inclinations from Hole 895E fall within a fairly narrow range and have a similar value (+36°) to that obtained for Hole 894G (+40°). As magnetite carries the bulk of the rock magnetization in the serpentized harzburgites, these data suggest that tectonic rotation occurred after the bulk of serpentinization was complete.

Physical properties of the ultramafic and mafic rocks at Site 895 are strongly influenced by the degree of serpentinization and recrystallization. Peridotites display low densities and porosities (mean value of 2.66 g/cm³ and 2.31% for harzburgites, and 2.54 g/cm³ and 3.54% for dunites, respectively), as opposed to the gabbroic rocks (2.81 g/cm³ and 0.65%, respectively). Compressional-wave velocities measured at atmospheric pressures and temperatures, in horizontally oriented water-saturated samples, have a mean of 5548 m/s ± 746 m/s. Low velocities correlate with high porosity-low density values. Velocities measured in several vertical samples show systematically lower velocities than adjacent horizontal samples. These differences in directional velocities might be attributed to mineral fabric or to preferred microcrack orientation. Thermal conductivity measurements have a mean value of 2.83 W/m°C. The large standard deviation for all the different rock types suggests that serpentinization of the peridotites and alteration of the gabbros play an important role in the thermal conductivity of the lower crust and upper mantle. Electrical resistivity measurements performed in several water-saturated minicores show a strong inverse correlation with porosity, which suggests that ionic pore-fluid conduction dominates in these samples, with the dunites having the lowest measured resistivities.

OPERATIONS

Site 895 is located along the slope south of the intrarift ridge, where *Nautile* Dive 17 recovered ultramafic rocks (Francheteau et al., 1990). The plan was to survey in the vicinity of this dive track, close to the location where harzburgite (Sample NZ17-13), dunite (Sample NZ17-14), and cumulate gabbro-norite (Sample NZ17-15) were collected, to find an appropriate site for a bare-rock spud-in. However, the exact position where these samples were collected is not clear because of a discrepancy between the depth recorded by the *Nautile* and the depth obtained from the SeaBeam map at the Global Positioning System (GPS) coordinates for the samples.

Three surveys were conducted in the same manner as at Site 894 (Fig. 1), allowing construction of a bathymetric map based on drill-string depth data (Fig. 2). This bathymetric map shows that the holes drilled at Site 895 are located on the flanks of a well-defined, almost north-south-trending spur. The terrane observed during these surveys differed dramatically from that at the top of the intrarift ridge. In contrast to the low-dipping sedimented surface at Site 894, we passed steep cliffs, several tens of meters high, along each side of the spur, before arriving at rugged surfaces covered with debris and boulders. In the following section, times are recorded in Universal Time Coordinated (UTC).

Survey 1

We left Site 894 at 1000 hr, 29 December 1992, and moved to Site 895 using dynamic positioning. After we arrived on location on 30 December at 1424, a beacon was dropped, the TV camera was lowered, and we started a camera survey. Survey 1 was conducted between 1640 hr and 2040 hr. The area surveyed is 350 m × 200 m, on the southern slope of the intrarift ridge, at depths between 3980 and 3820 m. The general slope dips toward the south, and the seafloor is largely sedimented with abundant talus piles. Heading east, we crossed several spurs bound by north-south-trending scarps. After heading northwest, we passed a north-south-trending, nearly vertical cliff, several tens of meters high, before reaching a flat, sedimented plateau. A punch test on this plateau, 30 m west of the edge, indicated a sediment thickness of 1–1.5 m. This site was selected for an unsupported spud-in.

Hole 895A

Hole 895A was spudded with a rotary core barrel (RCB) bit at 2045 hr, 30 December 1992. Core 147-895A-1R to -2R cored 17.2 m and recovered 2.38 m of foraminiferal nannofossil clay, serpentinite drilling breccia, and serpentinite and gabbro clasts. Another 9.7-m core was cut but could not be recovered because the bottom-hole assembly (BHA) broke 5.5 m below the mud line. The hole was abandoned at 0845 hr, 31 December 1992.

Hole 895B

A new hole was started at the same location because the rocks recovered at Hole 895A were promising. Hole 895B was spudded about 20 m north of Hole 895A at 0415 hr, 1 January 1993. Core 147-895B-1R penetrated 10.3 m and recovered 1.02 m of serpentinitized peridotite. Drilling conditions deteriorated, and because the hole could not be cleaned out, it was abandoned at 0915 hr, 1 January 1993.

Hole 895C

Hole 895C was spudded about 25 m southwest of Hole 895B in 3820 m water depth at 1000 hr, 1 January 1993. Cores 147-895C-1R to -4R penetrated 37.6 m and recovered 5.79 m of serpentinitized peridotites locally impregnated with gabbroic melts. Core 147-895C-5R had penetrated 4.9 m when the BHA broke. An attempt was made

to fish the pipe broken in the hole, because the rocks recovered were extremely interesting and hole conditions were the best of the leg before the BHA broke. The top of the 39.12 m pipe was 3.5 mbsf. The drill string was run with a 9-5/8-in. overshot. With no marker on the seafloor, the hole proved difficult to locate, but was reentered after four hours of surveying and positioning of the ship. The pipe was pulled out after two hours of unsuccessful attempts to recover the BHA, and the hole was abandoned.

Hole 895D

Hole 895D was spudded at 1600 hr, 3 January 1993, in 3821 m water depth, only a few meters from Hole 895C. Cores 147-895D-1R to -9R penetrated 93.7 m, 3821.0–3914.7 mbsf, and recovered 19.08 m of serpentinitized peridotites. After retrieval of Core 147-895D-9R, it was necessary to ream the hole from 3900.0 to 3910.0 m. On 6 January 1993, the bit was changed because of drilling problems. To facilitate reentry, a mini free-fall funnel was dropped around the drill pipe. Before the pipe was pulled out, inspection of the seafloor with the subsea camera revealed that the funnel was standing upright in the 2-m cavity corresponding to the entry of the hole. A beacon attached to the camera frame was successfully released to mark the hole. When the pipe was pulled out, the funnel was still attached to the bit and fell on the seafloor when the drill pipe swayed. Core 147-895D-10W, consisting of 0.91 m of washings, was recovered in the core barrel. Despite the absence of a reentry cone, Hole 895D was successfully reentered with a new RCB bit on 7 January 1993. While reaming the hole to reach bottom, the BHA broke 3.9 m below seafloor. An attempt was made to fish the BHA because of the high geological interest and the time already invested in the hole. A 9-5/8-in. overshot was run and was worked over the fish, but could not be engaged firmly. When the overshot grapple was examined, metal shavings were found, indicating that the fish had been swallowed completely but was too rusty to engage good metal. After this unsuccessful attempt at fishing, Hole 895D was abandoned.

Survey 2

Survey 2 was conducted from 0030 to 0500 on 9 January 1993, upslope from Hole 895D, to start a new hole higher in the stratigraphic sequence. The ship was first moved 300 m to the north. The slope remained low-dipping and covered with sediment. The ensuing ship track covered a 200 m × 100 m rectangle to the east. We passed over a spur covered with huge blocks that were unsuitable for drilling, then moved back to the west and to the south. An area with a more gentle, sedimented slope was selected, and a punch test indicated a sediment thickness of 3 m. This site was selected to start a new hole.

Hole 895E

Hole 895E was spudded with a RCB bit at 0730 hr on 9 January 1993 in 3753 m water depth. Cores 147-895E-1R to -8R penetrated 87.6 m and recovered 32.93 m. However, hole conditions started deteriorating after Core 147-895E-5R. Thereafter, the hole had to be reamed back to bottom after each core retrieval. After the wash barrel 147-895E-9W was retrieved and 0.46 m of core was recovered, the pipe became stuck. Because it could not be freed, the pipe was blown. A first charge was shot at the bit in an attempt to recover the BHA and leave enough hole for logging, but the pipe was not freed. A second charge, shot at 4 mbsf, was successful in freeing the pipe, but 65.35 m of BHA was lost in the abandoned hole.

Survey 3

Survey 3 was conducted from 2000 hr, 12 January to 0100 hr, 13 January 1993, upslope from Hole 895E to start a new hole higher in

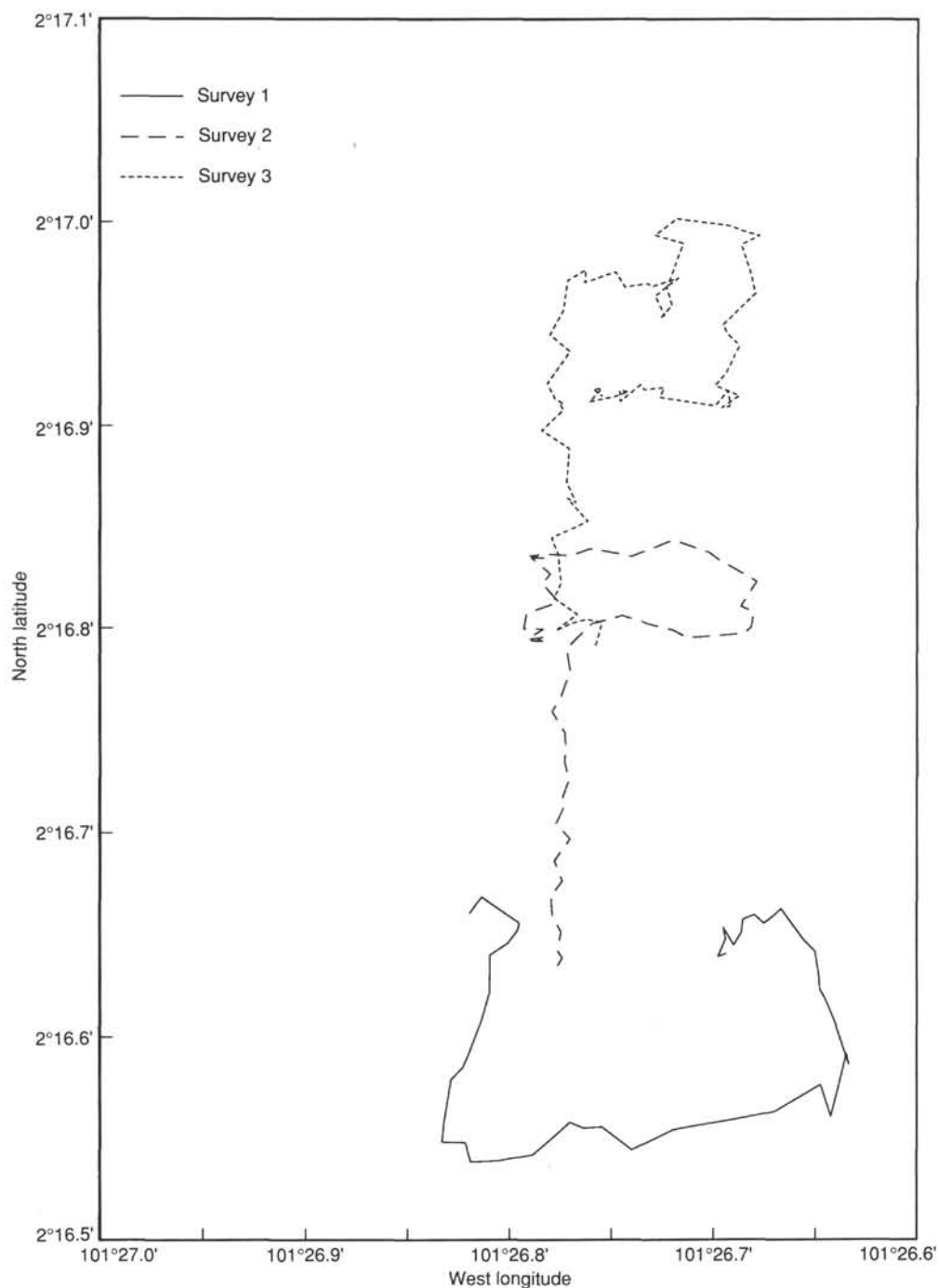


Figure 1. Map of the survey tracks for Site 895.

the stratigraphic sequence. The ship was first moved 200 m north of Hole 895E, then a 200 × 200 m east–north square was surveyed. However, from 3700 m depth upslope, the terrain became rugged and was covered with piles of large rounded blocks, some several meters in diameter. Because a gabbroic cumulate (Sample NZ17-5) was recovered by the *Nautila* in this area (Fig. 2), this sudden change in morphology is interpreted as a change in lithology from serpentinized peridotites to massive gabbroic rocks. However, the terrain was too rugged for a bare-rock spud-in, and a drill site was selected to the south, within the peridotites.

Hole 895F

Hole 895F was spudded with a RCB bit at 0300 hr, 13 January 1993, 3693 mbsl. The bit encountered 4 m of soft sediment. Cores 147-895F-1R to -2R penetrated 26.2 m and recovered 1.98 m of serpentinized peridotites. Coring conditions were poor, however, and the hole could not be kept open. The hole was therefore abandoned at 1230 on 13 January 1993. The bad hole conditions were interpreted as resulting from drilling in a pile of blocks and rubble. Because the remaining time was too short to conduct a new survey and start a hole

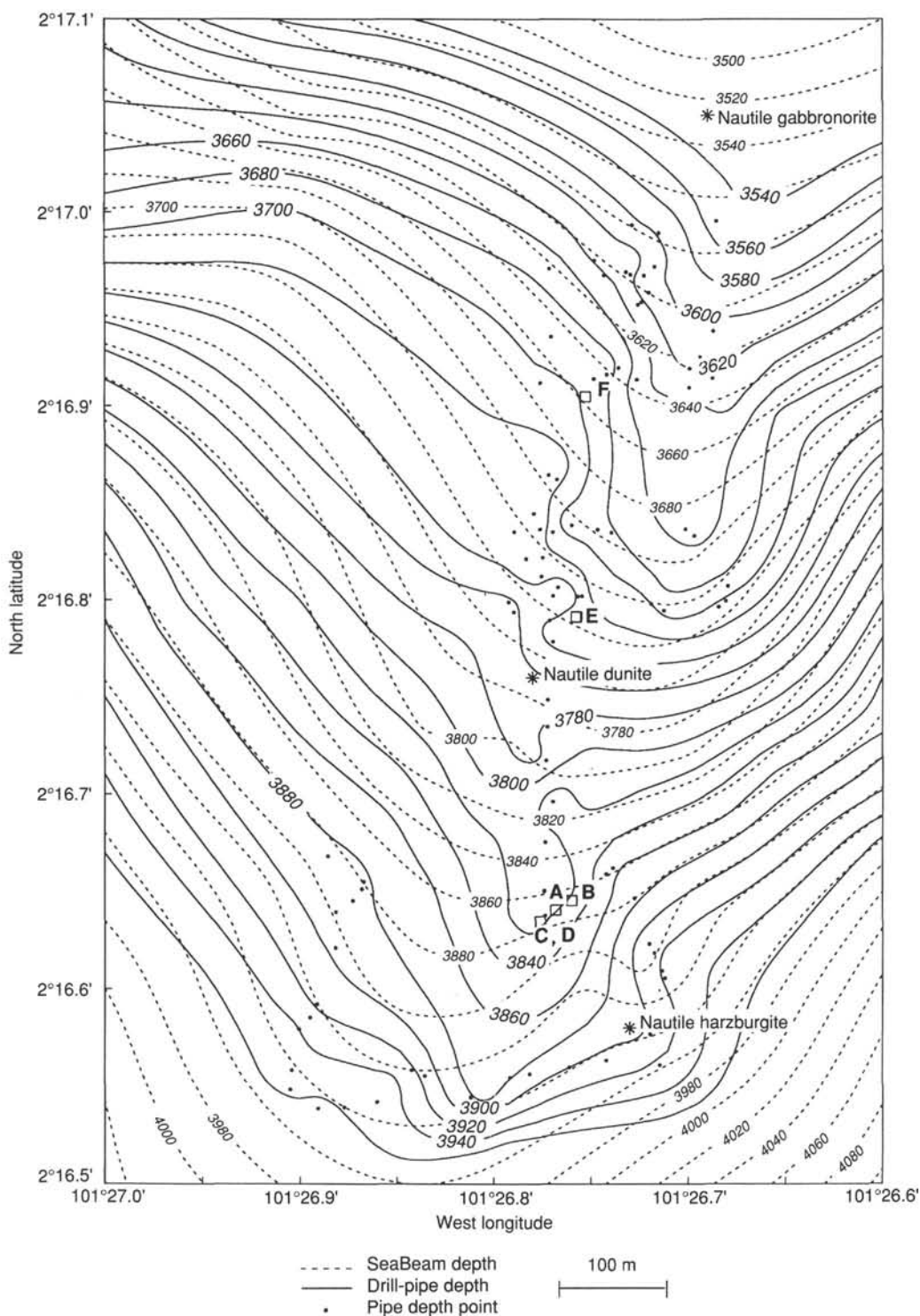


Figure 2. Refined bathymetric map (in meters) of Site 895 on the southern slope of the intrarift ridge, obtained from the depths measured during the Leg 147 site surveys (solid lines). Bathymetry derived from previous data also shown for comparison (dashed lines) (Cruise Report, *Sonne 60*, 12 March 1988–2 January 1989). Location of Holes 895A–F is shown.

with the potential of reaching a significant depth, we decided to leave Site 895 and return to Site 894 to log Hole 894G and retrieve the hard-rock guide base (HRB).

The six holes at Site 895 cored 272.9 m, yielding 64.56 m of serpentinized peridotites impregnated or crosscut by gabbroic melts (Table 1). Average recovery was 23.6%.

SEDIMENTS

At Site 895, sediments were only recovered in Core 147-895A-1R. A total of 1.78 m of material is spaced over two sections, but this does not represent full sediment recovery. No liner was run for this spud-in core, so the sediments had to be extruded from the core barrel. This

process normally results in highly disturbed sediment, but the situation was complicated further by the presence of loose, angular serpentinite fragments in soft ooze that had been caught up presumably from the top of the igneous basement and mixed into the ooze during coring. The clasts were individually removed from the ooze, which itself was scooped and scraped into pre-split archive and working sections of butyrate liner. The separate rock fragments were placed between pre-prepared spacers about midway in the half-liner of Section 147-895A-1R-1, between intervals of scraped-in ooze. In addition, a large quantity of serpentinite drilling breccia was washed from the inside of the core barrel and brought into the core lab in buckets. Some of this breccia was placed in the top 48 cm of Section 147-895A-1R-1, and the rest was used for a shipboard geochemical reference. There is no possibility of inferring sequence or stratigraphy among the breccia, the ooze, or the separate rock fragments in this section, except that they are above Section 147-895A-1R-2. This latter section includes rock fragments removed from the core catcher

Table 1. Coring summary, Site 895.

Core	Date (1992/93)	Time (UTC)	Depth (mbsf)	Cored (m)	Recovered (m)	Recovery (%)	
147-895A-1R	31 Dec	0000	0.0–9.2	9.20	1.50	16.3	
	31 Dec	0100	9.2–17.2	8.00	0.88	11.0	
Coring totals				17.2	2.38	13.80	
147-895B-1R	1 Jan	0900	0.0–10.3	10.30	1.02	9.9	
Coring totals				10.3	1.02	9.9	
147-895C-1R	1 Jan	1400	0.0–12.3	12.30	0.82	6.7	
	2R	1 Jan	12.3–18.3	6.00	0.21	3.5	
	3R	1 Jan	18.3–27.9	9.60	1.71	17.8	
	4R	2 Jan	27.9–37.9	10.00	2.99	29.9	
Coring totals				37.9	5.73	15.10	
147-895D-1R	3 Jan	2115	0.0–16.0	16.00	0.32	2.0	
	2R	4 Jan	16.0–26.0	10.00	1.95	19.5	
	3R	4 Jan	26.0–34.7	8.70	1.30	14.9	
	4R	4 Jan	34.7–43.3	8.60	4.88	56.7	
	5R	5 Jan	43.3–55.0	11.70	2.35	20.1	
	6R	5 Jan	55.0–64.6	9.60	1.17	12.2	
	7R	5 Jan	64.6–74.3	9.70	2.77	28.5	
	8R	6 Jan	0130	74.3–84.0	9.70	2.44	25.1
	9R	6 Jan	0900	84.0–93.7	9.70	1.90	19.6
	10W	7 Jan	0100	93.7–93.7	0.00	0.91	(wash core)
Coring totals				93.7	19.08	20.40	
Washing totals				0.0	0.91		
Combined totals				93.7	19.99		
147-895E-1R	9 Jan	1715	0.0–19.6	19.60	3.72	19.0	
	2R	9 Jan	19.6–29.6	10.00	2.21	22.1	
	3R	10 Jan	29.6–39.5	9.90	3.07	31.0	
	4R	10 Jan	39.5–48.9	9.40	3.24	34.4	
	5R	10 Jan	48.9–58.6	9.70	3.25	33.5	
	6R	10 Jan	58.6–68.2	9.60	6.60	68.7	
	7R	11 Jan	0000	68.2–77.9	9.70	5.25	54.1
	8R	11 Jan	0850	77.9–87.6	9.70	5.13	51.3
	9W	11 Jan	1400	87.6–87.6	0.00	0.46	(wash core)
Coring totals				87.6	32.47	37.10	
Washing totals				0.0	0.46		
Combined totals				87.6	32.93		
147-895F-1R	13 Jan	0830	0.0–18.2	18.20	0.13	0.7	
	2R	13 Jan	18.2–26.2	8.00	1.85	23.1	
Coring totals				26.2	1.98	7.60	

Note: The following cores were cut with a chrome core barrel: Cores 895A-1R and -2R; 895C-2R and -4R; 895D-2R, -4R, -6R, and -8R; 895E-2R, -4R, -6R, and -8R; and 895F-1R.

at its base and about 35 cm of firm ooze above this in stratigraphic sequence that was extruded fairly intact from the core barrel.

The drilling breccia at the top of Section 147-895A-1R-1 does not represent a sedimentary facies. It consists of extremely angular fragments of green serpentinite with abundant individual bits of orthopyroxene and numerous elongate chrysotile blades. The typical size of the fragments is 0.1–0.5 cm, with some pebbles reaching 3 cm in diameter. The protolith evidently was serpentinitized harzburgite that was veined with cross-fiber chrysotile.

Between 47 cm and 62 cm, and again from 82 cm to 117 cm in Section 147-895A-1R-1, the core liner is occupied by dark, extremely disturbed, yellowish brown to dark brown foraminifer-nannofossil ooze. The dark color of the sediment results either from pelagic biogenic deposition close to the carbonate compensation depth (CCD) in 3800 m of water or heightened input of a hydrothermal metalliferous component related to the proximal propagating tip of the Cocos-Nazca ridge. Foraminifers are in comparatively low abundance (<10%), and there appears to be no admixture of foraminifer-rich turbidites as there was at Site 894 (see "Site 894" chapter, this volume).

Igneous clasts are separated into five compartments between 62 and 82 cm in Section 147-895A-1R-1 and include serpentinites and metamorphosed gabbros. These clasts presaged the recovery of a dual gabbroic-ultramafic suite during basement coring. Sand-sized serpentinite grains are 1%–2% of the dark brown ooze on either side of this interval and are presumed to have been mixed in either during the process of coring or during extrusion of sediments from the pipe.

The firm ooze from 1 to 36 cm in Section 147-895A-1R-2 suggests that undisturbed sediment on the seafloor is layered, with some sediment being comparatively carbonate-rich (paler shades of yellowish brown) and other sediment being carbonate-poor (darker yellowish brown). Actual relationships were nearly lost because of core disturbance, but the material is still variegated in the manner of streaked, mixed-color taffy.

One additional type of sedimentary material was caught up in the sworl. This is distinctly greener (actually yellow-green), and may be serpentinous hydrothermal sediment produced by flux of water through the abundant ultramafic rocks in the immediate area. The sworl of this material is only 1–3 cm wide at most and is dispersed throughout about 20 cm of the core. Presumably, this means that the original layer on the seafloor was no more than a few centimeters thick.

Below this, from 35–60 cm in Section 147-895A-1R-2, is 10 cm of drilling breccia and angular pebbles, then three small cobbles of igneous rock, each in a separate compartment in the liner. The pebbles and two of the three rocks are serpentinitized harzburgite. The third rock, Sample 147-895A-1R-2 (Piece 2), is an aphyric basalt and resembles a fragment pillow lava or submarine extrusive flow. This and another fragment of pillow basalt near the top of Core 147-895A-2R are the only indications that at Site 895, as at Site 894, the surficial sediment may include fragmental basaltic material shed from fault exposures of shallow crust of the East Pacific Rise adjoining Hess Deep. Alternatively, the lava could be hill wash from upslope exposures of Cocos-Nazca eruptives. However, such exposures were not observed during *Nautile* dive operations on this portion of the intrarift ridge within Hess Deep (Francheteau et al., 1990), nor is the basalt at all porphyritic, as are most lavas from the nearby Cocos-Nazca rift tip (Hekinian et al., 1993).

IGNEOUS PETROLOGY

Introduction

Of the six holes drilled at Site 895, four Holes (895A, 895B, 895C, and 895F) cored to a maximum of 37.9 mbsf and had limited recovery (averaging less than 12.2%) before abandonment. Hole 895D was drilled to 93.7 mbsf, and Hole 895E to 87.6 mbsf; recovery was relatively high from both holes (averaging greater than 28.7%). Igneous lithologies sampled from Site 895 include dunitite, harzburgite, gabbroic rocks (gabbro, olivine gabbro, and troctolite), and

basalt (Table 2). Ultramafic rocks are moderately to pervasively serpentinized. Mafic rocks are generally, although not ubiquitously, moderately to pervasively altered as well. Descriptions of the various lithologies sampled at Site 895 and general descriptions of the primary minerals follow, subdivided by hole and mineralogy, respectively. As for Site 894, a lithostratigraphic unit number was assigned based on changes in modal mineralogy in ascending order with depth (Tables 3, 4, and 5). The data in these tables was used to produce igneous lithostratigraphic columns, which also show expanded recoveries for Holes 895D and 895E (Figs. 3 and 4).

Lithology

Hole 895A

Two cores were recovered from Hole 895A. Clasts of varying lithologies, including metamorphosed, sparsely plagioclase-olivine phryic basalt, fresh aphyric basalt, soapstone, serpentinite, serpentinized porphyroclastic harzburgite, and one piece of metamorphosed, coarse-grained gabbro were sampled. These cores correspond to a mixed rubble horizon and do not represent a stratigraphic sequence. The serpentinites are grayish white tinged with light green, have an almost schistose texture, and contain a small percent of chromite. Section 147-895A-2R-1 is composed of a mixed rubble horizon containing fragments of porphyroclastic, serpentinized harzburgite, greenstones, and fresh basalt fragments. The basalt lacks olivine and is oxide-rich, suggesting it is evolved. The harzburgite contains rounded, partially fresh orthopyroxene porphyroclasts (to 6 mm across), which are fragmented and partially to pervasively altered to bastite. The bastite pseudomorphs orthopyroxene and is also present in fractures and around the fragmented crystal margins. Bastite also

tends to change the morphology of the subrounded grains to a more irregular shape, intermingling with the surrounding serpentinized olivine matrix. Olivine preservation is poor. It is crosscut by multiple, anastomosing veinlets of serpentine and secondary magnetite, but adjacent kernels of relict olivine with a coherent extinction behavior define an approximate size-range of original crystals from 1 to 4 mm across. The harzburgite also includes a trace amount of dark brown, translucent, subequant spinel in elongate patches or weak stringers.

Hole 895B

Recovery from this hole includes an interval composed of sediment, mixed rubble clasts of porphyroclastic harzburgite, variably weathered and serpentinized dunite, and a single piece of metamorphosed gabbro. In thin section, the harzburgite exhibits clusters of fresh, optically continuous olivine kernels up to 5 mm across. These kernels occasionally display weak kink bands and have rare fluid inclusions. Orthopyroxene occurs as large (up to 5 mm) porphyroclasts with fragmented and rounded margins, commonly overgrown with bastite. Chromian spinel, with anhedral to vermicular habits, is also present. Small anhedral of higher birefringence pyroxene intergrown with orthopyroxene porphyroclasts occur. Spinel is intergrown with interstitial or exsolved clinopyroxene. The dunite fragments are moderately to intensely sheared and contain minor carbonate veinlets. A minor amount of pyroxene pseudomorphs is also part of the mineral assemblage. Section 147-895B-1R-1 (Piece 5) is an unoriented fragment of metamorphosed, coarse-grained, diallage gabbro with a preserved igneous contact against serpentinized dunite.

Hole 895C

The predominant rock type recovered from Hole 895C is porphyroclastic harzburgite, similar to the harzburgite from Holes 895A and 895B. The original olivine grain size is difficult to estimate because of pervasive serpentinization in anastomosing veinlets, but optical continuity between adjacent fresh kernels suggests anhedral crystals up to 5 mm across. Orthopyroxene porphyroclasts occur as large as 10 mm across, with morphologies similar to previously mentioned specimens (Fig. 5). Serpentinized dunites are variably weathered and serpentinized, but a few thin sections contain as much as 40% to 50% relict olivine. Anastomosing veinlets of serpentine and secondary magnetite, and rarely containing irregularly shaped, small patches of dark green, translucent serpentine, may be pseudomorphs after clinopyroxene. One small fragment of aphyric basalt was recovered, almost certainly an accidental lithic fragment fallen into the hole during the constant reaming and washing that interrupted coring intervals.

One interval of recovered core is so striking in appearance and unique in lithology, relative to the bulk of recovered core, that it merits particular attention. The uppermost pieces of Core 147-895C-4R are porphyroclastic harzburgite, grading into orthopyroxene-poor serpentinized dunite. From Section 147-895C-4R-1 (Piece 8) to Section 147-895C-4R-3 (Piece 3) the lithology varies locally from dunite through troctolite to olivine gabbro. Plagioclase appears in irregularly shaped patches, interstitial between clusters of olivine grains, and is almost ubiquitously mantled by light green, translucent serpentine, often intergrown with interstitial clinopyroxene. The modal percent of plagioclase-clinopyroxene patches increases from a few percent in Core 147-895C-4R-1 (Piece 8) to 40% of the rock in Core 147-895C-4R-2 (Piece 6) (Fig. 6), decreasing again to a few percent in Core 147-895C-4R-3 (Piece 3). This transition is gradational and can be traced between adjacent pieces. Clinopyroxene is consistently but not invariably in contact with plagioclase or the alteration products of plagioclase, and often is intimately associated with spinel. In the plagioclase-poorer representatives of this lithology, clinopyroxene often has an interstitial appearance within a serpentinized olivine matrix. Rare orthopyroxene is also present, in contact with plagioclase. Although orthopyroxene has essentially the same habit as in the

Table 2. Summary of recovered rock types for Site 895.

	Curated thickness (m)	Number of units	Recovery (%)
Hole 895A			
Harzburgite	1.01		79.53
Gabbro	0.03		2.36
Basalt	0.23		18.11
Total	1.27		100.00
Hole 895B			
Harzburgite	1.09	2	81.95
Dunite	0.19	1	14.29
Olivine Gabbro	0.05		3.76
Total	1.33	3	100.00
Hole 895C			
Harzburgite	3.46	4	54.06
Dunite	2.59	1	40.46
Gabbro	0.16	1	2.50
Basalt	0.19	2	2.97
Total	6.40	8	
Hole 895D			
Harzburgite	17.52	18	77.84
Dunite	2.44	15	10.84
Troctolite	1.22	4	5.42
Gabbro	0.95	8	4.22
Basalt	0.38	3	1.67
Total	22.50	48	100.00
Hole 895E			
Harzburgite	4.53	13	13.26
Dunite	24.18	28	70.84
Troctolite	1.38	11	4.03
Olivine Gabbro	3.74	5	10.94
Gabbro	0.32	3	0.94
Total	34.14	60	100.00
Hole 895F			
Harzburgite	2.39	1	100

Note: The curated thickness includes rock fragments interpreted to be rubble; these fragments are not included in the number of units.

Hole 895D

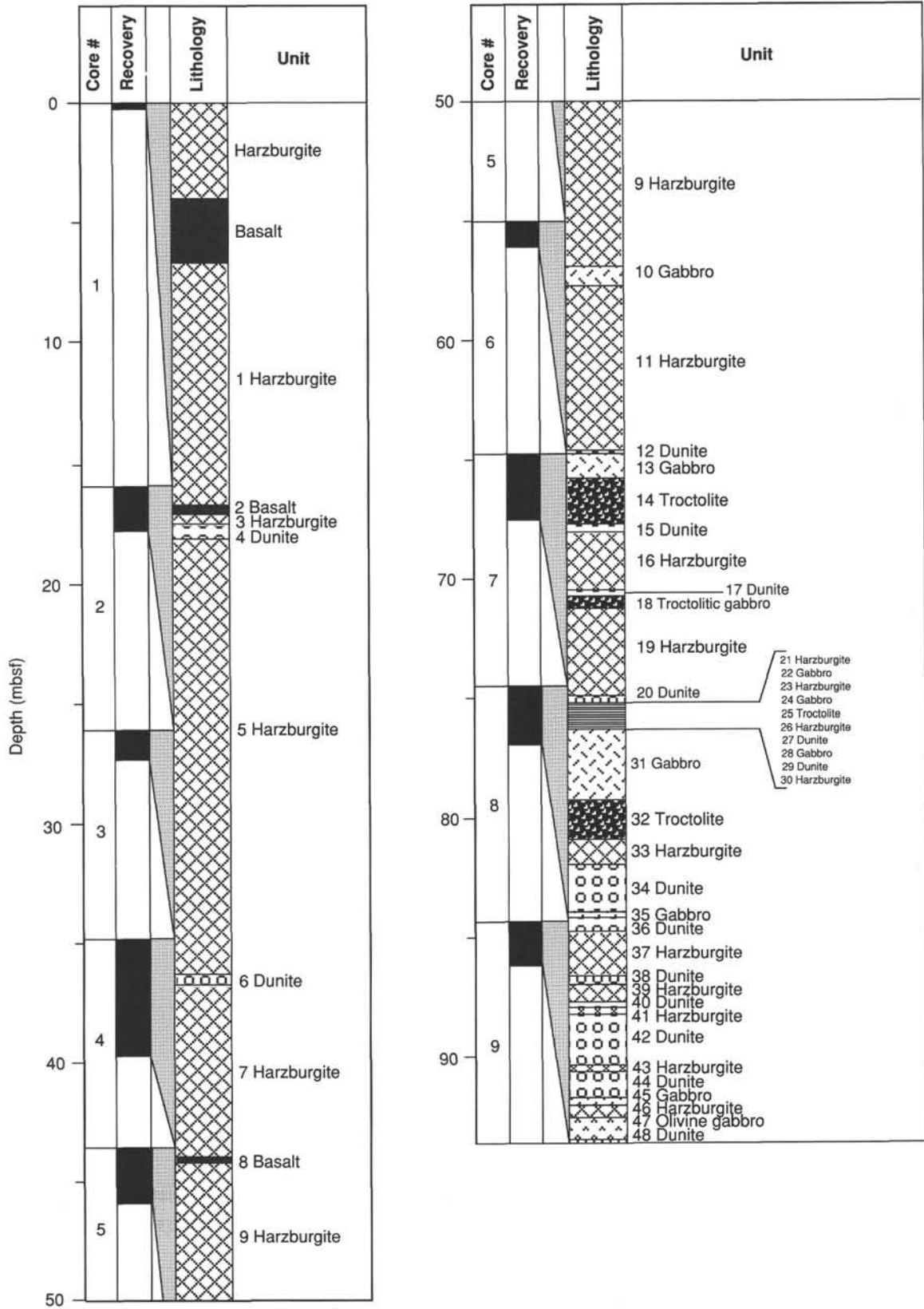


Figure 3. Schematic lithostratigraphic column for Hole 895D.

Hole 895E

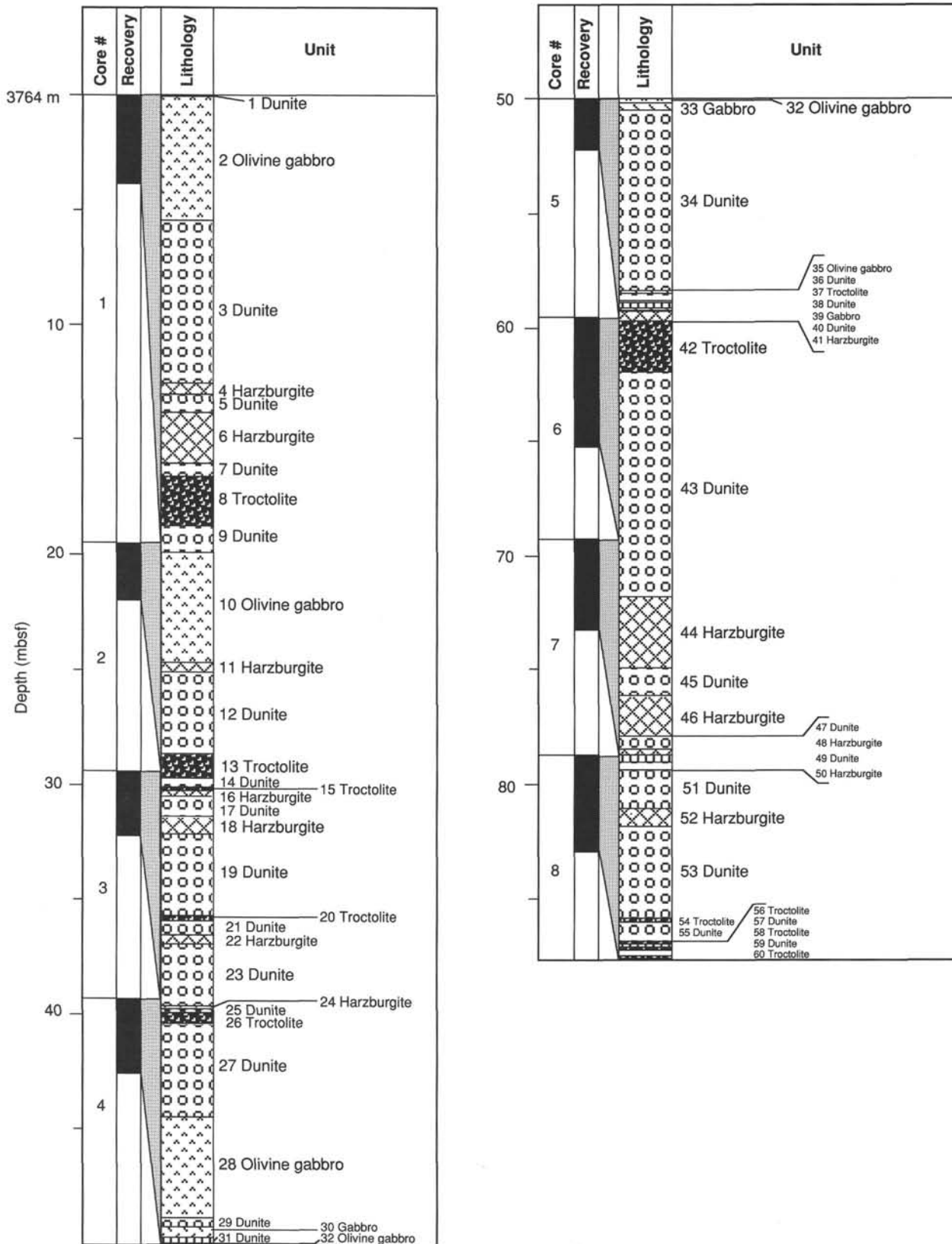


Figure 4. Schematic lithostratigraphic column for Hole 895E.



Figure 5. Photomicrograph of broken orthopyroxene porphyroblast. Wide fractures filled with fibrous serpentine, finer fractures filled with amphibole. Thin, subcontinuous mantle of amphibole surrounds orthopyroxene in serpentine matrix. Fresh olivine kernels are disseminated in serpentine near edges of photomicrograph (Sample 147-895C-1R-1, Piece 17, 105–109 cm; field of view = 6 mm).

associated harzburgite, it is incompletely mantled by, and partially recrystallized to clinopyroxene. The plagioclase and clinopyroxene tend to occur as anhedral crystals; where they occur together, pyroxene is commonly on the margins of the patches, and plagioclase makes up the bulk of the patch.

Serpentinized olivine is the most voluminous phase in this lithology, ranging from 95 to 50 modal percent. It is variably serpentinized from 60% to 90% and has a mesh-textured fabric defined by serpentine veinlets that can usually be shown to have a preferred orientation. The plagioclase-clinopyroxene patches are almost invariably interconnected by a series of serpentine-filled, thin veins that crosscut the general fabric present in the serpentinized olivine-rich part of the rock.

Hole 895D

Igneous lithologies recovered from Hole 895D included harzburgite, dunite, and gabbroic rocks (Table 2, Fig. 3). From Core 147-895D-1R to Core 147-895D-6R, harzburgite is predominant over dunite and mafic rocks. The relative proportion of dunite increases downhole and, in Cores 147-895D-8R and 147-895D-9R, surpasses harzburgite in abundance. Gabbroic and troctolitic rocks are also relatively common in the lower part of the hole.

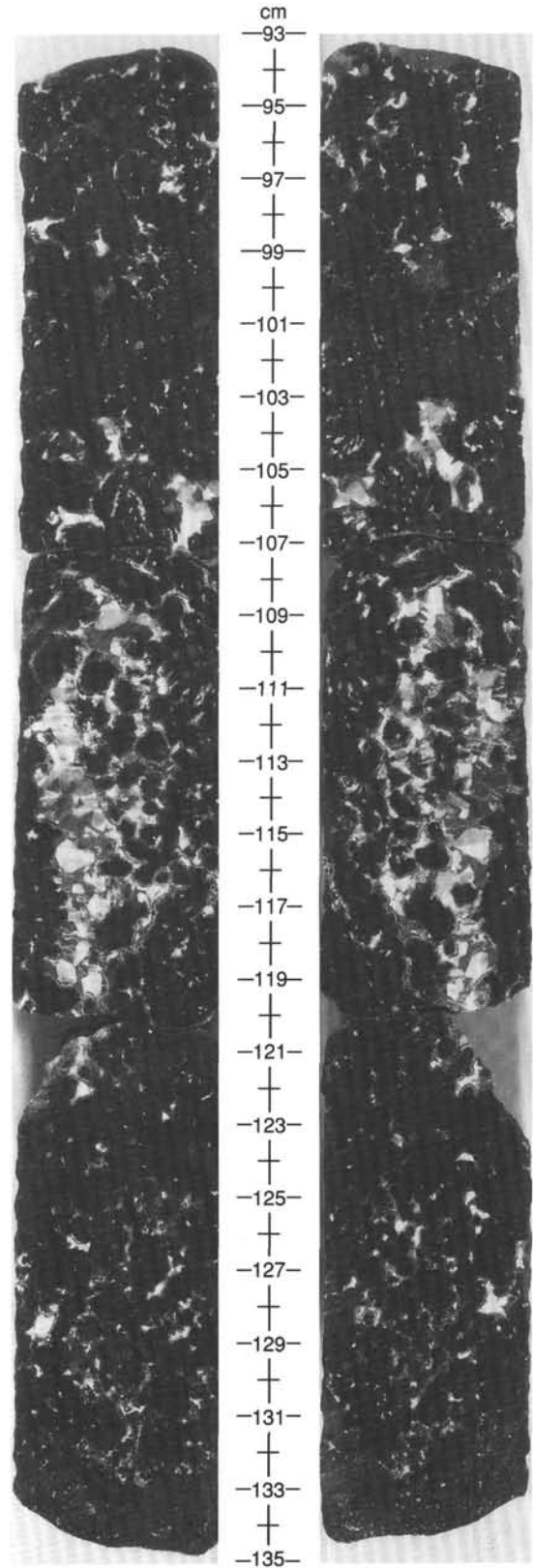


Figure 6. Closeup photograph of Section 147-895C-4R-2, 93–135 cm. Plagioclase (white) and clinopyroxene (light gray) intergrown with irregularly shaped patches of moderately serpentinized dunite (dark gray). Amount of plagioclase and clinopyroxene decreases away from center of this interval, grading from olivine gabbro to dunite. Left side: working half; right side: archive half.

Hole 895D rocks are strongly altered or metamorphosed; alteration of dunite is especially high, and in several intervals almost all primary minerals have been altered. In harzburgite, orthopyroxene is occasionally selectively altered, particularly along cracks. In some intervals, orthopyroxene is pervasively to completely altered (Fig. 7), making it difficult to distinguish harzburgite from troctolite in hand specimen. Where serpentinization is pervasive, peridotites are black to dark gray if fine-grained secondary magnetite is abundant and greenish if the amount of secondary magnetite is less. Weathered peridotites have a distinct yellowish or brownish tint, particularly in the olivine-rich horizons. In gabbroic and troctolitic rocks, plagioclase and olivine have been strongly altered.

In general, harzburgites are relatively poor in orthopyroxene (less than 15% by mode) throughout Hole 895D, although orthopyroxene is coarse-grained and more abundant (greater than 20% by mode) in some intervals (e.g., Section 147-895D-4R-3). Harzburgites often exhibit a gradational change to dunite (e.g., Section 147-895D-7R-1, Pieces 17–21, to Section 147-895D-7R-2, Pieces 1–2, and in Section 147-895D-8R-1, Piece 5). Small dunitic patches commonly occur in harzburgite, as do patches of porphyroclastic harzburgite in dunite.

Harzburgite usually exhibits a weak porphyroclastic to protogranular texture. In the weakly porphyroclastic-textured harzburgite, neoblasts of orthopyroxene and olivine, usually 0.2 to 0.4 mm across, are present only around orthopyroxene porphyroclasts, up to 6 mm across. Otherwise olivine is as coarse as or somewhat finer than orthopyroxene porphyroclasts. Tabular equigranular texture is rarely found (e.g., Sample 147-895D-5R-1, Piece 17, 126–129 cm). Clinopyroxene is characteristically sparsely present (typically less than 1% by mode, but rarely up to 3%). Small anhedral grains of clinopyroxene are attached to rounded orthopyroxene porphyroclasts or form vermicular intergrowths with chromian spinel. Chromian spinel, generally less than 2% by mode, is characteristically anhedral (“holly-leaf” shaped) and is closely associated with pyroxene, especially with clinopyroxene. Vermicular intergrowths of chromian spinel and clinopyroxene are also present. Spinel is reddish brown in thin section, suggesting that Cr# ($\text{Cr}/[\text{Cr} + \text{Al}]$ atomic ratio) is on the order of 0.5 to 0.6. In some clinopyroxene-poor (0.1% by mode) harzburgites, spinel is dark brown in color, and the Cr# may be higher, probably approaching 0.6.

Dunite is composed of olivine and chromian spinel (1% to 2% by mode) with or without pyroxene (less than 10% by mode). The most common habit of pyroxene is interstitial to olivine, and it is usually completely altered. Dunite is highly serpentinized relative to harzburgite; relict olivine is generally less than 10% in volume, but occasionally large clusters of fresh olivine kernels are preserved (Fig. 8). Chromian spinel is euhedral to subhedral and is brown to deep brown, noticeably darker than that in harzburgite, suggesting high Cr# (0.6 or higher). Olivine often has a dusty appearance in thin section, due to either minute fluid inclusions (or their relicts) or microgranular oxide minerals.

Mafic rocks recovered from the upper part of the hole are coarser grained than those from the lower part. An aphyric, fresh basalt fragment with a glassy selvage and scarce olivine microphenocrysts was recovered from Section 147-895D-1R-3. An intensely metamorphosed, diabasic-textured basalt was also recovered (Section 147-895D-2R-1, Piece 4). Porphyritic and ophitic textures are still preserved, but appreciable amounts of metamorphic minerals are present replacing olivine and plagioclase.

The lower part of Hole 895D is marked by the presence of coarse-grained gabbroic and troctolitic rocks, intercalated with serpentinized dunite and harzburgite. These mafic rocks are occasionally too strongly metamorphosed to specify igneous lithologies. Gradational transitions between troctolite and troctolitic gabbro are present. An interval of troctolite to troctolitic gabbro was recovered from Section 147-895D-7R-1 (Piece 7) to Section 147-895D-7R-1 (Piece 16); plagioclase was least abundant in the uppermost and lowermost

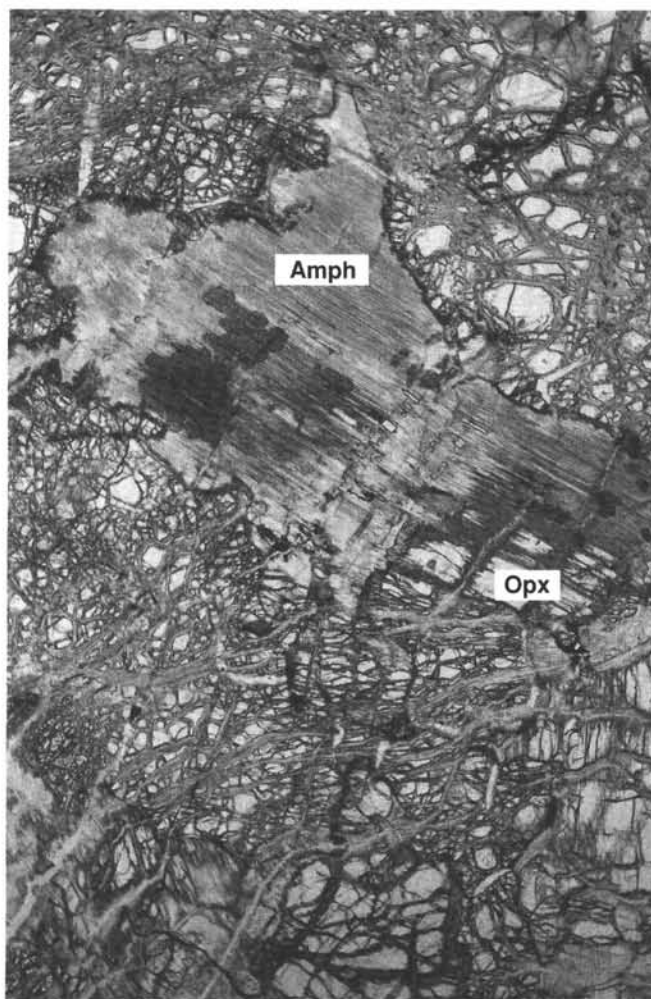


Figure 7. Photomicrograph of pervasively altered orthopyroxene (Opx). Amphibole (Amph) has nearly completely replaced orthopyroxene, and the morphology of the grain has become increasingly irregular, interfingering into serpentine matrix (Sample 147-895D-4R-3, Piece 12, 113–116 cm; field of view = 6 mm).

parts of the interval. In the gabbroic rocks, chromian spinel is characteristically anhedral and is usually associated with plagioclase. Metamorphosed troctolite and olivine gabbro were found in a wash core (Section 147-895D-10W-1, Piece 7, and Section 147-895D-10W-1, Piece 10), in which chromian spinel has a euhedral habit. Clinopyroxene-rich gabbro sometimes has olivine-rich aggregates, which are irregular in shape and are possible small xenoliths of dunite enclosed by gabbroic magma (e.g., Section 147-895D-8R-2, Piece 5, and Section 147-895D-10W-1, Piece 9).

Hole 895E

Hole 895E represents the most significant recovery of core from this site. Eight cores were recovered, averaging greater than 40% recovery (Table 2, Fig. 4). The predominant lithology sampled from this hole is variably serpentinized and weathered dunite (Table 2). Also recovered were significant volumes of harzburgite and mafic rocks that vary in modal composition from gabbro and olivine gabbro to troctolite. In general, all the rocks sampled in this hole are highly to pervasively altered.

Section 147-895E-1R-1 is composed of olivine gabbro with variable grain size and modal composition. Plagioclase ranges from 40

Table 3. Summary of igneous lithostratigraphic units for Holes 895A, 895B, 895C, and 895F.

Unit no.	Lithology	Top of unit		Bottom of unit			Expanded depth ^c (mbsf)	Curated thickness (m)	Contact description ^a			
		Core, type, section, piece	Depth (mbsf) ^b	Core, type, section, piece	Depth (mbsf) ^b	Depth (mbsf) ^b			Type	Nature	Morphology	
147-895A-												
	Harzburgite	1R-2, 1	40.0	1.87	1R-2, 1	45.0	1.92	3.45	0.05	M		
	Basalt	1R-2, 2	48.0	1.95	1R-2, 2	51.0	1.98	3.71	0.03	M		
	Gabbro	1R-2, 3	51.0	1.98	1R-2, 3	54.0	2.01	3.85	0.03	M		
	Harzburgite	1R-2, 4	54.0	2.01	2R-1, 3	13.0	9.33	10.10	0.19	M		
	Basalt	2R-1, 4	14.0	9.34	2R-1, 5	28.0	9.48	11.13	0.14	M		
	Harzburgite	2R-1, 6	30.0	9.50	2R-1, 14	87.0	10.07	15.20	0.57	M		
	Basalt	2R-1, 15	88.5	10.09	2R-1, 15	94.0	10.14	15.68	0.06	M		
	Harzburgite	2R-1, 16	96.0	10.16	2R-1, 18	116.0	10.36	17.20	0.20	M		
147-895B-												
	Harzburgite	1R-1, 2	3.0	0.03	1R-1, 2	11.0	0.11	0.79	0.08	M		
	Dunite	1R-1, 3	13.0	0.13	1R-1, 3	16.0	0.16	1.15	0.03	M		
	Harzburgite	1R-1, 4	16.0	0.16	1R-1, 4	21.0	0.21	1.51	0.05	M		
	Olivine gabbro	1R-1, 5	23.0	0.23	1R-1, 5	28.0	0.28	2.02	0.05	G	SI	I
	Dunite	1R-1, 5	28.0	0.28	1R-1, 5	30.0	0.30	2.16	0.02	M		
1	Harzburgite	1R-1, 6	30.0	0.30	1R-1, 9	80.0	0.80	5.76	0.50	M		
2	Dunite	1R-1, 10	81.0	0.81	1R-1, 11	95.0	0.95	6.84	0.14	M		
3	Harzburgite	1R-1, 12	97.0	0.97	1R-1, 18	143.0	1.43	10.30	0.46	M		
147-895C-												
1	Harzburgite	1R-1, 1	0.0	0.00	1R-1, 9	66.0	0.66	6.65	0.66	M		
2	Gabbro	1R-1, 10	69.0	0.69	1R-1, 12	81.0	0.81	8.17	0.12	M		
3	Harzburgite	1R-1, 13	82.0	0.82	1R-1, 18	122.0	1.22	12.30	0.49	M		
	Harzburgite	2R-1, 2	0.0	12.30	2R-1, 2	8.0	12.38	14.70	0.08	M		
	Gabbro	2R-1, 3	9.0	12.39	2R-1, 3	13.0	12.43	16.20	0.04	S	I	I
	Harzburgite	2R-1, 4	17.0	12.47	2R-1, 4	20.0	12.50	18.30	0.03	M		
3	Harzburgite	3R-1, 1	0.0	18.30	4R-1, 1	3.0	27.93	27.99	1.98	M		
4	Basalt	4R-1, 2	4.0	27.94	4R-1, 2	7.0	27.97	28.11	0.03	M		
5	Harzburgite	4R-1, 3	8.0	27.98	4R-1, 6	37.0	28.27	29.02	0.29	S	SI	I
6	Dunite	4R-1, 7	38.0	28.28	4R-3, 4	44.0	30.90	31.79	2.61	M		
7	Harzburgite	4R-3, 5	46.00	30.92	4R-3, 5	52.0	30.98	32.04	0.06	M		
8	Basalt	4R-3, 6	55.0	31.01	4R-3, 7	71.0	31.17	32.61	0.16	M		
147-895F-												
1	Harzburgite	1R-1, 1	0.0	0.00	2R-2, 9	77.0	20.45	25.70	2.39			

^a Contact description: Type: S = sharp, G = gradational, M = missing. Nature: SI = sutured igneous, I = intrusive. Morphology: I = irregular.

^b mbsf = curated depth in hole.

^c See "Igneous Petrography" section, "Explanatory Notes" chapter for definition. Depth of the bottom of the unit is given.

to 60 modal percent, and is moderately to pervasively altered. Individual plagioclase crystals range from about 1 to 5 mm, but aggregates of crystals form irregularly shaped patches in contact with other irregularly shaped patches of serpentinized olivine. In most pieces from this section, the olivine is completely altered, although several pieces contain at least minor amounts of fresh olivine. Clinopyroxene is present, generally as small, interstitial crystals with distinct light yellow-green color and closely spaced cleavage planes. Small patches of what appear to be altered clinopyroxene are present in part of this section, but are difficult to recognize in others. Some ambiguity exists as to nomenclature of the possibly clinopyroxene-barren parts of this section, but it should be resolved upon further examination.

Sections 147-895E-1R-2, -3, and -4 are composed of mesh-textured, serpentinized dunite, pervasively altered porphyroclastic harzburgite, and troctolite with abundant serpentinized olivine. The dunites from this part of the core are all greater than 95% serpentinized, with only a few relict olivine kernels. Anhedral to interstitial spinel is common along larger veins. Similarly, the harzburgites from this part of the core are pervasively altered, with usually less than 10% of primary phases still preserved. To an even greater degree than in Hole 895D, the relict orthopyroxene fragments are almost ubiquitously mantled with amphibole and talc that interdigitates with the surrounding serpentinized matrix, overprinting the subrounded habit of the orthopyroxene with an irregularly shaped morphology. Rare spinels,

occurring as discontinuous, diffuse stringers, define a foliation. The primary direction of serpentine veinlets appears to be parallel to this foliation. The troctolites in this section are also pervasively altered, although some pieces appear to preserve fresh olivine kernels in irregularly shaped patches. Olivine gabbro and dunite in Core 147-895E-2R are similar in appearance and composition to the lithologies in Core 147-895E-1R.

Cores 147-895E-3R and -4R are primarily dunite, intercalated with relatively thin intervals of troctolite and harzburgite. Whereas minor fresh olivine is recognized in the dunite from the overlying sections, none could be seen in most of the hand specimens or thin sections from this interval. Spinel appears to mark an incipient foliation, but it is not particularly well developed and generally occurs in discrete patches and diffuse stringers. The few pieces of troctolite have roughly equal proportions of altered plagioclase in aggregate patches up to 15 mm across and variably serpentinized olivine.

At the base of Core 147-895E-4R, olivine gabbro is composed of medium- to coarse-grained, fresh to moderately altered plagioclase, rare fresh olivine, and medium-grained to pegmatitic clinopyroxene. Plagioclase occurs in aggregated patches up to 10 mm across, and single clinopyroxene crystals are as long as 12 cm. Examination in thin section reveals a roughly equigranular matrix of plagioclase and clinopyroxene. Large clinopyroxenes, with distinct, finely divided and crenulated cleavage planes, are partially surrounded and crosscut

Table 3 (continued).

	Notes
Harzburgite gravel with light manganese coatings on some pieces. Fine-grained fresh aphyric basalt. Metamorphosed to calc-silicate minerals. Moderately to heavily weathered porphyroclastic harzburgite. Fine-grained fresh basalt. Porphyroclastic harzburgite.	
Porphyroclastic harzburgite.	
Serpentinized porphyroclastic harzburgite with ~15%-20% enstatite and <1% spinel. Contains subhedral rounded spinel and minor enstatite.	
Coarse-grained gabbro, metamorphosed to calc-silicate minerals, with a preserved contact with serpentinized dunite. May represent an occurrence similar to that of the gabbroic segregation in Hole 895C. Porphyroclastic harzburgite.	
Porphyroclastic harzburgite.	
Porphyroclastic harzburgite; Piece 14 to 18 moderately weathered with a dun-yellow sepiolite stain. Mixture of cross-fiber serpentine and calc-silicate vein fillings. Porphyroclastic harzburgite. Rubble caught in core catcher. Pervasively altered to calc-silicate minerals; contact in Piece 3; rubble caught in core catcher. Rubble caught in core catcher. Porphyroclastic harzburgite, locally weathered. Fine-grained aphyric basalt, metamorphosed to calc-silicate minerals. Porphyroclastic harzburgite; enstatite has local protogranular textural elements of deeply embayed interlocking smooth curved grain boundaries with the olivine. Dunite in 147-894C-4R-1, Piece 7, has gabbro attached to one side; plagioclase pseudomorphs first appear in Section 147-894C-4R-1, Piece 8; the upper portion of the dunite is plagioclase-bearing (<5% plagioclase); in Section 147-895C-4R-2, Piece 2, plagioclase-spinel-bearing dunite locally grades into patches of troctolite and gabbro; troctolitic patches define an irregular subvertical 5–10 cm segregation that extends down through this section of the core; the segregation consists of mixed, locally idiomorphic, olivine with intergranular plagioclase; plagioclase locally increases up to 20%–40% at the center of the segregation in association with coarse-grained intergranular clinopyroxene to form gabbroic patches; amount of plagioclase decreases down section from this concentration zone. Heavily weathered porphyroclastic harzburgite from the core catcher; similar to weathered harzburgite in 147-895C-3R1-8, 106–100 cm.	
Originally an intergranular to subophitic medium-grained basalt with 20% olivine pseudomorphs; altered to 60% amphibole, 20% secondary feldspar and a trace of epidote.	
Porphyroclastic harzburgite; 147-895F-1R-1, Piece 1, is a beautiful small serpentine shear polyhedron; 147-895F-1R-1, Piece 2, is a very fresh porphyroclastic harzburgite; 147-895F-2R consists of almost entirely of serpentinized harzburgite with a trace of relict enstatite, 5.8% relict olivine, and fractured chromian spinel; no evidence of diopside seen.	

by veins rich in prehnite and amphibole. In hand sample, the large pyroxenes have a bright, satiny sheen and occasionally appear to envelop small plagioclase crystals.

Cores 147-895E-5R and -6R are again primarily dunite with minor intervals of plagioclase-bearing, leucocratic rocks. Although still highly serpentinized, olivine in the dunites is somewhat better preserved than samples from further upsection, and sparse, interstitial clinopyroxene (to 1 mm) is present. Foliation defined by elongation and alignment of irregularly shaped spinel is discontinuous and generally weakly developed. Mafic rocks in this interval vary from sparsely clinopyroxene-bearing troctolites to olivine gabbro with up to 10 modal percent interstitial clinopyroxene. The clinopyroxene-rich samples have roughly equivalent modal plagioclase and olivine, but the troctolites contain substantially more olivine and pseudo-morphed olivine than plagioclase.

Core 147-895E-7R marks the top of an interval that is characterized by variably but highly serpentinized dunite and harzburgite. Transitions between these modal compositions are often missing; however, both sharp and gradational contacts have been sampled. Sharp contacts tend to be at high oblique angles (60°–70°) to horizontal, and are marked by a distinct mineralogical change from orthopyroxene-free dunite to porphyroclastic orthopyroxene-rich harzburgite (to 20 modal percent), over an interval of less than 1 cm. Gradational boundaries are much more difficult to recognize, as the first appearance of orthopyroxene in dunite is often veiled by intense alteration to dark green,

translucent amphibole or amphibole and chlorite in irregularly shaped, interstitial patches. This interval continues through Core 147-895E-7R and down to Section 147-895E-8R-4, where sparse, leucocratic troctolites supplant harzburgites as the lithology subordinately intercalated with dunite. These troctolites are variably plagioclase- to olivine-rich, with patches of serpentinized olivine separated by irregularly shaped patches of plagioclase and its alteration products. Pervasively serpentinized dunite is the most voluminous lithology in this interval, and persists to the bottom of the hole.

Hole 894F

Three cores were recovered from Hole 894F; the only lithology sampled was porphyroclastic harzburgite. Orthopyroxene porphyroclasts look fresh in a few pieces and exhibit the characteristic sheen recognized in the freshest harzburgites sampled at this site. Most of the orthopyroxene, however, appears to be altered to milky white to green-gray, soft amphibole and chlorite. The amount of orthopyroxene is variable (5 to 20 modal percent). A thin section from Sample 147-895E-2R-1 (Piece 15, 124–129 cm) exhibits 6 modal percent fresh olivine kernels in a mesh-textured, serpentinized matrix. Orthopyroxene in this sample is almost completely altered to intergrowths of bastite, amphibole, and talc. Deep brown, translucent spinel tends to occur in interstitial patches and disseminated stringers, intergrown and mantled by magnetite.

Table 4. Summary of igneous lithostratigraphic units for Hole 895D.

Unit no.	Lithology	Top of unit			Bottom of unit			Expanded depth ^c (mbsf)	Curated thickness (m)	Contact description ^a		
		Core, type, section, piece	cm	Depth (mbsf) ^b	Core, type, section, piece	cm	Depth (mbsf) ^b			Type	Nature	Morphology
	Harzburgite	1R-1, 1	0.0	0.00	1R-1, 2	9.0	0.09	4.00	0.09	M		
	Aphyric basalt	1R-1, 3	10.0	0.10	1R-1, 3	15.0	0.15	6.67	0.05	M		
1	Harzburgite	1R-1, 4	16.0	0.16	2R-1, 3	16.0	16.16	16.68	0.36	M		
2	Olivine-phyric basalt	2R-1, 4	17.0	16.17	2R-1, 4	24.0	16.24	17.03	0.07	M		
3	Harzburgite	2R-1, 5	25.0	16.25	2R-2, 1a	2.0	17.40	17.47	1.15	S	SI	I
4	Dunite	2R-2, 1a	2.0	17.40	2R-2, 1b	17.0	17.55	18.11	0.15	M		
5	Harzburgite	2R-2, 2	17.0	17.55	4R-2, 6	45.0	36.02	36.30	4.86	M		
6	Dunite	4R-2, 7	45.0	36.02	4R-2, 11	73.0	36.82	36.75	0.28	M		
7	Harzburgite	4R-2, 12	74.0	36.83	5R-1, 3	15.0	43.45	43.96	3.84	M		
8	Basalt	5R-1, 4	16.0	43.46	5R-1, 4	21.0	43.51	44.22	0.05	M		
9	Harzburgite	5R-1, 5	23.0	43.53	6R-1, 5	26.0	55.26	56.89	2.70	M		
10	Gabbro	6R-1, 6	27.0	55.27	6R-1, 6	36.0	55.36	57.62	0.09	M		
11	Harzburgite	6R-1, 7	39.0	55.39	6R-1, 17	132.0	56.32	64.60	0.93	M		
12	Dunite	7R-1, 1	0.0	64.60	7R-1, 1	5.0	64.55	64.75	0.05	M		
13	Gabbro	7R-1, 2	5.0	64.55	7R-1, 6	40.0	64.90	65.82	0.35	M		
14	Troctolite	7R-1, 7	40.0	64.90	7R-1, 16	101.0	65.51	67.69	0.61	M		
15	Dunite	7R-1, 17	102.0	65.52	7R-1, 19	113.0	65.63	68.06	0.11	G	SI	I
16	Harzburgite	7R-1, 19	112.5	65.63	7R-2, 6	48.0	66.42	70.48	0.80	M		
17	Dunite	7R-2, 7	48.0	66.42	7R-2, 7	57.0	66.51	70.75	0.09	M		
18	Troctolitic gabbro	7R-2, 8	58.0	66.52	7R-2, 9	74.0	66.68	71.27	0.16	M		
19	Harzburgite	7R-2, 10	75.0	66.69	8R-1, 3	18.0	74.48	74.91	1.16	M		
20	Dunite	8R-1, 4	20.0	74.50	8R-1, 4	26.0	74.56	75.18	0.06	M		
21	Harzburgite	8R-1, 5	27.0	74.57	8R-1, 7	51.0	74.81	76.02	0.24	M		
22	Gabbro	8R-1, 8	52.0	74.82	8R-1, 8	59.0	74.89	76.29	0.07	M		
23	Harzburgite	8R-1, 9	60.0	74.90	8R-1, 9	63.0	74.93	76.43	0.03	M		
24	Gabbro	8R-1, 10	65.0	74.95	8R-1, 10	67.0	74.97	76.56	0.02	S	I	P
25	Troctolite	8R-1, 10	67.0	74.97	8R-1, 10	75.0	75.05	76.83	0.08	M		
26	Harzburgite	8R-1, 11	75.0	75.05	8R-1, 13	91.0	75.21	77.38	0.16	M		
27	Dunite	8R-1, 14	92.0	75.22	8R-1, 14	97.0	75.27	77.58	0.05	M		
28	Gabbro	8R-1, 15	100.0	75.30	8R-1, 15	109.0	75.39	77.98	0.09	M		
29	Dunite	8R-1, 16	110.0	75.40	8R-1, 18	121.0	75.51	78.39	0.11	M		
30	Harzburgite	8R-1, 19	122.0	75.52	8R-1, 20	137.0	75.67	78.93	0.15	M		
31	Gabbro	8R-2, 1	0.0	75.67	8R-2, 2	19.0	75.86	79.23	0.19	M		
32	Troctolite	8R-2, 3	20.0	75.87	8R-2, 6	57.0	76.24	80.86	0.37	M		
33	Harzburgite	8R-2, 7	58.0	76.25	8R-2, 10B	89.0	76.56	81.94	0.31	M		
34	Dunite	8R-2, 11	91.0	76.58	8R-2, 19	147.0	77.14	83.90	0.56	S	I	I
35	Gabbro	8R-2, 19	147.0	77.14	9R-1, 1	4.0	84.04	84.18	0.07	M		
36	Dunite	9R-1, 2	5.0	84.05	9R-1, 3	17.0	84.17	84.76	0.12	M		
37	Harzburgite	9R-1, 4	19.0	84.19	9R-1, 7	56.0	84.56	86.50	0.37	M		
38	Dunite	9R-1, 8	58.0	84.58	9R-1, 9	66.0	84.66	86.95	0.08	M		
39	Harzburgite	9R-1, 10	67.0	84.67	9R-1, 12	83.0	84.83	87.71	0.16	M		
40	Dunite	9R-1, 13	84.0	84.84	9R-1, 13	89.0	84.89	87.98	0.05	M		
41	Harzburgite	9R-1, 14	89.0	84.89	9R-1, 14	95.0	84.95	88.25	0.06	M		
42	Dunite	9R-1, 15	98.0	84.98	9R-1, 21	142.0	85.42	90.35	0.44	M		
43	Harzburgite	9R-1, 22	143.0	85.43	9R-1, 22	148.0	85.48	90.62	0.05	M		
44	Dunite	9R-2, 1	0.0	85.48	9R-2, 4	26.0	85.74	91.78	0.26	M		
45	Gabbro	9R-2, 5	26.0	85.74	9R-2, 5	33.0	85.81	92.09	0.07	M		
46	Harzburgite	9R-2, 6	34.0	85.82	9R-2, 7	44.0	85.92	92.58	0.10	M		
47	Olivine gabbro	9R-2, 8	44.5	85.93	9R-2, 10	65.0	86.13	93.52	0.21	M		
48	Dunite	9R-2, 11	66.0	86.14	9R-2, 11	69.0	86.17	93.70	0.03	M		

^a Contact description: Type: S = sharp, G = gradational, M = missing. Nature: SI = sutured igneous, I = intrusive. Morphology: I = irregular, P = planar.

^b mbsf = curated depth in hole.

^c See "Igneous Petrography" section, "Explanatory Notes" chapter for definition. Depth of the bottom of the unit is given.

Relative Stratigraphies of Holes 895A–895F

The six holes drilled at Site 895 are staggered up a small north-south ridge or abutment of the east-west-trending Hess Deep intrarift high. Holes 895A, 895B, 895C, and 895D are situated together in a small area at about 3820 mbsl, with Hole 895E at 3753 mbsl, 270 m to the north, and Hole 895F at 3693 mbsl another 200 m to the north of Hole 895E. Holes 895D and 895E have very different stratigraphies (Figs. 3 and 4). The upper portion of Hole 894D is almost entirely harzburgite, whereas the lower portion is a complex intercalation of harzburgite, dunite, and gabbroic rocks. In contrast, Hole 895E is largely dunite, with more gabbro than harzburgite. To the north, Hole 895F recovered only harzburgite. These differences are highlighted when the proportions of all rock types from all holes are compared in Figure 9. There is a northward progression from dominantly harzburgite in the southernmost holes, to dominantly dunite and gabbro in the central holes, and then back to harzburgite in Hole 895F. Even when considering local disturbance caused by block rotation and local slumping of the section along the ridge, it is clear that the mantle

section drilled is laterally heterogeneous. This lateral variability in the shallow mantle section at Hess Deep may have major implications for the transport of magma from the mantle to the crust and for the consequent stratigraphy of the overlying crust.

Primary Mineralogy

Olivine

Olivine and its alteration products are the dominant minerals of the Site 895 rocks, composing more than 80% of the peridotites sampled. In general, olivine is moderately to pervasively serpentinized, but may be well preserved locally (e.g., Sample 147-895D-7R-2, Piece 9, an olivine gabbro). In thin section, fresh olivine occurs as small (generally less than 1 mm) subangular to subrounded kernels separated by anastomosing veinlets of mesh-textured serpentine and secondary magnetite. By observing clusters of olivine kernels that exhibit optically continuous extinction behavior, original grain sizes are estimated to be a minimum of 2 to 3 mm. Commonly, adjacent clusters of olivine

Table 4 (continued).

Notes
<p>Variably serpentinized and moderately weathered porphyroclastic harzburgite with ~20% enstatite. Aphyric basalt fragment with olivine and plagioclase microphenocrysts; fresh glass on one side. With ~20% enstatite and trace diopside. With >10% olivine and trace spinel phenocrysts; diabasic texture; metamorphosed. With ~20% enstatite and trace diopside; contact with lower dunite dips 70°.</p> <p>With 15%-20% enstatite and <1% diopside; harzburgite in 147-895D-2R-2 is more altered than the overlying dunite. Contains variable amounts of medium-grained irregular intergranular pyroxene pseudomorphs. Variably serpentinized with 15%-20% enstatite and trace to 3% diopside. Fine-grained basalt altered to calc-silicate assemblages. With trace to 3% diopside; enstatite is generally well preserved. Coarse-grained gabbro altered to calc-silicate assemblages. Variably serpentinized.</p> <p>Olivine-bearing gabbro with narrow olivine gabbro intervals; contains sharp, contact dipping 45° between coarse- and medium-grained zones at 24 cm; medium-grained gabbro is in the lower half. Contains skeletal chromite in plagioclase. Contains 1% spinel, no plagioclase; contact in Piece 19 is not oriented. Single thin section contains ~4% diopside. Contains 0.5% chromite and no plagioclase. Coarse-grained troctolite at top of Piece 8 grades into gabbro; Piece 9 is olivine gabbro.</p> <p>Medium-grained heterogeneous gabbro with olivine pseudomorphs, <5% is fresh. Two small fragments. 4-cm-wide gabbro zone intrudes troctolite. Coarse-grained troctolite with 30%-50% plagioclase.</p> <p>Very coarse-grained gabbro with subophitic clinopyroxene megacryst (>4 cm). Pink carbonate veins. With 10%-15% porphyroclastic enstatite. Coarse-grained gabbro. Medium- to coarse-grained granular troctolite with coarse-grained patches appear to be angular partially digested harzburgite and/or dunite xenoliths.</p> <p>Spinel subhedra are ubiquitous; contact in Piece 19 is unoriented. Medium-grained at contact with dunite in Piece 19; coarse-grained at top of Core 147-895D-9R; foliation sub-parallel to inclined to the contact.</p> <p>Coarse-grained, pervasively altered to calc-silicate assemblages.</p> <p>Coarse-grained with clinopyroxene up to 2.5 cm.</p>

preserve continuous kink bands, indicating that the original olivine grains may have been considerably larger than 3 mm in size. Olivine in several samples contains linear arrays of silicate inclusions.

Orthopyroxene

Orthopyroxene composes 0%–20% of the sampled peridotites, with an average of 12 to 15 modal percent in the harzburgites. It ranges from 1 to 20 mm in size, and generally occurs as subrounded to slightly subangular porphyroclasts. Fragmented grain boundaries are common, as is fracturing and a vaguely concentric orientation of marginal fragments, neoblasts, and serpentinization. A continual gradation can be seen in various samples from reasonably fresh, tabular to subrounded orthopyroxene to irregularly shaped patches of bastite, amphibole, and chlorite that interdigitate with surrounding serpentinized olivine and are often interconnected by a series of chlorite and serpentine veinlets. In hand specimen, it is often difficult to distinguish between irregularly shaped patches of dark green, translucent chlorite and serpen-

tine, which is alteration after orthopyroxene, and alteration products after plagioclase, which have similar morphologies and appearance. Usually, these can only be distinguished in thin section, thus causing ambiguity in some of the rock names afforded to various specimens that are classified as either troctolite or harzburgite.

Plagioclase

In harzburgites, trace amounts of interstitial altered crystals have been tentatively interpreted as plagioclase (see “Structure” section, this chapter). Plagioclase is common in dunites, where it forms interstitial, occasionally fresh crystals. The dunites may grade into troctolites as the modal proportion of plagioclase increases. Plagioclase and its alteration products typically make up 40 to 50 modal percent of the mafic rocks (troctolites, olivine gabbros, and gabbros). However, its distribution is more heterogeneous in troctolite, where its proportion varies between several percent up to 80%.

Table 5. Summary of igneous lithostratigraphic units for Hole 895E.

Unit no.	Lithology	Top of unit		Bottom of unit			Expanded depth ^c (mbsf)	Thickness	Contact description ^a		
		Core, type, section, piece	cm	Depth (mbsf) ^b	Core, type, section, piece	cm			Depth (mbsf) ^b	Type	Nature
1	Dunite	1R-1, 1	0.0	0.00	1R-1, 1	2.0	0.08	0.02	S	I	I
2	Olivine gabbro	1R-1, 1	2.0	0.08	1R-1, 16	143.5	1.44	5.45	1.42		
3	Dunite	1R-2, 1	0.0	1.44	1R-3, 1	9.0	2.93	12.56	1.53	G	
4	Harzburgite	1R-3, 1	9.0	2.93	1R-3, 2a	21.0	3.05	13.05	0.12	G	SI
5	Dunite	1R-3, 2a	21.0	3.05	1R-3, 3	39.5	3.24	13.82	0.19	M	
6	Harzburgite	1R-3, 4	39.5	3.24	1R-3, 5	93.0	3.77	16.04	0.54	G	SI
7	Dunite	1R-3, 5	97.0	3.81	1R-3, 6	107.0	3.91	16.62	0.10	M	
8	Troctolite	1R-3, 7	108.0	3.92	1R-4, 2	19.0	4.53	18.77	0.61	M	
9	Dunite	1R-4, 3	20.0	4.54	2R-1, 2	8.0	19.68	19.92	0.27	M	
10	Olivine gabbro	2R-1, 3	9.0	19.69	2R-2, 1	14.0	21.10	24.65	1.41	M	
11	Harzburgite	2R-2, 2	16.0	21.12	2R-2, 2	25.0	21.21	25.10	0.09	M	
12	Dunite	2R-2, 3	26.0	21.22	2R-2, 15	111.0	22.07	28.59	0.85	M	
13	Troctolite	3R-1, 1	0.0	29.60	3R-1, 1	3.5	29.64	29.70	0.04	M	
14	Dunite	3R-1, 2	3.5	29.64	3R-1, 3	19.0	29.79	30.12	0.16	M	
15	Troctolite	3R-1, 4	21.0	29.81	3R-1, 4	23.0	29.83	30.23	0.02	M	
16	Harzburgite	3R-1, 5	24.0	29.84	3R-1, 6	33.0	29.93	30.51	0.09	M	
17	Dunite	3R-1, 7	34.0	29.94	3R-1, 10	65.0	30.25	31.39	0.31	M	
18	Harzburgite	3R-1, 11	67.0	30.27	3R-1, 13	93.0	30.53	32.16	0.26	M	
19	Dunite	3R-1, 14	94.0	30.54	3R-2, 7	87.0	31.83	35.75	1.30	S	SI
20	Troctolite	3R-2, 8	88.0	31.84	3R-2, 8	93.0	31.89	35.92	0.05	S	I
21	Dunite	3R-2, 9	94.0	31.90	3R-2, 11	117.0	32.13	36.58	0.23		
22	Harzburgite	3R-2, 12	119.0	32.15	3R-2, 13	131.0	32.27	36.97	0.12	M	
23	Dunite	3R-2, 14	131.0	32.27	4R-1, 1	6.0	39.56	39.66	0.22	M	
24	Harzburgite	4R-1, 2	6.0	39.56	4R-1, 2	10.0	39.60	39.76	0.04	M	
25	Dunite	4R-1, 3	11.0	39.61	4R-1, 4	18.0	39.68	39.98	0.07	M	
26	Troctolite	4R-1, 5	18.0	39.68	4R-1, 7	35.0	39.85	40.43	0.17	M	
27	Dunite	4R-1, 8	37.0	39.87	4R-2, 15	134.0	42.28	44.49	2.41	M	
28	Olivine gabbro	4R-2, 16	135.0	42.29	4R-3, 8	63.0	43.04	48.87	0.75	M	
29	Dunite	5R-1, 1	0.0	48.90	5R-1, 3	14.0	49.04	49.26	0.14	M	
30	Gabbro	5R-1, 4	15.0	49.05	5R-1, 6	32.0	49.22	49.73	0.17	M	
31	Dunite	5R-1, 7	35.0	49.25	5R-1, 7	39.0	49.29	49.95	0.04	M	
32	Olivine gabbro	5R-1, 8	40.0	49.30	5R-1, 9	49.0	49.39	50.17	0.09	G	SI
33	Gabbro	5R-1, 10	51.0	49.41	5R-1, 11	61.0	49.51	50.49	0.10		
34	Dunite	5R-1, 12	62.0	49.52	6R-1, 3	13.5	58.34	58.39	3.25		
35	Olivine gabbro	6R-1, 4	14.0	58.34	6R-1, 4	21.0	58.41	58.50	0.07		
36	Dunite	6R-1, 5	21.0	58.41	6R-1, 8	43.0	58.63	58.82	0.22		
37	Troctolite	6R-1, 9	43.0	58.63	6R-1, 9	49.0	58.69	58.90	0.06	M	
38	Dunite	6R-1, 10	50.0	58.70	6R-1, 11	65.0	58.85	59.13	0.15	M	
39	Gabbro	6R-1, 12	66.0	58.86	6R-1, 12	71.0	58.91	59.22	0.05	M	
40	Dunite	6R-1, 13	72.0	58.92	6R-1, 13	74.0	58.94	59.26	0.02	M	
41	Harzburgite	6R-1, 14	76.0	58.96	6R-1, 14	78.0	58.98	59.71	0.02	M	
42	Troctolite	6R-1, 15	80.0	59.00	6R-1, 18	94.0	59.14	61.93	0.14	M	
43	Dunite	6R-1, 19	96.0	59.16	7R-2, 5	49.0	70.19	71.74	7.71	M	
44	Harzburgite	7R-2, 6	50.0	70.20	7R-3, 5	75.0	71.95	74.86	1.75		
45	Dunite	7R-3, 6	76.0	71.96	7R-3, 13	150.0	72.70	76.19	0.74	M	
46	Harzburgite	7R-4, 1	0.0	72.70	7R-4, 8	96.0	73.66	77.90	0.96	M	
47	Dunite	8R-1, 1	0.0	77.90	8R-1, 6a	36.0	78.26	78.48	0.36	G	SI
48	Harzburgite	8R-1, 6a	36.0	78.26	8R-1, 8b	55.0	78.45	78.78	0.19	S	SI
49	Dunite	8R-1, 8b	55.0	78.45	8R-1, 8b	69.0	78.59	79.01	0.14	M	
50	Harzburgite	8R-1, 9	71.0	78.61	8R-1, 10	93.0	78.83	79.39	0.22	M	
51	Dunite	8R-1, 11	94.0	78.84	8R-2, 5b	52.0	79.87	81.06	1.52	S	SI
52	Harzburgite	8R-2, 5b	52.0	79.87	8R-2, 7	101.0	80.36	81.84	0.13	M	
53	Dunite	8R-2, 8	104.0	80.39	8R-4, 10	65.0	82.88	85.88	0.99	M	
54	Troctolite	8R-4, 11	67.0	82.90	8R-4, 11	72.0	82.95	86.00	0.05	M	
55	Dunite	8R-4, 12	72.0	82.95	8R-4, 17	124.0	83.47	86.83	0.52	M	
56	Troctolite	8R-4, 18	125.0	83.48	8R-4, 18	130.0	83.53	86.93	0.05	M	
57	Dunite	8R-4, 19	130.0	83.53	8R-4, 19	141.0	83.64	87.10	0.11	M	
58	Troctolite	8R-4, 20	141.0	83.64	8R-4, 20	148.0	83.71	87.22	0.07	M	
59	Dunite	8R-5, 1	0.0	83.70	8R-5, 3	18.0	83.88	87.49	0.18	M	
60	Troctolite	8R-5, 4	19.0	83.89	8R-5, 4	25.0	83.95	87.60	0.06	M	
	Dunite	9W-1, 1	0.0	87.60	9W-1, 7	42.0				na	
	Troctolite	9W-1, 8	42.0		9W-1, 8	48.0				na	
	Dunite	9W-1, 9	48.0		9W-1, 9	51.0				na	

^a Contact description: Type: S = sharp, G = gradational, M = missing. Nature: SI = sutured igneous, I = intrusive. Morphology: I = irregular, P = planar.

^b mbsf = curated depth in hole.

^c See "Igneous Petrography" section, "Explanatory Notes" chapter for definition. Depth of bottom of unit is given.

Table 5 (continued).

Notes
<p>Medium-grained with 50%-60% plagioclase and variable proportions of olivine and clinopyroxene; local pegmatoidal patches with very coarse plagioclase and/or diallage; variably deformed from weak to strongly foliated. Contact steep at 45°, 147-895E-1R-1, 4-8 cm. With 3%-10% enstatite; contact between 21-26 cm.</p> <p>With 3%-10% enstatite; contact between 93-98 cm.</p>
<p>Medium- to coarse-grained with 55%-60% plagioclase and a few olivine-rich pods in 147-895E-1R-4, Piece 1; weak to moderately foliated with a penetrative foliation in 147-895E-1R-3, Piece 8-9, dipping about 30°. Coarse- to medium-grained igneous contact with an apparent dip of 27° in 147-895E-1R-4, Piece 2; rare small spinels at the bottom and top of the interval, but none seen in 147-895E-1R-4, Piece 10-11.</p>
<p>Medium- to coarse-grained with 55%-60% plagioclase; 1 cm, olivine-rich pods at bottom of 147-895E-2R-2, Piece 1; locally, weakly foliated with a 15° dip; rare spinels seen at top and bottom of unit, but not in 147-895E-2R-1, Piece 8-13. With 10%-15% enstatite. 147-895E-2R-2, Piece 4-5, are cut by 1-cm-wide coarse-grained troctolite veins with 60% plagioclase, with a sutured igneous contact and no evidence of a chill zone. Medium-grained with ~60% plagioclase; 0.2 mm, equant spinel in plagioclase.</p>
<p>Coarse-grained with ~60% plagioclase; a sharp intrusive contact on one edge with harzburgite, no chill zone; a single 0.1 mm equant spinel in plagioclase.</p>
<p>Weathered. Coarse-grained troctolite vein (1 to 2 cm width) with 50% plagioclase; sutured igneous contact with no evidence of a chill zone; a single 0.3 mm equant spinel seen in plagioclase. Coarse-grained troctolite with 40% plagioclase in contact with dunite within unoriented piece; sharp, sutured igneous contact; 0.2-0.5 mm equant spinels locally abundant in patch in olivine.</p>
<p>Medium- to coarse-grained with ~60% plagioclase; a weak to moderate foliation; 0.2 mm spinels rare in 147-895E-4R-1, Piece 5-7, but 0.2-0.5 mm equant spinels are abundant (0.5%) in Piece 7; small olivine-rich pod in Piece 7. Troctolite vein in 147-895E-4R-2, Piece 8 dips 14°. Highly variable grain size from medium to pegmatoidal patches with diallage >7 cm in length (147-895E-4R-3, Piece 7); with up to 50% plagioclase with some very diallage-rich zones; internal sharp planar sutured igneous contact between coarse- and medium-grained gabbro in 147-895E-4R-3, Piece 1 dips 70°; a weak foliation locally parallels contact.</p>
<p>Medium- to coarse-grained with coarse diallage oikocrysts, 1%-5% olivine, and ~50% plagioclase; rare equant spinels seen in intergranular diallage in 147-895E-5R-1, Piece 6.</p>
<p>147-895E-5R-1, Piece 8, is coarse-grained with <10% plagioclase, clinopyroxene- and olivine-rich; 147-895E-5R-1, Piece 9, is medium-grained equigranular with ~50% plagioclase; rare 0.1-0.2 mm equant spinel. Medium-grained with ~50% plagioclase; a pyroxene-rich layer in 147-895E-5R-1, Piece 10; moderately to strongly deformed; no spinel seen in hand specimen. Three fragments comprise Section 147-895E-6R-1: two are dunite, one is of unknown lithology—rubble? Medium-grained with 40% plagioclase, 50% olivine, 10% diallage; contains a weak foliation; rare 0.5 mm equant spinels and ~1%-2% intergranular diallage present.</p>
<p>Coarse-grained with ~50% plagioclase; rare 0.1-0.3 mm spinel present; very weakly deformed.</p>
<p>Coarse pegmatoidal diallage; rare 0.1 mm spinel in plagioclase in gabbroic patch; moderately deformed.</p>
<p>Porphyroclastic harzburgite in sharp planar contact with strongly foliated, medium-grained troctolite; unoriented piece. Coarse-grained troctolite less deformed and may contain less plagioclase (<10%); the latter appears to form an interconnected intergranular mesh around olivine-rich pods; abundant 0.2 to 0.5 mm equant spinels in plagioclase.</p>
<p>With a steep sharp lower contact with the dunite with an apparent dip of 81°.</p>
<p>Contact is irregular on a thin-section scale, but planar on a hand-specimen scale; it has a strike of 323° and dips 62°NE in core co-ordinates.</p>
<p>Undeformed, equigranular, coarse-grained with 50% plagioclase, 48% olivine, and 2% intergranular clinopyroxene; rare equant spinel in olivine and plagioclase.</p>
<p>Undeformed, very coarse-grained with ~45% plagioclase; equant 0.5-1 mm spinel present.</p>
<p>Undeformed, coarse-grained with ~10%-15% plagioclase forming an interconnected mesh around rounded, olivine-rich pods; equant 0.5-1 mm spinels in plagioclase.</p>
<p>Medium-grained weakly or undeformed, troctolite with ~50% plagioclase enclosing ragged irregular olivine-rich pods; small 0.1-0.3 mm equant spinels present. Wash core, no penetration. Wash core, no penetration; weakly or undeformed, medium-grained troctolite with about 50% plagioclase; spinel present. Wash core, no penetration.</p>

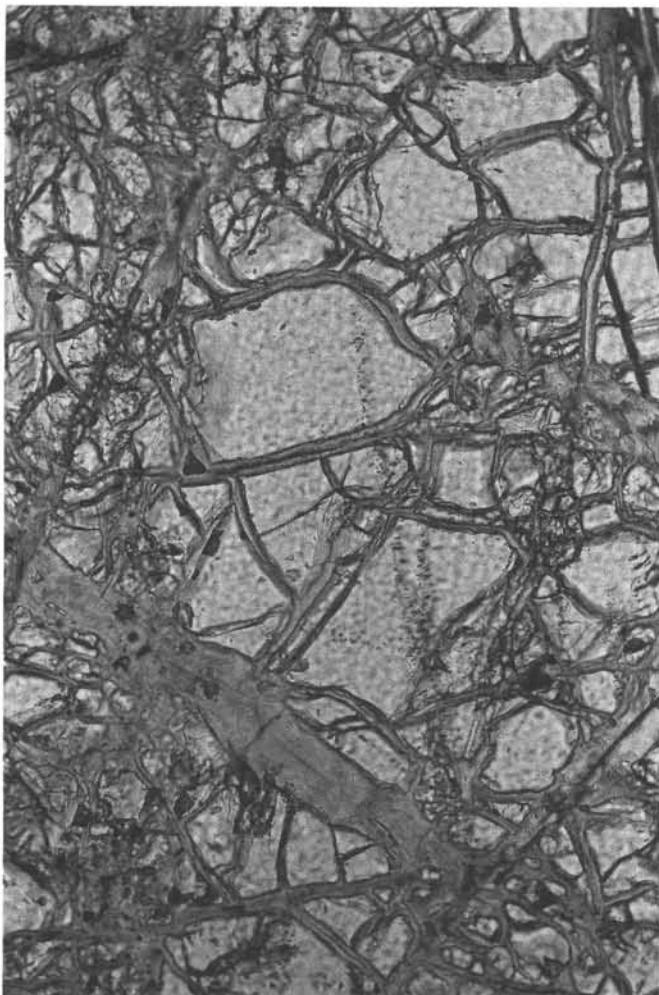


Figure 8. Photomicrograph of well-preserved olivine kernels in serpentine matrix (Sample 147-895D-5R-01, Piece 14, 103–105 cm; field of view = 1.5 mm).

Clinopyroxene

Clinopyroxene abundance is low (usually less than 1 modal percent), but where present it is usually remarkably fresh, given the degree of alteration of the other primary silicate phases. Clinopyroxene occurs in trace amounts as small (about 1 mm), interstitial, crystals in ultramafic rocks often associated with plagioclase. In harzburgite, clinopyroxene is recognized as sparse irregular anhedral exsolution patches along margins and in lamellae of orthopyroxene, and as granular exsolution in patches of orthopyroxene neoblasts recrystallized from primary orthopyroxene porphyroclasts. Clinopyroxene is common in the gabbroic rocks, where it is characterized by well developed, finely spaced cleavage that imparts a distinct satiny sheen to the cut face of hand samples. In some pieces of gabbro, clinopyroxene exceeds 10 cm in length. In the coarser-grained examples of this phase, the fine, wavy cleavage often appears to be crenulated, both along crystal margins and within crystals. Altered clinopyroxene is typically recognized by the aggregation of microgranular magnetite along cleavage planes and around grain margins.

Spinel

The abundance of spinel in these rocks is variable, ranging from up to 10% in one thin layer in dunite to a virtual absence in some metamorphosed gabbros. Spinel is disseminated throughout the dunites and harzburgites. The greatest concentration of spinel is associated with

troctolites, which can have up to 1%–2% spinel, ranging from 3 mm to more than 1 cm in diameter between altered olivine and plagioclase. Spinel also occurs as smaller (<0.2 mm) inclusions in plagioclase and ferromagnesian minerals. Spinel in harzburgites and dunites is generally 1–3 mm in size (rarely to 6.5 mm) and less abundant. Locally, dunite hosts slightly higher concentrations of spinel than does the adjacent harzburgite. In the longest section of dunite (Section 147-895E-6R-1, 96 cm, to Section 147-895E-7R-2, 50 cm), numerous concentrations of spinel occur as layers, especially toward the bottom of this interval, where thin, 1- to 2-cm-wide patches or layers may have up to 10% spinel. Several of the other dunite intervals have up to 5% spinel concentrated in thin layers.

In thin section, spinel has distinct colors (indicating variable composition) from red through brown to black in plane polarized light. Its morphology also changes from perfect euhedral and equant to subrounded and elongate to holly-leaf to vermiform with common pull-apart textures. Spinel occurs in four main textural sites:

1. In dunite, and where associated with olivine, the spinel has a deep red to black color, often is elongate and usually has rounded edges. It often occurs in rows or forms in echelon patches with elongated spinels aligned parallel to the long axes of these patches. It may also have a holly-leaf texture with concave edges pointing in towards the center of the spinel. This is an interstitial texture, and the spinel often partially or wholly encloses olivine.
2. Commonly, spinel is entwined within clinopyroxene to give a vermicular or wormy appearance. This spinel is characteristically brownish green in color. This texture is most common in clinopyroxenes that are situated on the edge of larger orthopyroxene crystals.
3. In troctolites containing interstitial patches of plagioclase, subrounded spinel is dark brown to black in transmitted light and is found within plagioclase and in adjacent mafic minerals. It sometimes has a holly-leaf form and exhibits cockscomb texture. It commonly encloses round inclusions filled with silicates, including possible phlogopite.
4. In gabbroic lithologies, spinels are dark brown to black. Although these lithologies may be completely barren of spinel, in rare instances they contain perfectly euhedral equant crystals in plagioclase, or seeded throughout the rock, or in lines.

Igneous Contacts

Several types of igneous contacts are found at Site 895. Two relationships exist between harzburgite and dunite. In long sections of the core, the percentage of enstatite decreases gradually, such that in some cases there are areas with less than 5% enstatite (technically dunite) that in turn appear to pass locally into pyroxene-free dunite. These gradational contacts are hard to define, so contacts were picked where the dunite was nearly pyroxene-free. In addition, there were numerous sharp harzburgite-dunite transitions where the modal percentage of enstatite dropped abruptly to zero or near zero. At these “contacts,” there is no evidence of chilling, and the dunite has the same approximate grain size as the adjacent harzburgite, with the olivine and pyroxene across the contact interlocked in a sutured igneous contact invisible except for the disappearance of pyroxene. The orientation of a number of sharp harzburgite-dunite contacts could be determined in long sections of core in Hole 895E. These were largely steep (60°–70°), and one of these when reoriented (using paleomagnetic declination and inclination) was found to have been subvertical at the time magnetization was acquired (see “Paleomagnetism” section, this chapter).

A variety of contact relationships exists between the gabbroic rocks and the dunites. The contacts of plagioclase-poorer, coarser-grained troctolites were gradational with dunite. At these contacts, a small percentage of intergranular plagioclase is scattered throughout the dunite, increasing in abundance to form an interconnected network with local segregations or pools where the plagioclase increases sharply in abundance to 30% or 40% of the rock. Locally, intergranu-

lar clinopyroxene is present in the center of these segregations to constitute a gabbroic mineralogy.

Discussion

Petrology of the Harzburgites

The harzburgites recovered at Site 895 are typical of residual mantle peridotites with porphyroclastic textures and contain a mineral assemblage consisting largely of olivine and lesser orthopyroxene with minor amounts of clinopyroxene and spinel. Clinopyroxene is usually low in abundance (less than 1%), though locally it may amount to 3% of the peridotite. In places, it is found as exsolution lamellae within primary orthopyroxene or attached to orthopyroxene, either around the rims of porphyroclasts or recrystallized in a matrix of orthopyroxene neoblasts. Vermiform intergrowths with fine-grained spinel are occasionally found. Clinopyroxene may also occur as interstitial crystals, associated with pseudomorphs of an interstitial mineral that was likely plagioclase (see "Structure" section, this chapter). The peridotites contain dark red chromian spinel, a color that suggests a Cr/(Cr + Al) ratio in the spinel of approximately 0.5 to 0.6.

The low abundance of clinopyroxene and the likely chrome-rich spinel composition suggest that the harzburgite from Hess Deep is refractory and represents melting of the Pacific mantle to a clinopyroxene-out or nearly clinopyroxene-out residue (e.g., Jaques and Green, 1980; Dick and Fisher, 1984). Compared with the large suites of abyssal peridotites dredged from fracture zones and rift valley walls in the Atlantic and Indian oceans, which contain on average 3.5% diopside (Dick, 1989), the rocks from Hess Deep are moderately to highly depleted. The low amounts of clinopyroxene (0% to 3%) suggest that they are as major-element-depleted as the more refractory Indian Ocean and Atlantic Ocean peridotites dredged in the vicinity of mantle hot spots (Dick and Fisher, 1984; Shibata and Thompson, 1986), but are not as depleted as the anomalous Mid-Atlantic Ridge 15°20'N Fracture Zone peridotites (Bonatti et al., 1992; Dick and Kelemen, 1992), which represent the most depleted abyssal peridotites dredged in the oceans to date. This latter suite, in contrast to the Site 895 peridotites, contains no primary clinopyroxene, and rarely exhibits any exsolution, granular or otherwise.

Petrology of the Dunites and Associated Rocks

At Site 895, dunite is abundant and consists of a rather monotonous association of highly serpentinized olivine and accessory spinel. The texture of the dunite was likely allotriomorphic granular before alteration, and is characterized by equant anhedral to subhedral relatively coarse-grained spinel, which is concentrated in places. The dunites are also associated with a suite of apparently coeval troctolites, olivine gabbros, gabbros, and gabbro-norites. Preliminary reconnaissance suggests the possibility that cyclic intervals marked by the repeated sequence harzburgite-dunite-troctolite-olivine gabbro-gabbro-olivine gabbro-troctolite-dunite-harzburgite may have been sampled. This sequence is occasionally complete, but more typically is only present in part, in some cases perhaps due to low core recovery. An apparent crystallization sequence can be extracted from these lithologies, starting with olivine and spinel in the dunites, followed by olivine, spinel, and plagioclase in the troctolites and troctolitic dunites, proceeding to olivine-spinel-plagioclase-clinopyroxene and olivine-plagioclase-clinopyroxene in the olivine gabbros and finally to clinopyroxene-plagioclase in the gabbros. However, because the contacts between these lithologies were rarely sampled, this interpretation is speculative.

The relatively common occurrence of dunite associated with refractory harzburgite may be characteristic of the Hess Deep upper mantle. In general, harzburgite is often modally gradational to dunite in the Site 895 peridotites, though there are sharp transitions between the two, where the transition occurs over a few centimeters or less. Possibly, the dunites are a simple residue of melting formed by more melt extraction

than from the harzburgites, but such a high degree of partial melting should be reflected in higher Cr# (>0.8; Jaques and Green, 1980) than that suggested by the spinel color. The possibility that the dunites are simple cumulus products of melt crystallization also cannot be ruled out. However, a combination of these processes—including melt-rock interaction with local consumption of pyroxene and the precipitation of olivine from a melt migrating through the shallow upper mantle—is a possibility for the Hess Deep dunites. If this is the case, the forsterite content of the olivine and the Cr# of spinel in the dunite should be lower than that expected for a simple dunite residue and similar to that of the harzburgite, as the compositions of these phases would be effectively buffered by the melt-rock interaction.

Frequent melt injection is consistent with the appearance of gabbroic and troctolitic rocks within dunite-dominant intervals of the Site 895 cores, particularly those from Hole 895E and the lower part of Hole 895D, as suggested by Hekinian et al. (1993) and Girardeau and Francheteau (1993). The survival of partly digested orthopyroxene in a plagioclase-poor troctolite strongly suggests an interaction between mantle orthopyroxene and melt, and also suggests that the troctolite might be a melt-peridotite interaction product. If the melt had been effectively eliminated, dunite would have been formed instead of the troctolite. Some troctolitic gabbros, which in places have relatively large amounts of euhedral chromian spinels, may have been formed from contaminating magnesium and chrome-rich melts near the peridotite wall. Some of the olivine in the olivine gabbros may also be modified xenocrysts and xenoliths of mantle olivine.

In the Hess Deep intrarift ridge suite, the dunites and related gabbroic rocks were most abundant in Hole 895E, where they constituted four-fifths of the total recovery in the 87 m drilled. By contrast, they were much less abundant in Holes 895A to 895D (less than 270 m downslope to the south) and at Hole 895F (less than 250 m upslope to the north) (Table 2 and Fig. 9). These results suggest a laterally heterogeneous mantle beneath the EPR before Hess Deep rifting, associated with nonuniform distribution of flow of melt out of the mantle. The association of the Hole 895E massive dunites, which may have formed by melt-rock interaction, with a considerable proportion of gabbroic rocks suggests that Hole 895E was drilled through a sequence representing a conduit for melt percolation through the shallow mantle to the crust.

Comparison with Ophiolitic and Abyssal Peridotites

The Hess Deep harzburgites are similar to tectonite peridotites described from a number of ophiolite occurrences (e.g., Oman, Troodos, Bay of Islands). The relative abundance of dunite suggests that the drilled sections at Site 895 are close to the mantle-crust boundary as recognized in these complexes. We also note that the close association of gabbroic and troctolitic rocks with dunite in the Site 895 cores is similar to the gabbroic intrusions and dunite envelopes described from the shallow mantle sections of the Semail ophiolite (Nicolas, 1989). The Hess Deep peridotites may be derived from such a transition zone at the crust/mantle boundary.

A notable difference between the suite of peridotitic and related rocks drilled at Hess Deep and those dredged elsewhere from fracture zones and rift valley walls at slow-spreading ridges is the abundance of dunite and primitive gabbroic rocks. Both of the latter are quite rare in abyssal peridotite suites from slow-spreading ridges (Dick, 1989; Cannat et al., 1992), indicating that these suites do not represent points at which substantial melt flow from the mantle beneath the ridge occurred (i.e., this occurs instead beneath rift valleys, away from fracture zones).

Another difference between the Hess Deep peridotites and peridotite suites from slow-spreading ridges is the abundance of highly evolved gabbros, diorites, and trondhjemites associated with the latter. This association is attributed to the shallow emplacement of the peridotites dredged from slow-spreading ridges on major faults at the

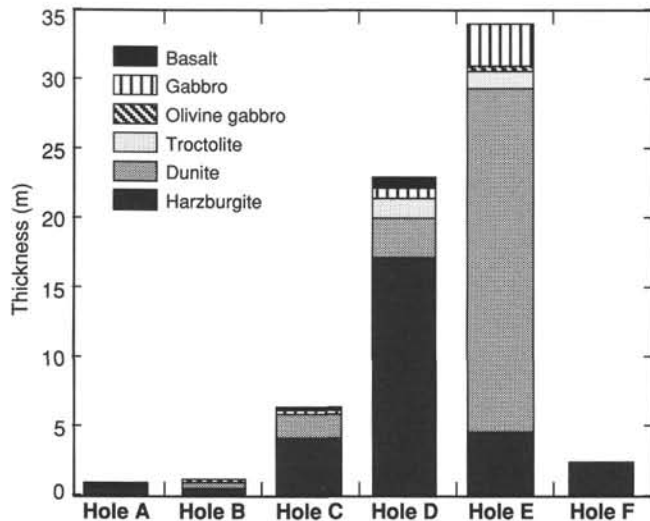


Figure 9. Cumulative curated thickness of the rock types recovered from each hole at Site 895.

rift valley walls at ridge transform intersections—faults that may also act as conduits for tapping of late-stage differentiates from the underlying crystallizing plutonic section (Bloomer et al., 1989; Dick et al., 1992) or represent small magma bodies enclosed within the peridotites (Cannat et al., 1992; Mével et al., 1991). Such was evidently not the case for the Site 895 suite that was exposed by faulting during the early (amagmatic) phase of Hess Deep opening.

METAMORPHISM

Introduction

Variably altered harzburgite, dunite, troctolite, and gabbroic rocks recovered from Site 895 record metamorphism ranging from greenschist to zeolite facies conditions. Amphibolite facies mineral assemblages are uncommon and occur only in the rare basaltic rocks. Static metamorphism is the dominant process controlling background alteration. The intensity of this alteration within and between holes is heterogeneous, and no systematic variation in metamorphic mineral zones was observed.

Estimated volumes of secondary minerals in the ultramafic lithologies are at least 50%, with numerous intervals containing 90%–100% (Table 6). Alteration is dominated by serpentine after olivine, with lesser amounts of bastite, talc, magnetite, chlorite, brucite, clay, and trace antigorite. The dunites and harzburgites in Holes 895A–895D are less altered (50%–90%) than those in Hole 895E (>90%).

Troctolitic and gabbroic rocks are moderately to pervasively altered and commonly exhibit well-developed coronitic replacement of olivine and plagioclase. Secondary minerals include chrysotile, tremolite, and magnetite after olivine and prehnite, chlorite, zeolite ± hydrogrossular after plagioclase (Table 6). Though the modal abundance of the hydrous calcium aluminum silicates typically associated with rodingitization is generally low, all plagioclase-bearing samples contain at least minor amounts of these phases. This indicates limited, incipient rodingitization similar to that reported by Honnorez and Kirst (1975).

In the peridotites at Site 895, six types of macroscopic (≥ 0.01 mm wide) and microscopic veins crosscut the pervasive background mesh-textured serpentine (Table 7), but not all of them are seen in one given sample. The earliest veins are uncommon and occur only in the harzburgites. They consist of composite veins of tremolite, Mg-chlorite, possible antigorite, and magnetite. Chrysotile and magnetite veins represent the first veining event in the dunites and the second vein

generation in the harzburgites. These may be followed by serpentine + magnetite + chlorite veins. These veins are cut by subparallel white serpentine + magnetite ± clay ± brucite veinlets. A fourth generation of serpentine + clay ± zeolite veins occurs in the dunites of Hole 895E. Veins filled by aragonite ± chrysotile form the latest generation.

Veins are uncommon in the gabbroic rocks. They are typically monomineralic, discontinuous, and filled by amphibole, talc, chlorite, prehnite, and zeolite. Adjacent to these veins, plagioclase is altered to net-textured albite and clinopyroxene to actinolite. In basaltic rocks, rare brown amphibole forms crosscutting veinlets and replaces clinopyroxene in the wall rock.

The moderate to pervasive metamorphism and associated vein formation in ultramafic and mafic rocks recovered from Site 895 reflect extensive interaction with seawater-derived fluids at greenschist to zeolite facies conditions. The strong control of primary mineralogy on the spatial distribution of secondary minerals in the serpentinized peridotites suggests that fluid-rock interaction was rock dominated.

Static Metamorphism

Variably altered harzburgites, dunites, troctolites, gabbros, and basalts from Site 895 record static metamorphism under greenschist to zeolite facies conditions (Table 6). Mineral assemblages defining distinct metamorphic zones are absent, and alteration within and between holes is heterogeneous (Appendix B on CD-ROM; see Fig. 11 of “Explanatory Notes” chapter for example). All ultramafic lithologies drilled at Site 895 are affected by at least 50% background replacement of primary minerals, with numerous intervals displaying 90%–100% alteration. Plagioclase-bearing lithologies are typically less altered than the plagioclase-free ultramafic rocks.

Alteration of Primary Minerals in Harzburgites and Dunites

Static metamorphism dominates the background alteration of harzburgites and dunites. The extent of background alteration is governed by the serpentinization of olivine, which represents at least 80% of the rock by volume. The average range of alteration of the harzburgites varies from 50% to 80% in Holes 895A through 895D. However, the harzburgites from Hole 895E are more than 90% altered. The dunites are always strongly altered, containing between 80% and 100% secondary minerals in Holes 895A through 895D and more than 90% secondary minerals in Hole 895E.

Orthopyroxene

Orthopyroxene porphyroclasts vary widely in extent of alteration (30% to 100%). They are less altered in harzburgites than in dunites, but the extent to which they are altered depends on the presence or absence of vein networks (Fig. 10). Where veins are present, alteration is >80%; where absent, alteration is <50%. Orthopyroxene is replaced by tremolite, Mg-rich chlorite, talc, bastite, and magnetite. All these secondary minerals can be found within the different generations of veins that crosscut the peridotites (see “Veins in Harzburgites and Dunites” section, this chapter). Tremolite and chlorite occur as 0.5- to 2-mm patches located in the cores of the porphyroclasts, chlorite is colorless to pale green with a blue birefringence, bastite pseudomorphs the primary crystals, and talc occurs as thin rims along the orthopyroxene-olivine grain boundaries. The abundance of talc is directly linked to the modal abundance of orthopyroxene in harzburgites; therefore, it is particularly abundant in Hole 895D. Talc is not pervasive in the peridotites; its occurrence is spatially restricted to orthopyroxene grains (Fig. 11).

Olivine

Olivine is highly to pervasively altered (60% to 100%) to lizardite, magnetite (up to 5%), patches of chlorite (up to 5%), yellowish clays

Table 6. Summary of metamorphic characteristics at Site 895.

Lithology	Mineralogy		Vein types	Alteration intensity
	Primary	Secondary		
Dunite	Olivine	Chrysotile, antigorite ?, talc, clay, brucite, magnetite	(1) Serpentine + magnetite; (2) Serpentine + magnetite + chlorite; (3) Serpentine + magnetite ± brucite ± clay; (4) Aragonite	Greenschist to zeolite facies, 50%→90% altered
Harzburgite	Olivine	Chrysotile, antigorite ?, chlorite talc, clay, brucite, magnetite	(1) Tremolite + Mg-chlorite, + serpentine; (2) Serpentine + magnetite; (3) Serpentine + magnetite + chlorite; (4) Serpentine + magnetite + talc + clay (5) Aragonite	Greenschist to zeolite facies, slightly rodingitized, 60%-90% altered
	Orthopyroxene	Tremolite, Mg-rich chlorite, talc, bastite, magnetite		
	Clinopyroxene	Tremolite, pyrite, magnetite		
	Plagioclase	Chlorite		
Gabbroic Rocks	Olivine	Chrysotile, cummingtonite, tremolite, chlorite, mixed-layer clay/chlorite, talc, magnetite	Typically monomineralic: amphibole, talc, chlorite, prehnite, zeolite	Greenschist to zeolite facies, slightly rodingitized, 60%-90% altered
	Clinopyroxene	Pale brown amphibole, green amphibole, colorless amphibole, chlorite, secondary clinopyroxene, pyrite, magnetite		
	Orthopyroxene	Cummingtonite, tremolite, chlorite, magnetite		
	Plagioclase	Tremolite-actinolite, prehnite, chlorite, clay, secondary plagioclase, hydrogrossular, zeolite, epidote, calcite		
Basalt	Olivine	Clay?	Brown amphibole	Amphibolite to zeolite facies, 75%-80% altered
	Clinopyroxene	Brown amphibole, magnetite, green amphibole		
	Plagioclase	Clay, amphibole?		

that occur as patches in the cores of relict olivines (0.1–0.2 mm in diameter), and platy aggregates or micron-sized irregular overgrowths of brucite. This mineral assemblage forms a mesh texture typical of the static metamorphism that dominates the peridotites. Whereas brucite is scarce in harzburgites and its occurrence is restricted to olivine-rich zones, it may compose up to 5% of the total alteration of the dunites in Holes 895D and 895E. Brucite occurs as radiating fibers of prismatic crystals that are typically associated with trains of magnetite grains. The crystals, which can reach a size of 0.5 mm, are colorless with a honey-yellow birefringence commonly characterized by anomalous interference colors. Rare antigorite (0.03–0.07 mm) is characterized in thin section by a platy habit, gray to yellow birefringence, and a refringence slightly higher than for chrysotile and lizardite. It occurs mainly along the veins and was probably one of the earliest minerals to form during metamorphism. The pervasive alteration of olivine is linked to a dense, microscopic, mesh-like network of veins (0.01–0.05 mm in width) comprising serpentine, magnetite, and brucite (see “Veins in Harzburgites and Dunites” section, this chapter).

Where olivines are in contact with orthopyroxene grains altered to tremolite, radiating colorless acicular diopside may form thin

fringes (0.1–0.2 mm in width) replacing olivine crystals. The occurrence of this metamorphic reaction is discrete downhole.

Clinopyroxene

Clinopyroxene in harzburgites is commonly interstitial. Alteration is highly variable, ranging from <2% to 100%, and is dominated by colorless, fibrous tremolite. With increasing extent of clinopyroxene alteration, tremolite replacement textures change from being limited to clinopyroxene cleavages to occurring as pervasive patches independent of clinopyroxene structure or morphology.

Alteration of Primary Minerals in Troctolitic and Gabbroic Rocks

Variably altered and deformed troctolitic and gabbroic rocks recovered from Site 895 are moderately to pervasively altered and commonly exhibit well-developed coronitic replacement of olivine and plagioclase (Fig. 12). Static alteration dominates the background alteration, and overprinting of higher-temperature secondary minerals by lower-temperature phases is common. Secondary minerals

Table 7. Summary of vein types in rocks from Site 895.

Major minerals	Color	Width	Comments
Pervasive Serpentine + magnetite	Dark green to black	0.3 to 1 mm	Associated with pervasive background alteration of olivine to form mesh serpentine and bastite after orthopyroxene. Form straight to wavy individual sets of veins ($n < 10$) or branching networks ($n > 10$) defined by the alignment of fine-grained magnetite.
Discrete fracture-filling Tremolite + Mg-chlorite \pm serpentine	Dark green	5 μ m to 1 mm	Rare. Identified in thin section only. Restricted to harzburgitic lithologies. Cut early mesh serpentine texture.
Serpentine + magnetite	Diverse shades of green to blue	1 to 5 mm	In both dunitic and harzburgitic lithologies. Typically brittle variety, rarely platy or fibrous. Commonly crosscut by white irregular chrysotile \pm brucite \pm talc veinlets. Locally deformed and associated with alteration haloes.
Serpentine + magnetite \pm chlorite \pm clay	White	0.1 to 1 mm	In both dunitic and harzburgitic lithologies. Straight to wavy, discontinuous vein networks, commonly as subparallel or conjugate sets, steeply dipping.
Serpentine + magnetite \pm clay \pm brucite/talc	White	0.1 to 1 mm	In both dunitic and harzburgitic lithologies. Commonly as straight to wavy, discontinuous, subparallel vein sets, shallowly dipping. Locally brucite-dominated in dunites, talc-dominated in harzburgites. Represent second stage of pervasive serpentinization.
Serpentine \pm magnetite \pm clay \pm zeolite	White	0.3 to 1 mm	In dunitic lithologies, typically in Hole 895E. Straight to wavy, discontinuous, locally steeply dipping.
Aragonite	White	to 1.5 cm	Fills discrete, straight to wavy fractures and microfractures. Commonly forms radiating fibrous clusters on subparallel fracture surfaces, with local incipient brecciation. Associated with tremolite in discontinuous veinlets, patches, and as pseudomorphs after pyroxene.

typically include chrysotile, tremolite, and magnetite after olivine, and prehnite, chlorite, zeolite \pm hydrogrossular after plagioclase.

Olivine

Olivine alteration is highly variable, involving complex and heterogeneous coronitic replacement by chrysotile, cummingtonite, tremolite, chlorite, mixed-layer clay/chlorite, and, less commonly, talc. Mineral zonations are extremely well developed in troctolitic samples such as 147-895D-7R-1 (Piece 4, 14–30 cm) and 147-895D-8R-2 (Piece 4, 31–41 cm) (Fig. 12). Replacement is typically moderate to pervasive, although several samples contain up to 90% relict olivine (e.g., Sample 147-895D-7R-2, Piece 9, 70–75 cm). Fine-grained magnetite is abundant along crosscutting microfractures, as are healed microfractures defined by arrays of fine-grained silicate inclusions. Olivine grain boundaries are commonly embayed and rimmed by radiating sprays and aggregates of well-developed tremolite and, less commonly, coarse-grained cummingtonite. Tremolite-rich patches may be locally intergrown with, or enclose, talc and/or chlorite with anomalous blue interference colors. Pods of olive-green to green-yellow mixed-layer clay/chlorite with abundant fine-grained oxides are rare. Irregularly shaped fibrous aggregates of tremolite completely pseudomorph olivine in the most pervasively altered samples. In Sample 147-895D-8R-2 (Piece 4, 35–38 cm) tremolite-dominated patches are rimmed by thin bands (0.7 mm wide) of oxide-rich clinopyroxene that define podiform coronas and that are bounded by translucent chlorite and plagioclase (Fig. 12).

In troctolitic samples such as those found in Section 147-895D-7R-1, clusters of optically continuous olivine kernels are rimmed by serpentine and oxide-rich veins. These clusters exhibit well-developed corona structures, which, from the core outward, involve variable amounts of very fine-grained turbid tremolite and chlorite. Chlorite-rich bands between olivine and plagioclase are zoned with chlorite adjacent to tremolite, commonly exhibiting anomalous blue birefringence, and chlorite next to plagioclase displaying first-order gray birefringence.

Plagioclase

Plagioclase alteration is typically patchy and highly variable, ranging from <10% to 100% and involves the formation of tremolite-

actinolite, prehnite, chlorite, clay, secondary plagioclase, hydrogrossular, zeolite, and trace epidote and calcite. Strongly altered interstitial plagioclase is commonly rimmed by chlorite or serpentine and fibrous tremolite, which rims adjacent olivine (Sample 147-895D-7R-1, Piece 11, 71–74; Fig. 13). In highly altered zones, plagioclase is typically turbid and dusty due to abundant fine-grained fibrous tremolite(?) and poorly developed inclusions of prehnite with clay and zeolite. X-ray diffraction determinations were carried out on the altered plagioclase domains, as the fine grain size makes optical identification of the secondary minerals difficult. The results indicate that milky white, altered plagioclase grains consist primarily of chlorite, Na-Ca zeolites (thomsonite and natrolite?), diopsidic clinopyroxene, and hydrous garnet (a Ca-Fe³⁺ variety), with minor kaolinite (Fig. 14). Tremolitic amphibole was also identified by X-ray diffraction in more translucent white, altered plagioclase domains, and prehnite was identified in thin section. Secondary plagioclase forms irregular microveinlets and bands that crosscut and rim primary plagioclase and that rarely form well-developed crosscutting veins in the gabbros.

Locally, in extensively altered patches, secondary plagioclase contains abundant anhedral liquid-dominated fluid inclusions (<5 to 25 μ m in size). Cogenetic liquid and vapor-dominated secondary inclusions, which occur along healed microfractures in Sample 147-895D-7R-2 (Piece 9, 70–75 cm), may be immiscible H₂O-CH₄-bearing fluids similar to those in 735B gabbroic rocks (Kelley and Frantz, unpubl. data). Formation of prehnite and tremolite after plagioclase is much more common than that observed at Site 894, with a corresponding reduction in replacement by secondary plagioclase. Coarse-grained fibrous sprays of tremolite are rare; however, very fine-grained “dusty” tremolite commonly rims grain boundaries and more rarely occurs as anastomosing veinlets. Trace epidote forms fine-grained granular grains that may preferentially replace cleavage planes. Locally, plagioclase is replaced by very fine-grained, high relief granular crystals (“fish roe”), which may be the hydrogrossular garnet identified by X-ray diffraction.

Clinopyroxene

Clinopyroxene exhibits a variety of textures in the troctolitic and gabbroic lithologies of Site 895, including fine-grained coronas between plagioclase and olivine crystals, fine- to medium-grained intergranular anhedral grains, and coarse-grained pegmatitic diallage

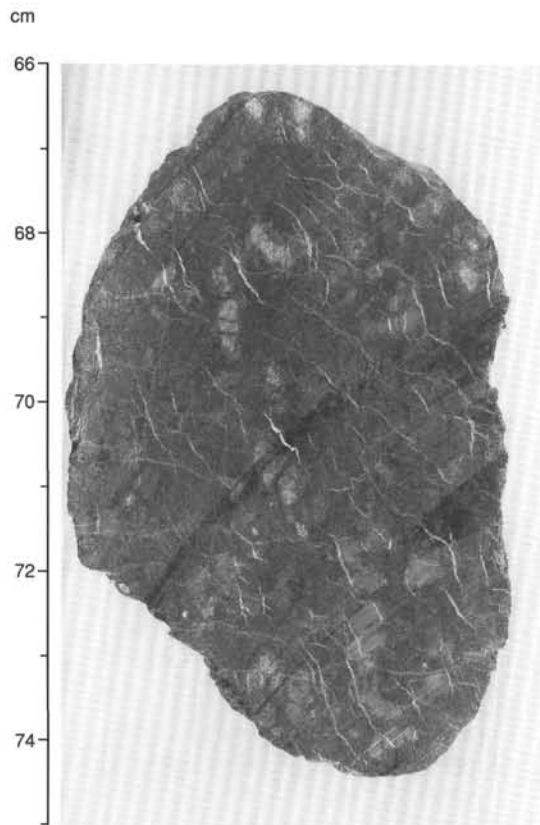


Figure 10. Photograph showing harzburgite alteration. Bastite textures after orthopyroxene are well developed in the portion of the sample between 70 and 74 cm (Sample 147-895D-8R-2, Piece 8, 66–75 cm).

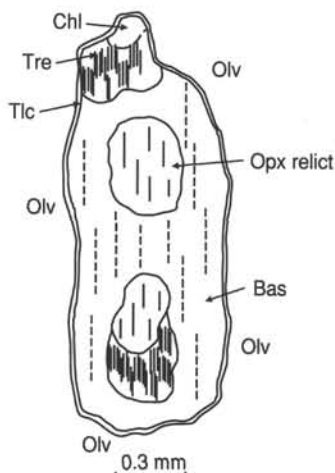


Figure 11. Schematic sketch of orthopyroxene alteration in harzburgites in Holes 895D and 895E. The sketch shows a porphyroblast of orthopyroxene (Opx) surrounded by olivine (Olv), replaced by patches of tremolite (Tre) and bastite (Bas), and rimmed by a micron-size crown of talc (Tlc).

crystals. Alteration of the coronitic and intergranular clinopyroxenes is minor. In Sample 147-895D-8R-2 (Piece 4, 35–38 cm), secondary clinopyroxene and pale brown amphibole locally replace intergranular grains, but the principal secondary phase is minor pale green amphibole. In many cases, abundant fine-grained magnetite is concentrated at the margins of coronas and may indicate incipient or submicroscopic alteration.

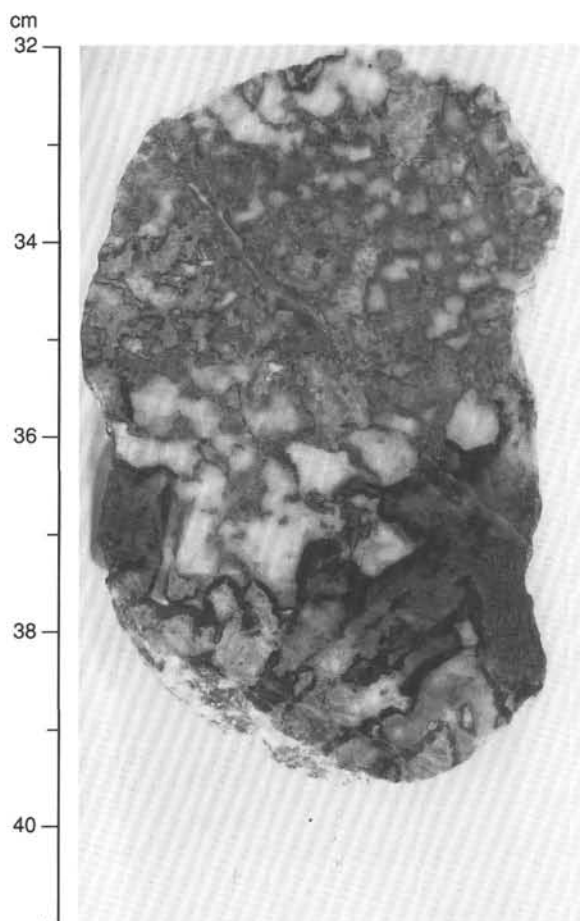


Figure 12. Photograph showing textures of olivine alteration in troctolites (Sample 147-895D-8R-2, Piece 4, 32–41 cm).

Samples 147-895E-4R-3 (Piece 1, 4–8 cm) and 147-895D-7R-1 (Piece 4, 23–27 cm), contain pegmatitic (up to 10 cm long) first-order birefringent clinopyroxene with classic diallage morphology (Fig. 15). The crystals exhibit {100} partings that are turbid and dusty due to abundant fine-grained inclusions. Grains exhibit sigmoidal deformation zones (0.6 mm wide) defined by bent diopside with second-order birefringence, undulose and wavy extinction, and partial replacement by colorless tremolitic(?) clinoamphibole and chlorite-rich pods. Grains are fragmented and cut by abundant subparallel microveinlets and veinlets of prehnite ± epidote, which contain diopside selvages, and, more rarely, colorless chlorite. Veining predates deformation of diopside as veins are offset in deformation zones. Grain boundaries are commonly embayed and rimmed by very fine-grained low birefringent amphibole(?) and radiating sprays of tremolite-actinolite, but may also be sharp. Diopside exhibiting second-order birefringence contains bleb-shaped exsolution lamellae replaced by very fine-grained, colorless fibrous amphibole. Patches of clear diopside, which occur in cores of grains and adjacent to veins, contain abundant vapor-dominated secondary and primary fluid inclusions.

The origin of the large diallage crystals is uncertain. Though there appears to be a general textural continuum between finer-grained clinopyroxenes that are clearly of magmatic origin, the exceptional grain size and high potential for calcium metasomatism of the gabbroic rocks suggest that a secondary origin cannot be ruled out.

Orthopyroxene

Orthopyroxenes exhibit slight to high degrees of alteration, predominantly due to variable replacement by cummingtonite, tremolite,

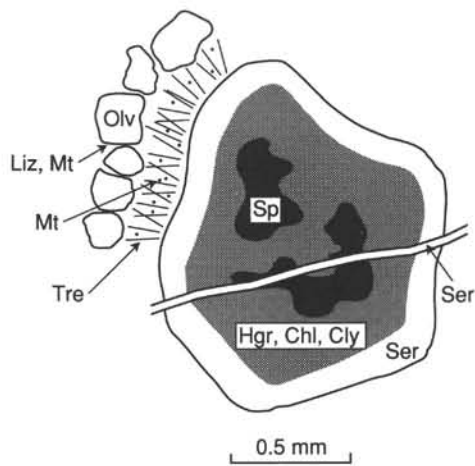


Figure 13. Sketch of plagioclase alteration from a thin section of Sample 147-895D-7R-1 (Piece 11, 71–74 cm). The interstitial plagioclase enclosing the spinel (Sp) is altered to a fine-grained mixture of hydrogrossular (Hgr), chlorite (Chl), and clays (Cly). Plagioclase develops a first crown of serpentine (Ser) and a second one of fibrous tremolite (Tre) at the contact with partly serpentinized olivines (Olv). Liz = lizardite, Mt = magnetite.

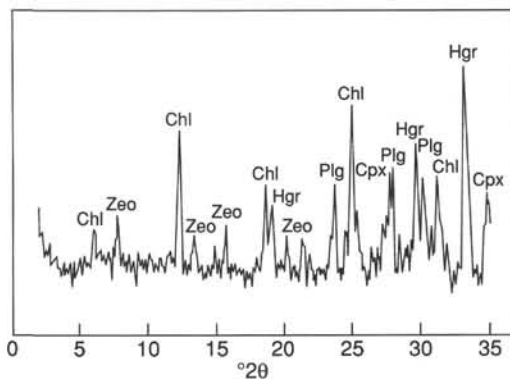


Figure 14. X-ray diffraction pattern of milky white alteration minerals after plagioclase, in gabbroic Sample 147-895D-10W-1, 53–54 cm. Cpx = clinopyroxene, Chl = chlorite, Hgr = hydrogrossular, Zeo = zeolite, Plg = plagioclase.

and fine-grained oxides. Irregular and embayed grain boundaries are common, as are crosscutting microfractures and schiller structures. Cummingtonite is commonly fine-grained, forming subradiating aggregates that rim grain boundaries and microveinlets, and is rarely associated with talc. Where orthopyroxenes are bounded by plagioclase, fine-grained tremolite and cummingtonite may be intergrown and rimmed by anomalous blue to olive-green birefringent chlorite. Microveinlets of chlorite cut some grains.

Oxide and Sulfide Minerals in the Ultramafic and Gabbroic Rocks

Oxide Minerals

Magnetite forms the most common secondary oxide, occurring as an alteration product of spinel and olivine, and is typically associated with serpentine. Rare, patchy magnetite completely replaces spinel and contains radiating bundles of needle-shaped crystals with low reflectance. In highly altered samples, non-pitted magnetite forms an overgrowth on spinel grains, giving the spinel a ragged outline. In some grains these overgrowths are euhedral and are similar in appearance to euhedral magnetite crystals commonly associated with serpentine. Magnetite is most abundant as fine-grained crystals produced

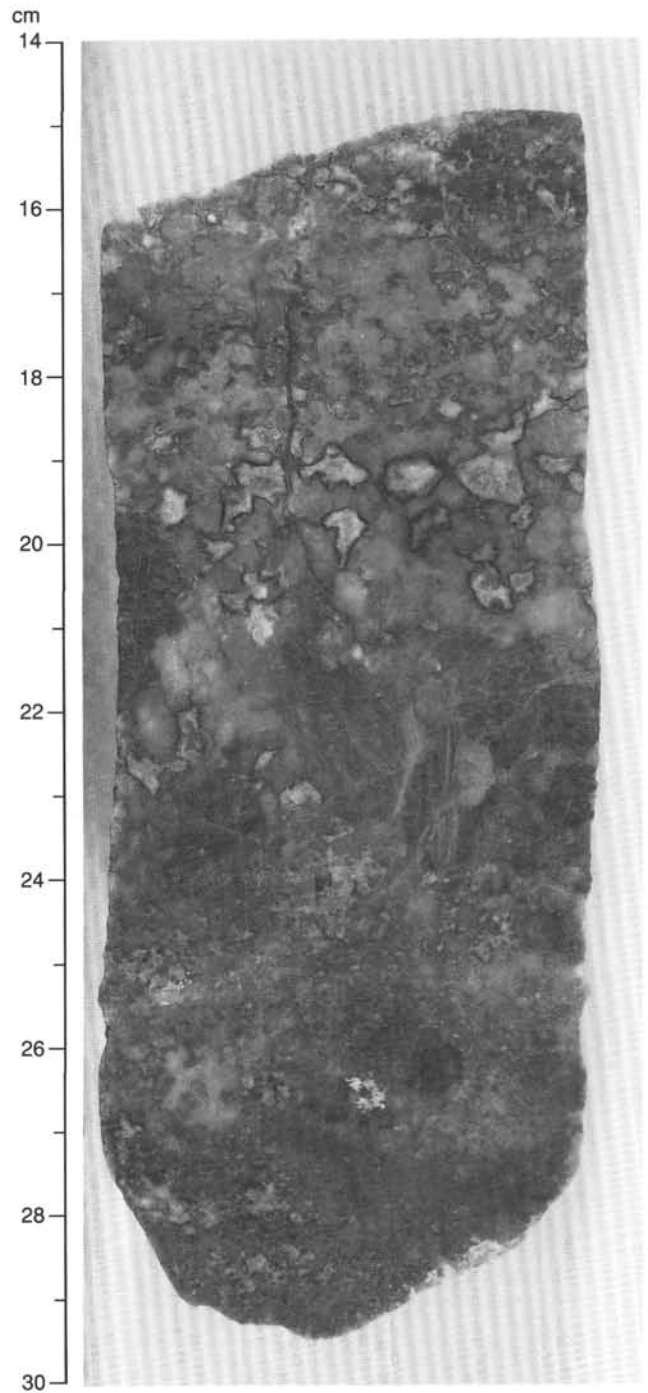


Figure 15. Photograph of olivine gabbro showing large clinopyroxenes with diallage texture (Sample 147-895D-7R-1, Piece 4, 14–30 cm).

during alteration of olivine and is ubiquitous throughout the ultramafic suite. Magnetite characteristically forms elongate stringers that form a network surrounding partially or wholly serpentinized olivine grains; magnetite abundance is greatest where the network rims are adjacent to olivine grains. In highly serpentinized samples and in veins, irregular magnetite stringers are joined by euhedral crystals of magnetite, which commonly are hexagonal in shape.

Spinel

Alteration of spinel is most intense where serpentinization is greatest. In some spinel grains, reflectivities may indicate the pres-

ence of magnetite and ferritchromit. In many crystals, a bright rim of alteration occurs on spinel grain boundaries, and a lower reflectance mineral, typically with a pitted surface, occurs as patches within this rim. In the harzburgites, Cr-spinel is moderately altered (10% to 30%), whereas it is moderately to pervasively altered in the dunites (30%–100%). Black, spongy, iron-rich spinel defines irregular overgrowths on preserved cores of red-brownish Cr-spinel. Magnetite overgrowths on secondary spinel are in contact with serpentinized or chloritized olivine. Microscopic cracks in spinel are filled by brucite or chlorite. In dunites recovered from Hole 895E, spinel may be completely replaced by patches of chlorite, and aligned magnetite grains pseudomorph the anhedral spinel grain boundaries. Fibrous crystals of Mg-rich chlorite (0.05–0.1 mm) are commonly associated with the altered spinels.

Secondary Sulfide Minerals in Ultramafic and Mafic Rocks

Sulfide minerals occur in all ultramafic and gabbroic lithologies recovered from Site 895 (Table 8). Sulfide mineral abundance varies among Holes 895A through 895F with generally more sulfide in samples from Hole 895D. Sulfide minerals in harzburgite from Hole 895D are commonly accompanied by native copper.

Numerous sulfide minerals occur as secondary phases and are commonly associated with alteration products after clinopyroxene and in veins. Pentlandite and lesser pyrite are enclosed and divided by laths of magnetite and form the most common sulfide mineral assemblage. These clusters are rounded or elongate in shape, and the sulfides commonly are entirely surrounded by magnetite, which exhibits a slight purple hue. The composite grains typically occur within magnetite stringers or at triple junctions of the magnetite network associated with alteration of olivine. In some samples, pentlandite-pyrite-magnetite clusters are accompanied by copper minerals, which include native copper, chalcocite, covellite, and bornite. Native copper typically forms irregular stringers around sulfides and rarely is symplectically intergrown with chalcocite. Pentlandite alters locally to violarite, and bornite occurs as exsolution lamellae in pentlandite. Finer-grained, isolated euhedral pyrite is dispersed throughout the rocks and is especially common in serpentine veins.

Highly altered gabbroic rocks are typically barren of sulfide minerals but may contain pyrite intergrown with fibrous tremolite; chalcopryrite is rare.

Alteration of Basaltic Dikes

Fine-grained basaltic rocks recovered at Site 895 are highly to pervasively altered. Grain boundaries are diffuse and relict primary grains are turbid. Subhedral to euhedral pseudomorphs of equant phenocrysts are composed of fine-grained amorphous to fibrous low-birefringent minerals (clays?), which probably represent original olivine crystals. Similar secondary minerals replacing finer-grained anhedral patches suggest that olivine was also a groundmass phase.

Clinopyroxene is replaced by pale brown to pinkish amphibole and fine-grained anhedral magnetite. This assemblage is rimmed by green amphibole. The extent of clinopyroxene replacement is variable. For example, near a 0.6-mm-wide brown amphibole vein in Sample 147-895D-2R-1 (Piece 4, 17–19 cm), clinopyroxene is completely replaced by brown amphibole and magnetite; elsewhere in this sample, alteration only occurs at grain margins.

Plagioclase is pervasively altered to clay(?) and is turbid and dusty due to abundant fine-grained inclusions. Grain boundaries are irregular and diffuse because of alteration; however, relict twinning is locally present.

Groundmass minerals are completely replaced by fine-grained aggregates and radiating sprays of fibrous, low-birefringence minerals (amphibole?) and flakes and sheaves of colorless chlorite that form interlocking aggregates. The low-birefringence amphibole(?) forms

Table 8. Summary of secondary sulfide minerals and their characteristics.

Mineral	Characteristics
Pentlandite	Pale brown with blocky cleavage.
Violarite	As an alteration product of pentlandite. Preserves common texture of pentlandite, but is darker brown in color.
Pyrite	Isotropic and pale yellow, appearing bright next to pentlandite, but with a lower relief and smoother surface. Commonly forms euhedral isolated crystals in veins.
Copper	Native copper is pale pink in color and forms stringers.
Chalcocite	Pale blue-gray in color and commonly forms adjacent to native copper.
Covellite	Bright blue in color and rims pentlandite.
Bornite	Reddish brown in color and tarnishes to a purple color.

rounded pods that are locally rimmed by coarser-grained brown amphibole. Plagioclase in the groundmass is completely replaced by extremely fine-grained, low-birefringence minerals. Groundmass clinopyroxene is relatively fresh.

Sheared, Fine-grained Metagabbroic Rocks

Several fine-grained, gray to white sheared zones bounded by serpentinized dunite were observed in cores recovered from Site 895 (Samples 147-895C-4R-1, Piece 7; 147-895D-8R-2, Piece 19; and 147-895E-8R-4, Piece 9; see Fig. 16). Because they locally contain indistinct metamorphosed shear polyhedra with internal textures similar to the finer-grained troctolites and gabbros, these zones were interpreted as sheared dikelets of these lithologies. Their whitish color and fine grain size are similar to rodingites observed in the ultramafic portions of many ophiolites; however, X-ray diffraction results on Sample 147-895D-8R-2 (Piece 19, 146–147 cm) yielded peaks for chlorite and calcic amphibole only (Fig. 17). Thus, these zones are not regions of metasomatic replacement by calc-silicate assemblages that are typical of rodingites, but rather gabbroic rocks that have been more extensively metamorphosed to the same mineral assemblage that characterizes the static metamorphism of these lithologies.

Veins and Associated Alteration

Macroscopic veins are a common feature in the peridotites at Site 895. Identification of fine-grained vein fillings was facilitated by shipboard X-ray diffraction studies on air-dried samples cut or scraped from representative veins. In the following sections, we discuss the characteristic features of veins in the harzburgites, dunites, and gabbroic lithologies at Site 895.

Veins in Harzburgites and Dunites

The heterogeneous background alteration of olivine to serpentine and bastite after orthopyroxene in the peridotites at Site 895 is typically associated with pervasive anastomosing networks of dark green to black, 0.3- to 1-mm-wide serpentine + magnetite veins and veinlets that form a characteristic mesh serpentine texture. The vein networks are defined by the alignment of fine-grained magnetite along precursor olivine grain boundaries or lining microfractures to form individual or sets of subparallel veins. Multiple generations of discrete fracture fillings with varying mineralogies, sizes, colors, and morphologies crosscut mesh-textured serpentine. Although crosscutting relationships are commonly ambiguous, six types of veins are distinguished, many of which occur on both macroscopic (≥ 0.01 mm wide) and microscopic scales (Table 7). Mineralogical variations of the fracture-filling phases are observed on a grain-size scale within one lithology and as a function of host-rock lithology. The multiple

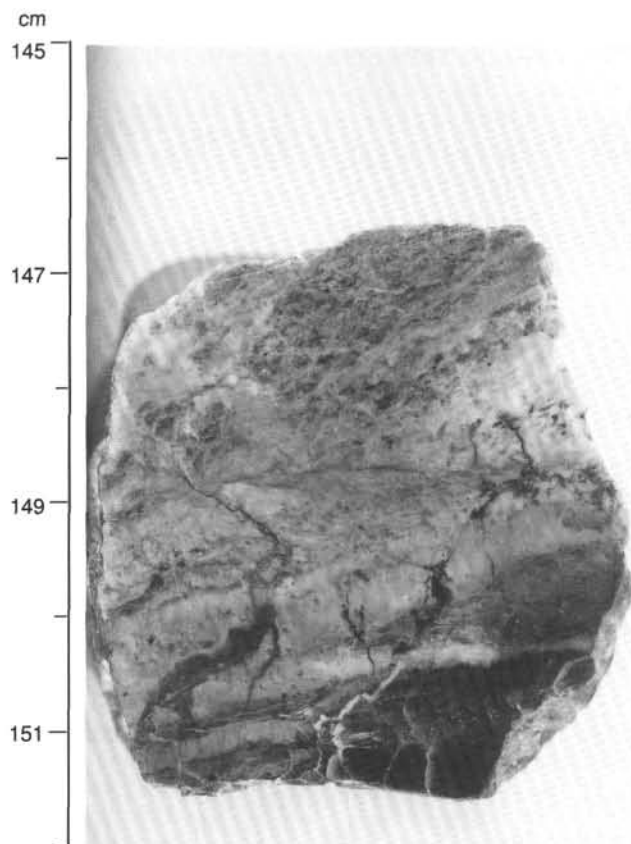


Figure 16. Photograph of sheared metagabbro (Sample 147-895D-8R-2, Piece 19, 145–151 cm).

generations of veins show varying deformation textures, such as kink bands, weak crenulations, undulatory extinction, as well as pull-apart and en echelon, sigmoidal-shaped structures.

Tremolite + Mg-chlorite ± Serpentine Veins

Rare veins of tremolite and Mg-chlorite with minor serpentine (antigorite?) and magnetite, identified in thin section, represent the earliest fracture-filling assemblages in the harzburgitic lithologies. The tremolite-bearing veins are 5 μm to 0.3 mm wide and are locally composite in nature, lining microfracture surfaces with colorless, anomalous blue birefringent Mg-chlorite and serpentine (predominantly chrysotile) in the cores. Monomineralic tremolite veins are typically magnetite-poor and occur locally as isolated microscopic veinlets cutting orthopyroxene. Early chlorite-dominant veins are associated with very fine-grained dusty magnetite grains lining vein walls. The optical properties of chlorite in these veins indicate that it is Fe-rich.

Serpentine ± Magnetite Veins

In general, fractures filled with green to bluish-green serpentine ± magnetite postdate the harzburgite-hosted tremolite-chlorite veins and represent the first veining event in the dunites. Brittle serpentine (chrysotile?) typically forms steeply dipping, straight to slightly wavy individual veins, or more rarely, sets of subparallel veins, 1 mm to 5 mm wide. The veins are commonly deformed and are locally faulted or have incipient brecciation. Deformation of these blue-green serpentine veins is most common in dunitic lithologies of Hole 895E. These veins are distinct in that they are cut nearly perpendicularly by thin (0.1

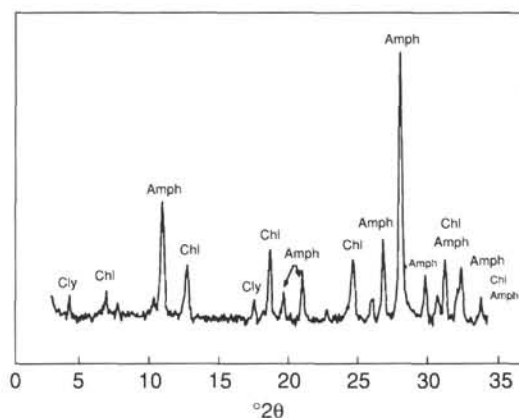


Figure 17. X-ray diffraction pattern of light greenish-gray material from sheared metagabbro, Sample 147-895D-8R-2 (Piece 19, 146–147 cm). Amph = amphibole, Chl = chlorite, Cly = clay.

to 1 mm wide) white, wavy, discontinuous veins with variable fillings of serpentine ± clay ± brucite (discussed in more detail in the following section; Fig. 18). The crosscutting veins occur as subparallel arrays along the vertical axes of the brittle serpentine, giving a characteristic “zipper-like” appearance. An example of X-ray diffraction patterns of the late crosscutting veins is shown in Figure 19A.

In thin section, the thick chrysotile veins may show a zonal distribution of grain sizes and/or composite mineralogies. For example, some veins have fine-grained, gray birefringent serpentine (most likely chrysotile) in the centers and coarser-grained, blocky serpentine (possibly antigorite) and fine-grained magnetite along the rims. The degree of wall-rock alteration is variable, but is generally characterized by more extensive serpentinization of olivine, local patches of chlorite, and yellow-brown clay. Chrysotile in the veins commonly shows undulating extinction and, in rarer cases, has crack-seal textures. A well-developed crack-seal vein occurs in Sample 147-895D-4R-2 (Piece 18, 126–129 cm). It is characterized by kink banding of the fibrous serpentine and contains acicular crystals of secondary diopside that grew during a second stage of opening perpendicular to the primary phase (Fig. 20).

Serpentine + Magnetite ± Chlorite Veins

An additional type of serpentine vein forms steeply dipping, straight to wavy, discontinuous white individual veins or vein networks (0.1 to 1 mm wide) with conjugate or subparallel sets. These occur in both harzburgites and dunites and are particularly well developed in Hole 895E. The serpentine is commonly fibrous, gray birefringent serpentine and may occur with fine-grained rims of magnetite along vein walls or in vein centers. X-ray diffraction studies confirm the presence of chrysotile as the principal serpentine polymorph in these veins.

Serpentine ± Magnetite ± Brucite/Talc ± Clay Veins

Thin irregular veins that crosscut the green to blue chrysotile veins, forming the “zipper” appearance, are a third and relatively abundant set of discrete, subparallel, white fracture-fillings that typically have variable mineralogies. These veins are composed of varying proportions of serpentine, brucite or talc, clay, and magnetite, which form shallowly dipping, straight to wavy, discontinuous vein sets (Fig. 10). The veins are 0.1 to 1 mm wide and may have composite mineralogies. For example, in Sample 147-895E-1R-2 (Piece 18B, 110–114 cm) fine-grained dusty magnetite grains line vein walls, followed by brucite, serpentine, and clay in the centers (Fig. 21).

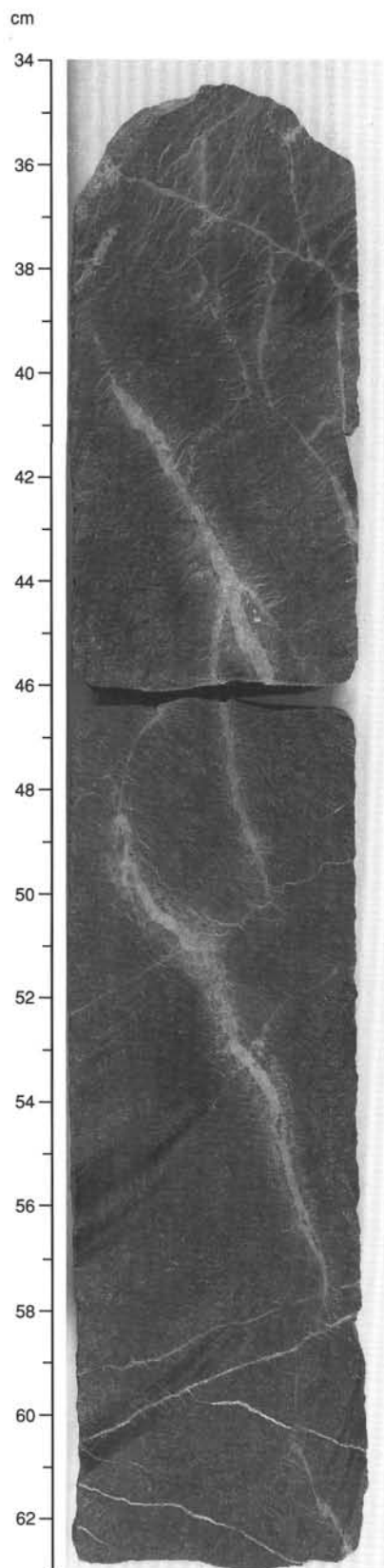


Figure 18. Photograph of crosscutting vein relations in dunite (Sample 147-895E-6R-4, Pieces 2A and 2B, 34–63 cm). Early wide chrysotile veins are crosscut by thin, subparallel brucite veins. From 58–63 cm, straight conjugate serpentine veins cut the wider chrysotile veins and in turn are cut by wavy discontinuous brucite veins.

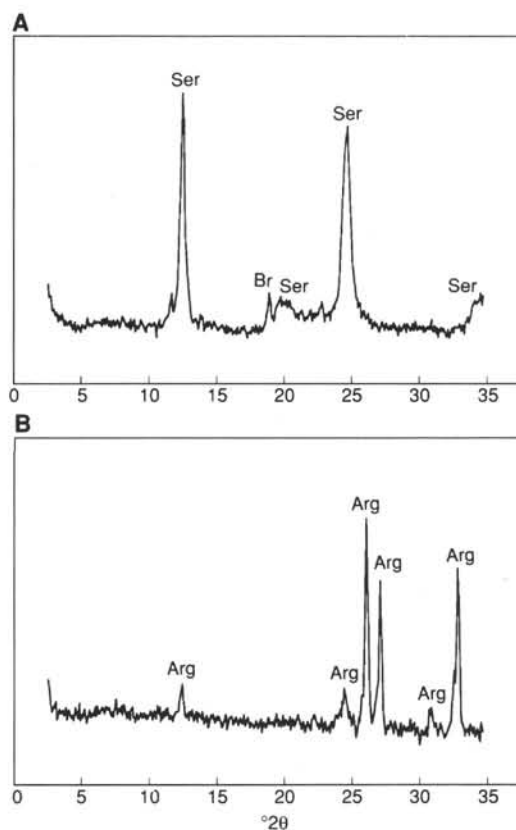


Figure 19. Representative X-ray diffraction patterns of vein material in porphyritic harzburgites from Site 895. A. Sample from thin white wavy veins crosscutting brittle serpentine, giving a characteristic scar- or zipper-like appearance (Sample 147-895D-4R-2, 48–49 cm). B. Sample from late-stage aragonite vein along fracture surface (Sample 147-895D-4R-4, 97–98 cm). Arg = aragonite, Br = brucite, Ser = serpentine.

Brucite and talc never coexist in the same vein. Brucite-rich assemblages, commonly occurring in pull-apart veins, are restricted to dunites or olivine-rich intervals in the harzburgites. Discontinuous veins of talc are limited to the harzburgites and typically form adjacent to, or crosscutting, orthopyroxene. This phase of veining represents a second phase of pervasive serpentinization, resulting in 90%–95% alteration of the dunites in Holes 895D and 895E.

Serpentine ± Magnetite ± Clay ± Zeolite Veins

In the dunites of Hole 895E, a late-stage vein event cuts the more pervasive serpentine-brucite vein sets. Serpentine ± magnetite ± clay ± zeolites fill straight to wavy, locally steeply dipping, discontinuous veins.

Aragonite Veins

Carbonate veins are composed of aragonite (confirmed by X-ray diffractometry; Fig. 19B), which fills discrete, straight to wavy fractures and commonly forms radiating fibrous clusters on subparallel fracture surfaces. Incipient brecciation of the serpentinized wall rock, with millimeter- to centimeter-sized clasts incorporated in the carbonate matrix, commonly occurs along the fracture surfaces. The carbonate veins are associated with discontinuous, 0.1- to 1-mm-wide, branching and an echelon microfractures that are filled with aragonite ± clay and crosscut or parallel the early generations of serpentine veins. Locally, aragonite veining is coeval with the formation of tremolite in discontinuous veinlets, patches, and as pseudomorphs after pyroxene. In dunitic lithologies, aragonite veins may be associated with a 2- to

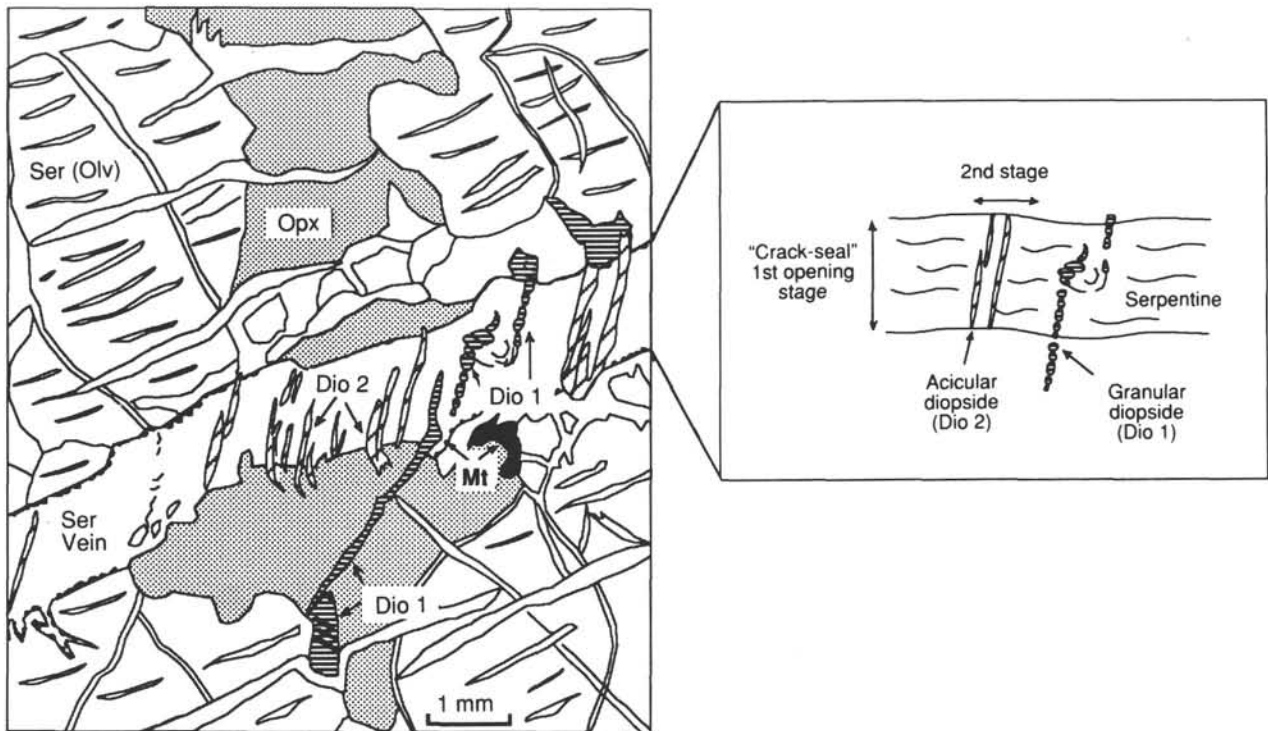


Figure 20. Thin-section sketch of harzburgite Sample 147-895D-4R-2 (Piece 18, 126–129 cm), with primary olivine grains (Olv) completely altered to serpentine + magnetite ± clays, relict primary clinopyroxene (Dio 1), and orthopyroxene porphyroclasts (Opx), moderately altered to bastite. The sample is cut by multiple generations of serpentine ± clay veinlets with a major crack-seal fibrous serpentine vein in the center. Enlarged sketch of crack-seal vein shows a first stage of opening, which disaggregates a primary diopside grain. A discrete but perpendicular stage of opening is marked by the crystallization of acicular secondary diopside (Dio 2). Ser = serpentine, Mt = magnetite.

5-mm-wide, discontinuous alteration halo characterized by a concentration of micron to submicron-sized aggregates of magnetite in the cores of relict olivine grains. Clusters of euhedral radiating crystals indicate that the aragonite grew in open cracks (Fig. 22).

Veins in Gabbroic Rocks

Veins in gabbroic rocks are thin (<0.5 mm), discontinuous, and typically monomineralic. Sample 147-895D-8R-2 (Piece 4, 35–38 cm) is cut by veins filled by green amphibole, talc, chlorite, and prehnite. The green amphibole veins in plagioclase are cut by chlorite alteration of plagioclase in the wall rock, indicating that the veins may predate the static background alteration. Coarse-grained gabbros are cut by monomineralic prehnite and zeolite veins (e.g., Sample 147-895D-7R-1, Piece 4, 23–27 cm). Wall-rock alteration near these veins includes alteration of plagioclase to net-textured albite and clinopyroxene to actinolite. Colorless, high-relief, inclusion-rich clinopyroxenes occur in both prehnite and zeolite veins where large clinopyroxenes are cut. These grains may represent either brecciated and replaced wall-rock clinopyroxene or authigenic crystals. Similar clinopyroxene occurrences have been noted in prehnite-rich veins and metasomatic zones in dikes in East Greenland (Rose and Bird, 1987; Rose, 1989).

Veins in Basaltic Dikes

Veins in the basaltic dikes were not visible macroscopically, but shipboard petrography revealed a variety of microscopic vein types. Sample 147-895D-2R-1 (Piece 4, 17–19 cm) is cut by a discontinuous 0.6-mm-wide monomineralic brown amphibole vein. The optical properties of the amphibole in the vein are identical to those of the amphibole-replacing clinopyroxene in the wall rock. Alteration of clinopyroxene in the diabase is more extensive near this vein.

Sample 147-895C-4R-3 (Piece 6, 60–64 cm) is cut by sets of subparallel, discontinuous, 0.1- to 1-mm-wide colorless chlorite veins. Several of these veins contain tabular, subhedral to anhedral titanite grains, which locally occur where the veins cut wall-rock oxides.

Fluid Inclusions

Fluid inclusions in gabbroic and basalt samples recovered at Site 895 commonly occur along anastomosing arrays of healed microfractures in matrix minerals. Less commonly, they occur in alteration mineral phases as primary inclusions trapped during crystal growth. In vein minerals, primary and secondary inclusions are rare, probably because minerals such as tremolite, chlorite, and prehnite rarely trap inclusions. Based on petrographic analyses at room temperature, the inclusions were classified into two main types.

Type 1: Liquid-dominated, Daughter Mineral-absent Inclusions

Type 1 inclusions are liquid-dominated, are pervasive in primary and secondary plagioclase, and are less common in secondary amphibole and clinopyroxene. Inclusion sizes are widely variable, ranging from <1 μm to 23 μm . The liquid-dominated inclusions occur as two subtypes. Type 1a are liquid-dominated inclusions that exhibit subhedral to anhedral habits, contain a small aqueous liquid-rimmed vapor bubble (<50 vol%), and commonly form anastomosing cross-cutting arrays along healed microfractures. Type 1a inclusions are most commonly secondary in nature; however, concentrated zones of irregularly shaped, ragged inclusions that occur in highly altered patches of plagioclase, and ubiquitous inclusions in plagioclase and clinopyroxene that exhibit subparallel to parallel alignment may be primary in origin. It should be noted that, as with inclusions in gabbroic rocks from Site 894, textural evidence for primary origin is

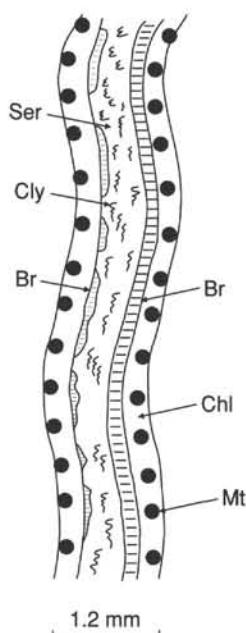


Figure 21. Sketch of macroscopic composite vein in serpentinized dunite, filled with magnetite (Mt), chlorite (Chl), brucite (Br), and serpentine (Ser) plus clays (Cly) (Sample 147-895E-1R-2, Piece 18B, 110–114 cm).

not conclusive. However, Type 1b inclusions, which are plagioclase hosted (e.g., troctolite Sample 147-895D-7R-2, 70–75 cm), occur as anastomosing arrays along healed microfractures, contain a vapor bubble comprising less than ≈ 20 vol% of the inclusion, and, along individual microfractures, are associated with inclusions that are completely vapor filled. These inclusions are similar in appearance to plagioclase-hosted inclusions in gabbros recovered from Site 735B in which immiscible liquid-dominated H_2O -rich and vapor-dominated CH_4 -rich inclusions are cogenetic (Kelley and Frantz, unpubl. data). It is probable that inclusions in the rocks from Hess Deep are similar, but further constraints await the results of shore-based raman spectrometric and microthermometric analyses.

Type 2: Vapor-dominated, Daughter Mineral-absent Inclusions

Vapor-dominated inclusions only occur in troctolite Sample 147-895D-7R-2, 70–75 cm, where they are moderately abundant as secondary inclusions in plagioclase. Individual inclusion arrays may contain solely vapor-dominated secondary inclusions; however, many arrays exhibit a bimodal distribution of vapor abundance ranging from completely vapor-filled to liquid-dominated inclusions.

Discussion

The variably altered peridotites recovered from Site 895 contain metamorphic mineral assemblages that reflect progressive hydration of peridotite under greenschist to zeolite facies conditions (see Table 6). Alteration is dominated by serpentine after olivine with lesser amounts of bastite, talc, magnetite, chlorite, brucite, tremolite, clay, and rare antigorite. The earliest metamorphic minerals include tremolite, antigorite, and secondary diopside in harzburgite, which suggests at least greenschist facies conditions. Fluid infiltration associated with the high-temperature event is restricted to (1) alteration of orthopyroxene to tremolite, (2) coronitic reactions along tremolite-orthopyroxene grain boundaries to form secondary diopside, and (3) rare macroscopic veins rimmed by antigorite. This paragenesis indicates that the early aqueous fluids were calcium-rich.

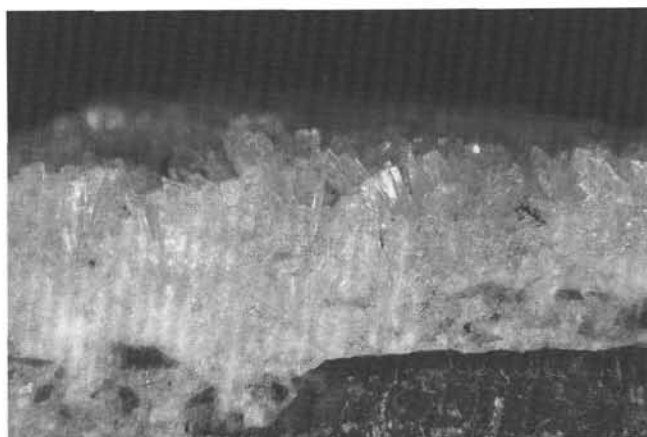
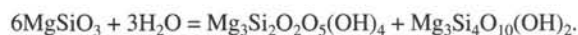


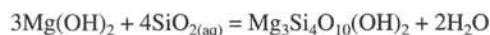
Figure 22. Photograph of aragonite vein in serpentinized harzburgite, with serpentine clasts and acicular to tabular elongate aragonite sprays (Sample 147-895D-4R-4, Piece 2A, 5–14 cm).

Later metamorphic phases in the peridotites include chrysotile, lizardite, magnetite, talc, chlorite, brucite, clays, and locally tremolite. The alteration phases and degree of serpentinization are mainly dependent on the protolith composition and extent of veining. The serpentinization products predominantly reflect hydration of olivine and orthopyroxene. The assemblage serpentine + brucite + magnetite tends to be restricted to dunitic lithologies, whereas the assemblage talc + serpentine \pm magnetite is chiefly associated with the presence of orthopyroxene. This assemblage may be described by the reaction:



enstatite serpentine talc

Brucite and talc never co-exist at a microscopic scale, but may locally be present in an individual sample of harzburgite. The reaction:



brucite talc

implies that the distribution of brucite and talc requires small-scale gradients in the activity of aqueous silica in the serpentinizing fluids. In general, the occurrence of secondary minerals in the peridotites from Site 895 is strongly governed by the distribution and geometry of primary phases. This suggests that fluid-rock interaction was dominated by diffusion of a Mg-rich fluid with varying silica activity depending on the proportion of olivine relative to orthopyroxene in the protolith.

The moderate to pervasive metamorphism and associated generations of vein formation in the ultramafic rocks reflect multiple phases of fracturing and extensive interaction with seawater-derived fluids during successive hydrothermal pulses. Temperatures of interaction are difficult to estimate due to the absence of mineral assemblages that define distinct metamorphic zones. However, the preliminary stable isotope studies of serpentinized peridotites at Hess Deep indicate temperatures of serpentinization between 350° and 250°C (Agrinier et al., unpubl. data). Fluid-rock interaction continued to low temperatures at zeolite facies conditions, as evidenced by the presence of low-temperature serpentine (chrysotile, lizardite), brucite, clays, and possibly iron-oxihydroxides. An influx of late-stage oxidizing fluids rich in CO_2 and Ca produced aragonite in discrete fractures and microfractures, and is associated with the formation of tremolite and magnetite-rich zones in individual samples.

The gabbroic and troctolitic lithologies at Site 895 record the early development of a greenschist facies mineral assemblage of green amphibole, chlorite, talc, and secondary plagioclase. Later formation of secondary minerals typically involves development of calcium aluminum silicate phases such as prehnite, zeolites, hydrogrossular garnet, tremolite, and rare epidote and clinopyroxene, which indicates local incipient rodingitization. The close association of the calc-silicate-bearing gabbroic and troctolitic rocks with the peridotites may reflect migration of calcium-rich fluids generated during serpentinization of the peridotites under greenschist facies conditions.

The metamorphic mineral assemblages and vein types in the peridotites and gabbroic rocks from Site 895 are similar to those of the Garret Transform (Bideau et al., 1991) and to those recovered at Site 670 (Hébert et al., 1990). At Hess Deep, crustal attenuation and faulting associated with formation of the rift valley may have enhanced penetration of seawater into the peridotites, resulting in pervasive static metamorphism and concomitant generation of calcium-enriched fluids.

STRUCTURE

Introduction

The ultramafic rocks encountered at Site 895 have plastic deformation fabrics indicative of deformation at extremely elevated temperatures, probably close to the peridotite solidus. We infer that these fabrics were acquired under asthenospheric mantle conditions.

The tectonized harzburgites and dunites from Site 895 may contain variable percentages of interstitial plagioclase accompanied in some instances by clinopyroxene (see "Igneous Petrology" section, this chapter). In general, these phases do not exhibit the deformation textures shown by the host olivine, orthopyroxene, and spinel; therefore we argue that they represent trapped partial melt products that have infiltrated the host peridotites at the end of the main high-temperature deformation episode. These observations, and the conclusions drawn from them, are similar to those proposed for ultramafic rock samples dredged from Hess Deep by Hekinian et al. (1993) and Girardeau and Francheteau (1993).

Some of the coarse-grained mafic rocks associated with the peridotites of Site 895, although variably rodingitized, display penetrative foliations. The intense metamorphic overprint that affects these rocks typically obscures the fabric, but in the least-altered samples it is possible to show that the fabrics probably were formed by a combination of both magmatic and solid-state flow.

The ultramafic rocks are highly serpentinized. Serpentine minerals are developed either in the groundmass or in discrete veinlets. Several generations of veins may be distinguished on the basis of their mineral assemblages, but no consistent relationship has been recognized with respect to their orientation. Except for localized centimeter-scale offsets along some of the late veins, little evidence exists for deformation of serpentine in any of the Site 895 cores; hence we surmise that serpentinization of the mantle peridotites of the Hess Deep intrarift ridge was essentially a static process.

High-temperature Deformation in Ultramafic Rocks

Macroscopic Appearance

The harzburgites from Site 895 exhibit varying modal proportions of orthopyroxene, and a complete gradation from harzburgite to depleted harzburgite to dunite is recognized (see "Igneous Petrology" section, this chapter). The high-temperature deformation of the Site 895 peridotites gives rise to a foliation that can be recognized in both harzburgites and dunites. Macroscopically, most harzburgites have a foliation delineated by the elongation of spinel grains. The orthopyroxene grains may also define a foliation, but are more difficult to recognize on the scale of a core sample. Foliation may also be marked by the orientation of trains of spinel crystals, or by the elongation of pyroxene and altered plagioclase impregnations.

Foliations in the dunites are also marked by the weak elongation of individual spinel grains or of strings of more equant spinel grains. In general, the fabric is less easy to recognize than in the harzburgites because of the erratic distribution of spinel in the dunites. In troctolites it was rarely possible to recognize any penetrative foliation, except for the orientation of the troctolite contacts themselves.

Microstructural Types

Harzburgite

Microscopically, the texture of harzburgite is porphyroclastic. Orthopyroxene porphyroclasts (2 to 5 mm in diameter) exhibit tilt sub-boundaries perpendicular to the {100} slip plane, and are surrounded by polygonal orthopyroxene neoblasts (0.5 to 1 mm) (Fig. 23). Orthopyroxene crystals are elongate parallel to their {100} slip planes and often show concave grain boundaries. In the least-serpentinized specimen (Sample 147-895D-5R-1, Piece 2), olivine crystals (5 to 7 mm) have curved grain boundaries meeting at triple junctions (Fig. 24). Sub-boundaries within the olivines are rare. Only in the vi-

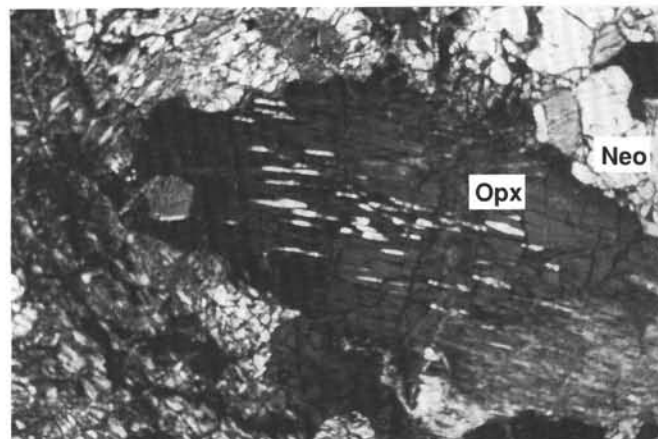


Figure 23. Photomicrograph of harzburgite. Orthopyroxene porphyroclast (Opx), elongate parallel to {100} crystallographic plane, with sub-boundaries perpendicular to this plane, concave grain boundaries, and recrystallized neoblasts (Neo) (Sample 147-895D-2R-1, Piece 6C, 56–60 cm; field of view = 1.75 mm).

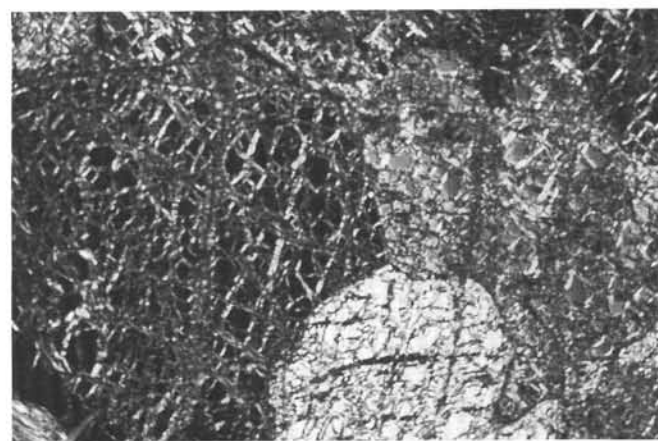


Figure 24. Photomicrograph of harzburgite. Rounded to euhedral olivine grains with a triple junction boundary, indicative of annealing and a high degree of recovery of the crystallographic lattice (Sample 147-895D-5R-1, Piece 2, 7–11 cm; field of view = 1.75 mm).

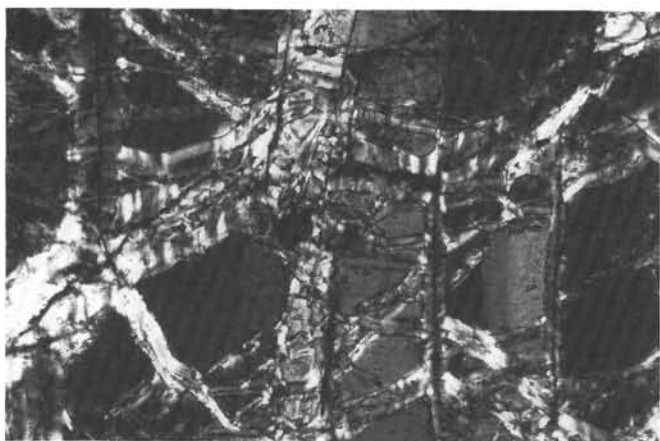


Figure 25. Photomicrograph of harzburgite. Sharp [100] sub-boundaries in olivine, characteristic of high-temperature plastic deformation (Sample 147-895D-5R-1, Piece 2, 7–11 cm; field of view = 1.75 mm).

cinity of orthopyroxene porphyroclasts do olivine crystals preserve sub-boundaries (Fig. 25), and these tend to be widely spaced and have a planar form. This implies a high degree of recovery of the olivine lattice. Despite its weak shape fabric, olivine appears to have a strong preferred orientation, as suggested by the common optical extinction of large olivine aggregates. Spinel occurs either in association with orthopyroxene aggregates or dispersed in the olivine matrix. It typically displays “pull-apart” textures and a strong shape fabric.

All of these characteristics have been interpreted as recording solid-state flow of peridotite at high temperatures and low deviatoric stresses in the asthenospheric mantle (Nicolas et al., 1973). The presence of orthopyroxene neoblasts and the high degree of annealing of the olivine crystals point to unusually high temperatures, probably very close to the peridotite solidus (in the order of 1200°C).

Clinopyroxene, associated with pseudomorphs that we think to be plagioclase, is present in the Site 895 harzburgites; it is interstitial, and often has lobate grain boundaries. Occasionally clinopyroxene has been observed poikilitically enclosing olivine (Fig. 26). Both clinopyroxene and plagioclase are undeformed. They therefore have not been affected by the plastic deformation recorded by the peridotite, and are interpreted as crystallizing from a melt percolating in and reacting with the harzburgite framework during the last stage of plastic deformation (Nicolas, 1989). Rocks with such textures have been collected previously from the Garrett Fracture Zone and Hess Deep, and have been described as impregnated peridotites (Cannat et al., 1990; Hekinian et al., 1993; Girardeau and Francheteau, 1993).

Dunite

Dunite from Site 895 is heavily serpentinized (see “Metamorphism” section, this chapter); however, the shapes and optical characteristics of the primary olivine crystals are often preserved. Olivine grains (2 to 5 mm diameter) are rounded to euhedral (Fig. 27), with numerous triple junctions. Large olivine crystals (5 to 7 mm) may have a shape fabric, but apparently no preferred orientation, and rare sharp sub-boundaries are observed. Small olivine (1 mm) crystals are euhedral. The presence of strained olivine crystals in the Site 895 dunites, rocks that otherwise appear to have cumulate textures, suggests that some, if not all, of the dunite olivines are of residual mantle origin.

Dunite may contain interstitial plagioclase and clinopyroxene located at the triple junctions of olivine grains, and at olivine grain boundaries (Fig. 27). The amount of plagioclase and clinopyroxene is highly variable: at maximum, it may be as high as 50%, isolating individual olivine grains or aggregates and giving rise to a troctolite/olivine gabbro assemblage.

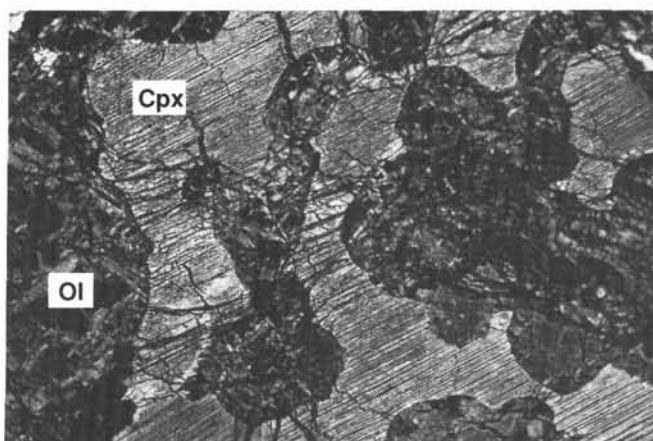


Figure 26. Photomicrograph of harzburgite. Poikilitic clinopyroxene (Cpx) including euhedral olivine (Ol). The clinopyroxene is undeformed (Sample 147-895C-4R-1, Piece 12, 85–88 cm; field of view = 1.75 mm).

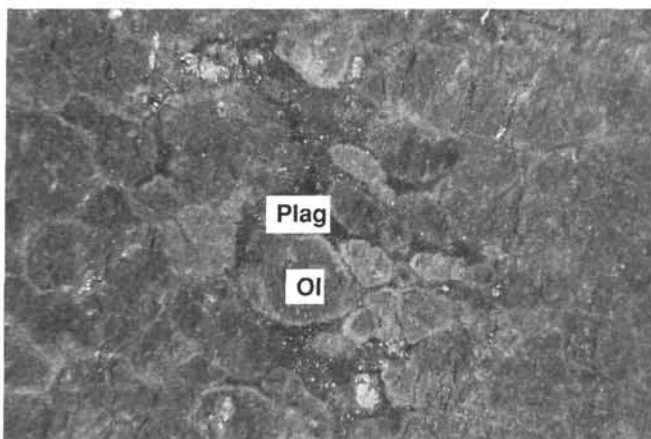


Figure 27. Photomicrograph of dunite. Olivine grains (Ol) have rounded to euhedral form, with interstitial altered plagioclase (Plag) locally embaying millimetric-sized euhedral olivine crystals (Sample 147-895D-8R-2, Piece 5A; field of view = 1.75 mm).

In conclusion, the transitional characteristics between textural types of the ultramafics recovered in Holes 895C, 895D, and 895E suggest that these rocks belong to a suite of tectonized residual mantle peridotites that have been variably impregnated by, and have reacted with, a percolating mafic magma.

Geometry of High-temperature Plastic Deformation

The foliation marked by spinel shape fabric was observed in 106 core pieces and measured in 74 pieces of harzburgite and dunite from Holes 895C, 895D, and 895E for which reliable orientations relative to the axis of the core were visible. Apparent dip and strike measurements were made on half-cut surfaces and on surfaces cut perpendicular to the axis of the core, respectively. Dip values measured relative to the axis of the core are moderately to steeply dipping in Holes 895C (mean 64°; Fig. 28) and 895D (mean 72°; Fig. 29A), and there is a suggestion of an increase of dip with depth in Hole 895E (mean 55°; Fig. 30A). A few measurements of the spinel lineation on half-cut surfaces close to the foliation plane indicate a steep plunge for this lineation.

Of the 74 foliation measurements made relative to core-liner coordinates, we were able to restore 21 relative to the stable remanent

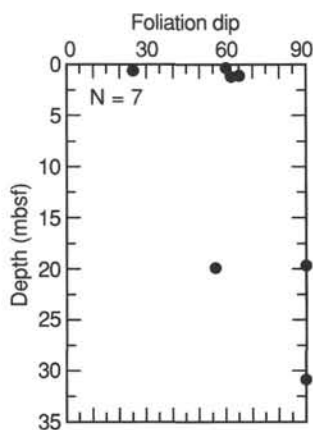


Figure 28. Dip of foliation vs. depth in peridotites from Hole 895C. Dips are measured relative to the core liner and have not been corrected for magnetic inclination.

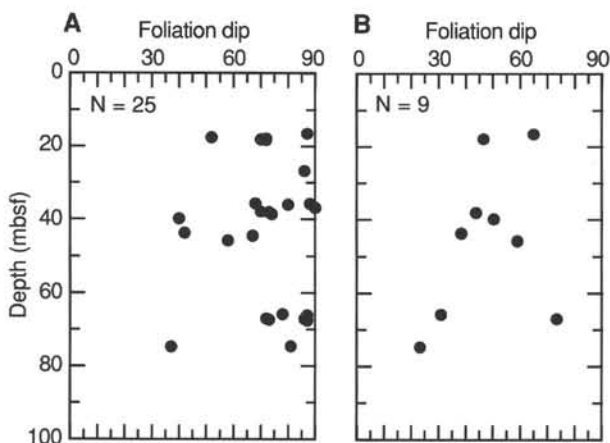


Figure 29. Dip of foliation vs. depth in peridotites from Hole 895D (A) relative to core, and (B) after restoration of the stable remanent magnetization to zero (the predicted inclination for these latitudes).

magnetization direction (see "Structural Geology" section, "Explanatory Notes" chapter, this volume). Of these 21 data points, one each was from Holes 895B and 895C, 9 were from Hole 895D, and 10 were from Hole 895E. Most paleomagnetic inclinations from Site 895 show the same moderate positive (downward) direction that was identified at Site 894; the only notable exceptions were five samples scattered through Hole 895D that have flat or negative inclinations (see "Paleomagnetism" section, this chapter). As for Site 894, the expected magnetic inclination for rocks of this age and latitude is approximately zero; the mean inclination of approximately 40° therefore implies a tectonic rotation or component of rotation of that magnitude down toward the magnetic declination direction (see "Structure" section, "Site 894" chapter, this volume). Again, the polarity of the rocks is not known with certainty but is inferred to be reversed (see "Paleomagnetism" section, this chapter). If so, the magnetic declination and, hence, tilting direction should be toward geographical south; however, in the absence of direct evidence for the magnetic polarity, we follow the convention used for the Site 894 structural reorientations and present all figures and quote all directions with the declination restored to north.

The high-temperature fabrics in the Site 895 peridotites must predate rotation of the magnetic vector; thus it is appropriate to correct the data so that the magnetic inclination is zero. Because of the variability in Hole 895D, we have applied an individual correction for each sample. The effect of correction for magnetic inclination on

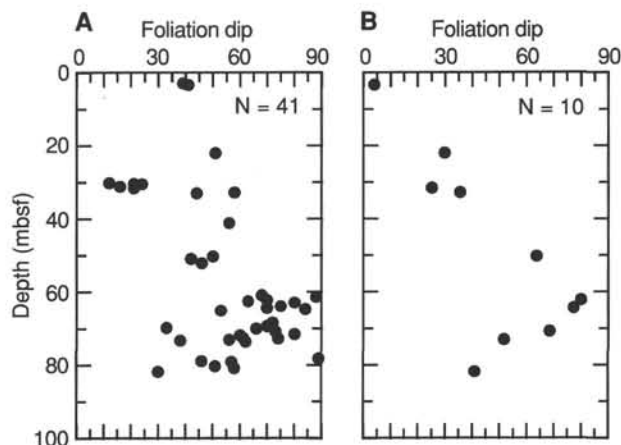


Figure 30. Dip of foliation vs. depth in peridotites from Hole 895E (A) relative to core, (B) after restoration of the stable remanent magnetization to zero (the predicted inclination for these latitudes).

the dip of the foliation (Figs. 29B and 30B) appears to correspond to a general shift toward lower values compared with the uncorrected data, and the suggested increase of dip with depth for foliations from Hole 895E is emphasized (Fig. 30B).

The strike of the peridotite foliations shows a preferred north to north-northeast trend when restored with respect to magnetic declination only (Fig. 31), and a stronger maximum in a north-northeast to northeast direction when magnetic inclination is taken into account (Fig. 32). This is roughly parallel to the supposed orientation of the East Pacific Rise spreading axis, and to the magmatic foliation trend found at Site 894 (see "Structure" section, "Site 894" chapter, this volume). The well-defined girdle of poles to planes (Fig. 32B) indicates that the preferred strike of the Site 895 peridotite foliations remains relatively constant when the dip varies. This observation, when coupled with the progressive increase of dip with depth in Hole 895E (Fig. 30B), suggests that the trajectory of mantle flow changes from steep (and ridge parallel) to flat with increasing stratigraphic depth in Hole 895E.

Deformation in Mafic Rocks

Mafic rocks recovered from Site 895 are variably altered and deformed gabbros, olivine gabbros and troctolites. They range from undeformed to well foliated; the fabric of the latter is defined by the elongation of irregularly shaped grains of plagioclase with coronae of light green amphibole/chlorite (Fig. 33; see "Metamorphism" section, this chapter). The dip of the foliation (measured relative to the axis of the borehole only) from one sample in Hole 895D is 70° (Sample 147-895D-8R-2, 26 cm; 75.9 mbsf); four samples from Hole 895E respectively measure 40° (Sample 147-895E-1R-3, 125 cm; 4.1 mbsf), 11° (Sample 147-895E-1R-3, 135 cm; 4.2 mbsf), 25° (Sample 147-895E-1R-4, 6 cm; 4.4 mbsf), and 20° (Sample 147-895E-1R-4, 17 cm; 4.5 mbsf). These measurements were made with respect to the core liner and, in the absence of magnetic data, have not been corrected for magnetic inclination; hence, it should be noted they may not be representative of the true (original) dips of the foliation.

Microscopic Observations

Microscopic observations (from the poorly foliated Sample 147-895E-6R-3, Piece 5, 97–100 cm) show foliation to be defined by the alignment and elongation of plagioclase and clinopyroxene, both of which are in various stages of alteration. Plagioclase has extensive undulatory extinction and commonly has deformation twins. Clinopyroxene locally displays strong undulose extinction and is elongate parallel to the foliation; however, more typically it has a shape fabric

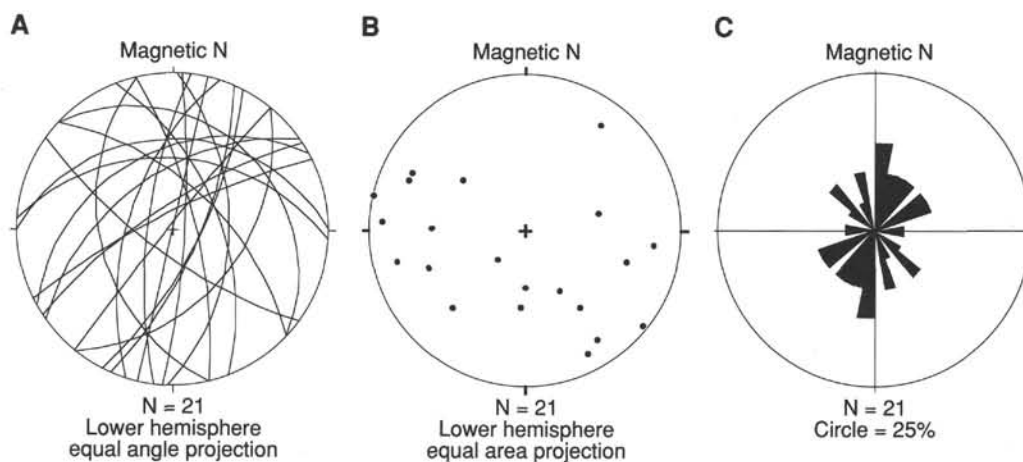


Figure 31. Foliations in peridotites from Site 895, restored relative to declination of the stable remanent magnetization, but with no inclination correction. **A.** Foliation planes. **B.** Poles to planes. **C.** Rose diagram of strike of foliation.

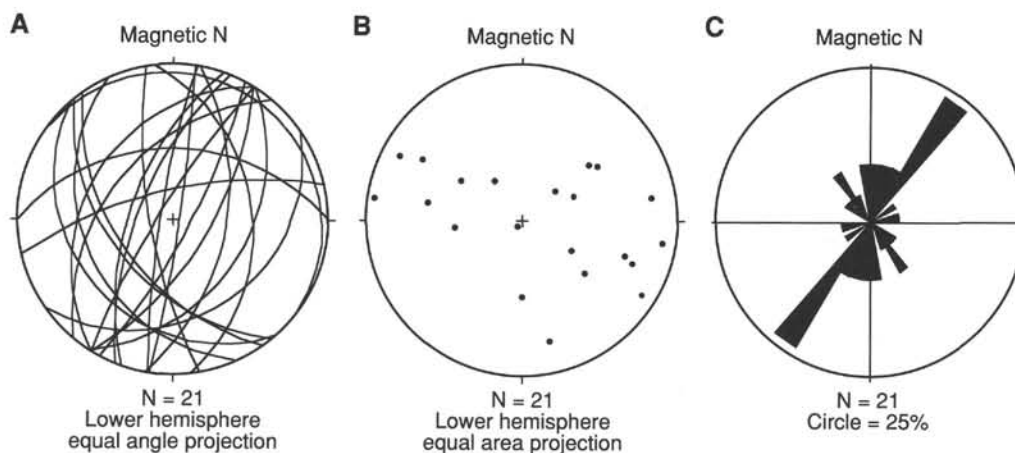


Figure 32. Foliation in peridotites from Holes 895D and 895E, restored relative to declination and assuming the inclination of the stable remanent magnetization to be zero. **A.** Foliation planes. **B.** Poles to planes. **C.** Rose diagram of strike of foliation.

parallel to the foliation but is not plastically deformed. Recrystallization has not been observed in plagioclase or clinopyroxene. Larger, low-birefringent clinopyroxene grains have both sharp kink bands and more openly folded areas. Plagioclase deformation twins are statically altered to varying degrees to a fine-grained tremolite/chlorite mixture. Deformed, elongate pyroxene grains are variably altered to tremolite, which has formed parallel to the foliation.

In another sample, a nonfoliated, highly altered olivine gabbro (Sample 147-895-E-2R-1, Piece 8, 36–39 cm), the plagioclase grains display minor undulose extinction and rare deformation twins. However, olivine grains display strong undulose extinction and, in one grain, a well-developed, planar subgrain boundary was observed. This suggests that olivine may be a residual phase that remained after percolation of a mafic melt, as suggested above for olivine in the dunites and troctolites.

Clinopyroxene and plagioclase have a poorly developed mineral shape fabric that defines the foliation seen in hand specimen. This shape fabric may be magmatic in origin; however, the observation of extensive undulose extinction and development of deformation twins in plagioclase indicates that plastic deformation contributed, at least in part, to the development of the foliation. The lack of dynamically recrystallized minerals and the associated metamorphic mineral assemblage indicate that the plastic deformation event probably occurred before or during greenschist facies metamorphism.

Igneous Contacts

Planar igneous contacts for which orientations could be ascertained were encountered at two locations in Hole 895D and two locations in Hole 895E. Modal variation in a rodingitized gabbro (Sample 147-895D-7R-1, 18 cm; 64.8 mbsf) dips at 45° relative to the axis of the borehole, and a 1-cm-wide troctolite segregation at 41.7 mbsf in Hole 895E (Sample 147-895E-4R-2, 80 cm) has a dip of 14° . One small, unoriented core piece (147-895E-6R-1, 78 cm; 59.4 mbsf) contains a sheared contact between highly deformed troctolite and harzburgite.

Two of the contacts are between harzburgite and dunite. These contacts are defined by the disappearance of orthopyroxene in the latter over a distance of a few millimeters. Dips of these contacts relative to the axis of the borehole are both steep: 70° (Sample 147-895D-2R-2, 6 cm; 17.5 mbsf) and 62° (Sample 147-895E-8R-2, 51 cm; 79.9 mbsf). Magnetic data for the latter show its true dip (corrected for magnetic inclination) to be 78° towards the southwest and strike 143.3° .

Veins

Veins in the harzburgites and dunites from Site 895 range in morphology from planar and continuous structures to thin, irregular, discontinuous veinlets. Six generations of macroscopic veins have

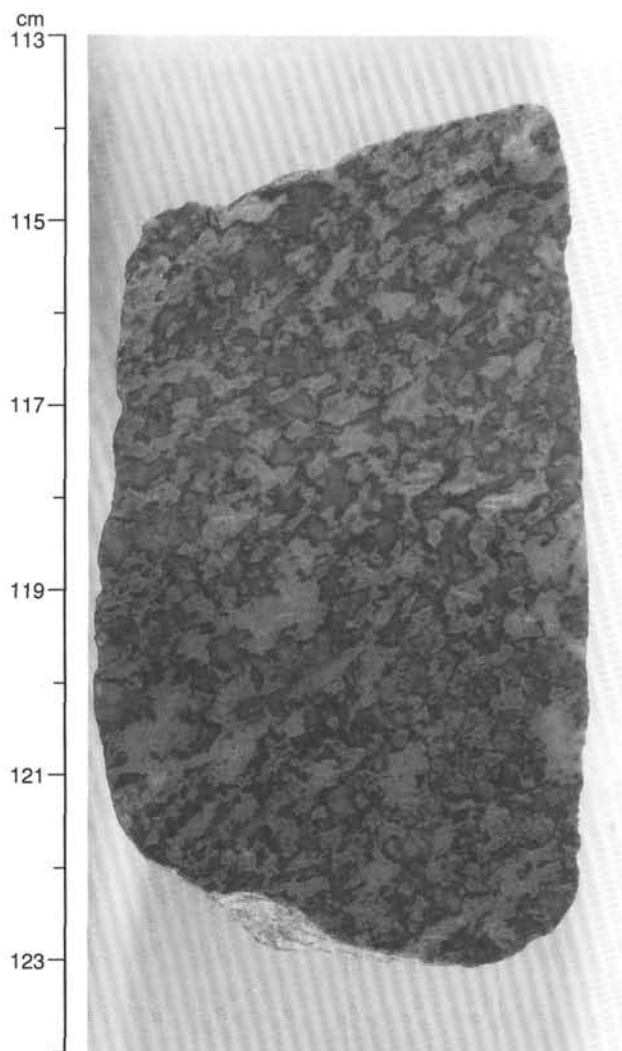


Figure 33. Photograph of a foliated olivine gabbro. Elongate plagioclase and tremolite/chlorite define the foliation (Sample 147-895-E-1R-3, Piece 9, 113–124 cm).

been identified. Their morphologies and mineral assemblages are described in detail in the “Metamorphism” section, this chapter, and summarized in Table 7.

Microscopic Characteristics

In thin section, the blue-green serpentine + magnetite vein type commonly possesses a zoned morphology, with a fine-grained serpentine core rimmed by a coarser, blocky serpentine. These veins are crosscut by an array of irregular, discontinuous brucite veinlets. Less commonly the chrysotile veins display a “crack-seal” morphology (Ramsay, 1980), with numerous parallel trains of wall-rock inclusions, indicating that the veins formed by successive opening/infilling events. In one section (147-895D-4R-2, Piece 18, 126–129 cm), the vein reopened perpendicular to the initial opening direction and was infilled with fibrous amphibole (see “Metamorphism” section, this chapter; Fig. 20). Both the amphibole and chrysotile are sheared with a normal sense of movement.

Serpentine + magnetite \pm chlorite \pm clay (\pm brucite/talc) veins are zoned. Serpentine and clay occur together and are commonly sheared, giving the serpentine a wavy, ribbon-like appearance. Both normal and reverse apparent shear senses are observed.

Vein Orientations

Veins at Site 895 show a variety of orientations. Their dips are widely scattered, whether plotted relative to the axis of the borehole (Fig. 34A) or corrected assuming the inclination of the stable magnetization to be zero (Fig. 34B). Their restored strikes, however, are more consistent, showing a general preferred southwesterly to westerly orientation when restored relative to declination only (Fig. 35), or a west to west-northwest trend when also corrected for magnetic inclination (Fig. 36).

We were unable to find a consistent relationship between vein assemblage and orientation, although, relative to the axis of the core, the pale green chrysotile veins appear to be more steeply dipping on average than the crosscutting brucite veins. Therefore, no attempt has been made to subdivide the data on Figures 34, 35, and 36.

The distribution of dips between the uncorrected and inclination-corrected histograms is markedly different (Fig. 34), and it is not implicit which of the two restorations is more justifiable. If the veins were formed before tilting, the distribution of vein dips in Figure 34A is meaningless, because the angle between the veins and the axis of restoration is not constant for all data. If, on the other hand, tilting of the intrarift ridge (as implied by the anomalous magnetic inclinations found at Sites 894 and 895) occurred before veining, it is not valid to restore the data relative to a magnetic inclination of zero. We have little basis for distinguishing between the two distributions; indeed, it is possible that some of the veins were formed during tilting and only partially rotated, in which case neither distribution is correct. The only constraint we have is that some of the serpentinization must have occurred before tilting, because peridotites will only acquire a significant remanence upon serpentinization and consequent formation of magnetite. We also note that the distribution of poles to planes for the

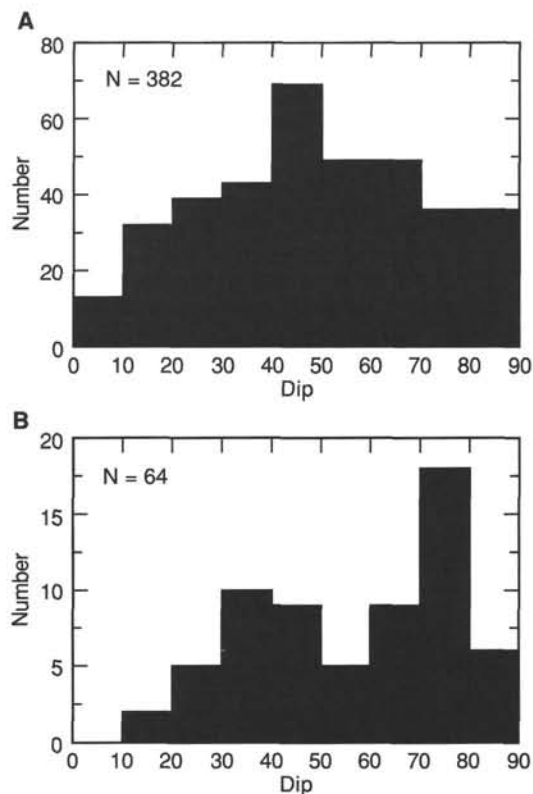


Figure 34. Histogram of the dips of serpentine veins from Site 895. A. Dips of all veins with respect to the axis of the core. B. Dips of veins for which magnetic data are available, corrected assuming a magnetic inclination of zero.

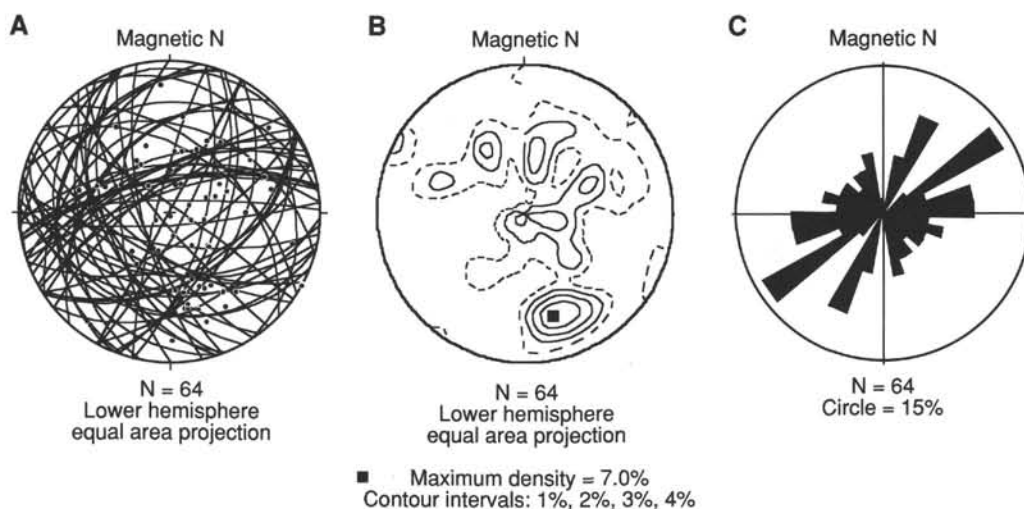


Figure 35. Orientations of serpentine veins in peridotites from Site 895, restored with the declination of the stable remanent magnetization pointing north, but making no correction for inclination. **A.** Foliation planes. **B.** Poles to planes. **C.** Rose diagram of strike of foliation.

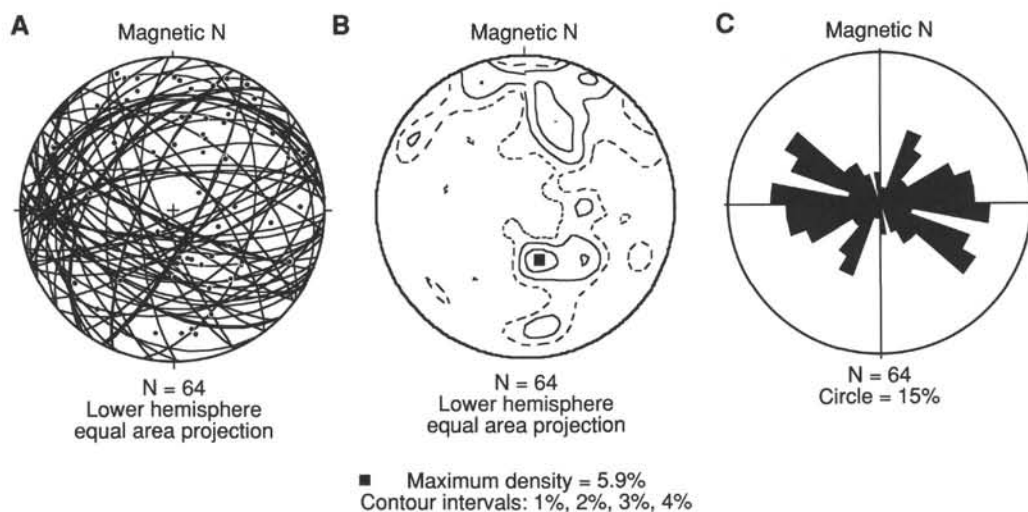


Figure 36. Orientations of serpentine veins in peridotites from Site 895, restored assuming the declination of the stable remanent magnetization to point north and the inclination to be zero. **A.** Foliation planes. **B.** Poles to planes. **C.** Rose diagram of strike of foliation.

Site 895 data shows a tighter clustering for the uncorrected (Fig. 35B) compared with the corrected (Fig. 36B) data; in effect, the data fail a “fold test” upon restoration.

The absence of widespread deformation of the serpentinite from Site 895 is notable. We see no pervasive deformation associated with the background serpentinite mesh network; minor centimeter-scale offset along some late brucite veins is the only evidence for tectonism associated with serpentinization. It therefore appears that serpentinization of the peridotites of the Hess Deep intrarift ridge was essentially a static phenomenon, and models invoking serpentinite diapirism to affect its uplift are not supported by observations from Site 895.

GEOCHEMISTRY

Fourteen whole-rock samples from Site 895 were analyzed using X-ray fluorescence (XRF) for major oxide compositions and abundances of the trace elements Nb, Zr, Y, Sr, Rb, Zn, Cu, Ni, Cr, V, Ce, and Ba. Nb and Rb are below detection limits for all samples (≤ 1 and

≤ 2 ppm, respectively); Ce and Ba are not reported due to high analytical errors. The samples were also analyzed using gas chromatography for H, C, and S contents. Sample preparation techniques and analytical procedures are outlined in the “Geochemistry” section of the “Explanatory Notes” chapter. Of the lithologies selected for geochemistry, five are dunites, seven are harzburgites, and one sample each is basalt and olivine gabbro. The results are presented in Table 9. Due to the nature of the ultramafic lithologies sampled at Site 895 (harzburgites and dunites), only the mafic rocks have Zr, Y, and Sr above detection limits (Table 9). The Ni and Cr abundances (Table 9) in the ultramafic rocks probably reflect the relative abundances of olivine vs. pyroxene and Cr-spinel, such that relatively low Cr/Ni ratios may reflect decreasing modal abundance of pyroxene (predominantly orthopyroxene) and Cr-spinel.

Considerable differences (~ 1 – 2 wt%) were observed between loss-on-ignition (LOI) values and the sum of $H_2O + CO_2 + N_2 + S$ as determined by gas chromatography with the totals of volatiles being typically higher (Table 9). The high H_2O content of the ultramafic rocks

Table 9. Chemical composition of rock samples from Holes 895A, 895D, and 895E.

Hole	895A	895D	895D	895D	895D	895D	895D	895D	895E	895E	895E	895E	895E	895E
Core-section:	2R-1	2R-1	3R-1	4R-3	6R-1	7R-1	7R-1	10 W	1R-3	3R-2	4R-1	6R-3	7R-4	8R-3
Interval (cm):	91-95	42-45	48-52	50-56	128-134	23-27	131-135	24-27	0-5	39-46	117-126	89-95	48-51	39-44
Piece:	15	6A	6D	6B	17	4	20B	3	1	4	17	5A	4	3
mbsf:	10.1	16.4	24.5	37.5	56.3	65	66.1	93.9	2.86	31.4	40.7	62.2	73.2	81.2
Igneous unit		3	5	7	11	13	16		4	19	27	43	46	53
Lithologic type:	B	HZ	HZ	HZ	HZ	G	HZ	D	HZ	D	D	D		HZ
SiO ₂	49.86	43.41	43.42	43.19	44.73	46.00		39.96	40.64	40.09	39.64	39.82	42.73	39.84
TiO ₂	1.61	0.01	0.01	0.01	0.01	0.11		0.03	0.01	0.02	0.02	0.03	0.01	0.01
Al ₂ O ₃	15.29	0.73	0.78	0.82	0.91	23.04		0.44	0.70	0.53	0.56	0.72	0.65	0.35
FeO	9.66	8.15	8.06	8.09	7.91	3.57		10.09	9.64	10.86	10.15	9.51	8.24	10.25
MnO	0.16	0.13	0.13	0.12	0.12	0.07		0.15	0.14	0.17	0.16	0.15	0.12	0.16
MgO	7.52	45.14	45.88	45.76	43.88	10.38		47.56	46.93	45.95	47.39	47.78	45.41	47.47
CaO	10.84	0.84	0.52	0.84	0.87	15.79		0.02	0.01	0.00	0.01	0.06	0.74	0.02
Na ₂ O	2.78	0.00	0.00	0.00	0.02	1.00		0.00	0.00	0.00	0.01	0.00	0.00	0.00
K ₂ O	0.18	0.00	0.00	0.00	0.01	0.04		0.00	0.00	0.00	0.00	0.00	0.00	0.00
P ₂ O ₅	0.14	0.01	0.00	0.00	0.01	0.01		0.00	0.01	0.01	0.00	0.01	0.00	0.00
Total	98.11	98.38	98.81	98.85	98.46	100.01		98.25	98.09	97.64	97.95	98.04	97.93	98.11
LOI	1.13	10.45	10.41	9.13	10.78	3.62		14.81	14.35	14.26	15.10	14.28	11.60	14.84
H ₂ O	1.72	11.16	10.71	10.08	11.61	3.82	12.36	14.72	14.09	13.69	14.90	14.58	13.14	16.29
CO ₂	0.00	0.15	0.10	0.07	0.15	0.00	0.18	0.29	0.42	0.92	0.77	0.18	0.07	0.18
S	0.08	0	0	0.01	0	0	0.01	0.03	0	0	0	0	0	0
Sr	128	0	1	0	1	279	0	0	0	0	0	1	0	0
Zr	104	0	0	0	0	2	0	0	0	0	0	0	0	0
Y	34	0	0	0	0	2	0	0	0	0	0	0	0	0
V	296	40	26	34	48	66	42	24	33	18	27	15	30	15
Cr	289	2331	2419	2891	2845	996	2922	2283	2182	1777	2102	1463	2062	1725
Ni	115	2312	2195	2296	2123	396	2298	2354	2481	2383	2320	2509	2393	2269
Cu	68	4	3	1	0	12	12	3	0	3	1	0	0	0
Zn	84	32	34	35	24	10	35	44	33	33	41	35	24	38
Mg/(Mg+Fe)	58.1	90.8	91.0	91.0	90.8	83.8		89.4	89.7	88.3	89.3	90.0	90.8	89.2
MgO/Al ₂ O ₃	71.2	61.8	58.8	55.8	48.2	0.45		108.1	67.0	86.7	84.6	66.4	69.90	134.6
Cr/Ni	2.51	1.01	1.10	1.26	1.34	2.52	1.27	0.97	0.88	0.75	0.91	0.58	0.85	0.76

Notes: HZ = harzburgite; D = dunite; G = gabbro; B = basalt. Mg/(Mg+Fe) multiplied by 100. Sample 147-895D-7R-1 (Piece 20B, 131-135 cm) not run for major elements.

(10–16 wt%; Table 9) is consistent with the high degree of serpentinization of these rocks (see “Metamorphism” section, this chapter).

In addition to the above lithologies, a portion of the wash core from 147-894D-10W (“Wash 10”) was selected as a reference sample for post-cruise geochemistry. “Wash 10” consists of approximately 10 kg of sand- to gravel-sized mixed mafic to ultramafic material. This reference material was homogenized (after grinding in small portions) by passing it through a sample splitter 15 times.

The significant results from the geochemistry of mafic and ultramafic rock samples from Site 895 are as follows:

1. The aphyric basalt with a glassy rind from Hole 895A (Sample 147-895-2R-1, Piece 15, 91–95 cm) has a composition similar to moderately evolved mid-ocean-ridge basalt (MORB) from the East Pacific Rise (Allan et al., 1989).

2. The olivine-bearing gabbro sampled from Hole 895D (Sample 147-895D-7R-1, Piece 4, 23–27 cm) is characterized by very low Zr, Y (2 ppm), low TiO₂ (0.10 wt%) and high Sr (279 ppm), Cr (996 ppm), Ni (396 ppm), and Mg/(Mg + Fe) compared with gabbroic rocks sampled at Site 894 (Table 14 of the “Site 894” chapter, this volume). Apart from the high Sr and Mg/(Mg + Fe), which could be attributed to secondary processes, the differences in trace element content of the gabbroic rocks from each site suggest that the olivine-bearing gabbro sample from Hole 895D represents a cumulate rock from a primitive magma.

3. Both the harzburgites and dunites exhibit a significant range in Ni and Cr abundances and Cr/Ni values (Table 9). Harzburgites with relatively low Cr and Ni contents and high Cr/Ni ratios have a higher proportion of modal orthopyroxene (~15–20 modal percent); clinopyroxene is present as exsolution lamellae in orthopyroxene and as discrete neoblasts associated with Cr-spinel. Harzburgites with relatively high Ni and Cr abundances and low Cr/Ni ratios have no clinopyroxene (rare as exsolution lamellae) and low modal abundance of orthopyroxene (~8–10 modal percent). These observations are

consistent with increasing degrees of melt extraction; however, mineral chemical data are required to confirm this preliminary conclusion.

4. As with harzburgites, dunites also show a significant range in Ni abundances (Table 9). As Ni is primarily concentrated in olivine and is generally correlated with the forsterite content of olivine, the variation in Ni abundances in the dunites may indicate a significant range in the forsterite content of olivine. As in the case of harzburgites, mineral chemical data are required to confirm this preliminary conclusion.

PALEOMAGNETISM

Introduction

Magnetic measurements were made on 36 minicore samples from Holes 895B, 895C, 895D, and 895E, with the majority of the samples taken from the two deepest holes (895D and 895E). The results of these measurements are displayed in Tables 10 and 11. The magnetic susceptibility of the whole core and the remanent magnetization of the archive half of the split core were also measured. Techniques for these measurements are described in the “Paleomagnetism” section of the “Explanatory Notes” chapter, this volume. Although the lithology of the cores recovered from Site 895 was variable, including small amounts of basalt and gabbro, core from Hole 895D was dominated by harzburgite, and core from Hole 895E was dominated by dunite. These ultramafic rocks provide an important contrast to gabbro, which was predominant in the cores recovered from Hole 894G.

Intensity of Natural Remanent Magnetization (J_0)

Natural remanent magnetization intensities are listed in Table 10 and shown in Figures 37 and 38. J_0 values obtained from the 36 minicores ranged from 0.0006 to 25.0 A/m (arithmetic mean of 2.0 A/m). This large variation was caused by a few weakly magnetized gabbros (e.g., Sample 147-895E-4R-3, 6–8 cm) and a strongly magnetized dunite (Sample 147-895D-9R-1, 120–122 cm). Figure 38A

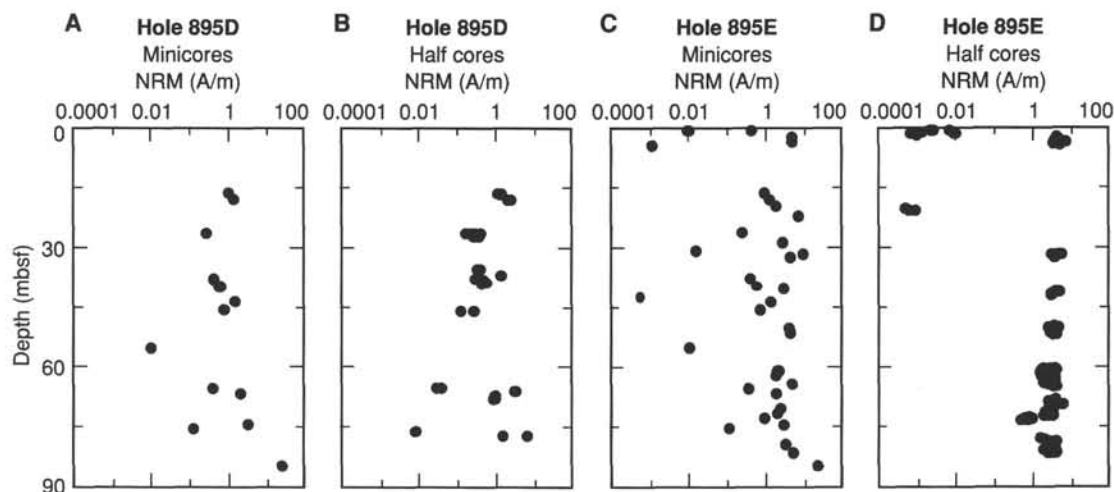


Figure 37. Plots of NRM intensity vs. depth in Holes 895D and 895E.

Table 10. Summary of magnetic property values for minicores sampled from Holes 895B, 895C, 895D, and 895E.

Core, section, interval (cm)	Piece number	Depth (mbsf)	NRM (A/m)	Susceptibility (SI)	Q	MDF (mT)	Stable declination	Stable inclination	Rock type
147-895B-1R-1, 64-66	9b	0.64	4.72E-01	7.42E-03	2.4	12.0	-63	39	Harzburgite
147-895C-3R-1, 139-141	22	19.69	2.03E+00	2.33E-02	3.3	15.0	-13	46	Harzburgite
4R-1, 83-85	12	28.73	2.84E+00	2.37E-02	4.6	10.0	10	46	Olivine gabbro
4R-3, 58-60	6	31.06	1.52E-02	7.85E-04	0.7	11.0	ND	ND	Basalt
147-895D-2R-1, 47-49	6b	16.47	1.02E+00	1.03E-02	3.7	14.0	-139	38	Harzburgite
2R-2, 47-49	3a	17.89	1.35E+00	3.65E-02	1.4	7.0	109	-34	Harzburgite
3R-1, 45-47	6d	26.45	2.60E-01	5.81E-03	1.7	12.5	116	-23	Harzburgite
4R-3, 110-112	12	38.09	4.34E-01	3.68E-03	4.5	15.0	49	38	Harzburgite
4R-5, 3-5	1	39.76	6.09E-01	4.84E-03	4.8	20.0	23	24	Harzburgite
5R-1, 52-54	8	43.82	1.48E+00	2.48E-02	2.3	12.0	-89	-26	Harzburgite
5R-2, 100-102	14	45.74	7.82E-01	1.15E-02	2.6	15.0	163	-3	Harzburgite
6R-1, 32-34	6	55.32	1.09E-02	3.49E-04	1.2	13.0	-152	6	Gabbro
7R-1, 119-121	20a	65.79	3.86E-01	2.80E-02	0.5	12.0	37	59	Harzburgite
7R-2, 92-94	12a	66.99	2.04E+00	3.25E-02	2.4	12.0	118	50	Harzburgite
8R-1, 45-47	7	74.75	3.21E+00	2.84E-02	4.3	10.0	-41	49	Harzburgite
8R-2, 4-6	1	75.72	1.24E-01	3.12E-04	15.1	19.0	ND	ND	Gabbro
9R-1, 120-122	18	85.20	2.50E+01	6.73E-02	14.2	18.0	52	-59	Dunite
147-895E-1R-1, 47-49	5b	0.47	1.05E-02	3.20E-04	1.2	44.0	-60	17	Olivine gabbro
1R-2, 72-74	15	2.16	5.06E+00	7.45E-02	2.6	10.0	-74	47	Dunite
1R-3, 49-51	4a	3.35	5.34E+00	1.13E-01	1.8	10.0	151	38	Harzburgite
1R-3, 122-124	9	4.08	1.14E-03	4.43E-04	0.1	4.0	ND	ND	Troctolite
2R-2, 107-109	15	22.03	7.58E+00	5.99E-02	4.8	13.0	1	59	Dunite
3R-2, 55-57	5	31.52	1.03E+01	1.15E-01	3.4	10.0	151	37	Dunite
3R-3, 14-16	3	32.61	4.67E+00	1.25E-01	1.4	9.0	-108	45	Dunite
4R-1, 102-104	15b	40.52	3.21E+00	5.84E-02	2.1	7.0	-47	30	Dunite
4R-3, 6-8	1	42.47	5.75E-04	2.78E-04	0.1	ND	ND	ND	Olivine gabbro
5R-1, 145-147	21	50.35	4.35E+00	6.75E-02	2.5	9.0	-143	45	Dunite
5R-2, 115-117	18	51.55	4.78E+00	7.63E-02	2.4	7.0	-74	27	Dunite
6R-2, 111-113	7	61.21	2.30E+00	2.72E-02	3.2	14.0	50	11	Dunite
6R-3, 101-103	5b	62.32	1.93E+00	2.55E-02	2.9	7.0	-27	58	Dunite
6R-5, 66-68	5	64.41	5.25E+00	4.65E-02	4.3	7.0	-115	17	Dunite
7R-2, 102-104	11c	70.72	2.79E+00	4.64E-02	2.3	12.0	94	30	Harzburgite
7R-3, 60-62	4b	71.8	2.12E+00	3.56E-02	2.3	10.0	20	35	Harzburgite
7R-4, 36-38	4	73.06	1.04E+00	1.27E-02	3.1	11.0	97	41	Harzburgite
8R-2, 57-59	5b	79.96	3.72E+00	5.92E-02	2.4	7.0	170	30	Harzburgite
8R-3, 103-105	6	81.83	5.84E+00	6.84E-02	3.3	13.0	40	-11	Dunite

Note: ND = values not determined.

shows that dunite samples have a stronger magnetization, whereas harzburgite and gabbro samples possess intermediate and weak magnetizations, respectively. The arithmetic mean of the J_0 of the 12 dunite samples is 6.7 A/m. This value was reduced to 5.0 A/m by leaving out the dunite sample with an anomalously high magnetization. The 17 harzburgite minicores have an arithmetic mean J_0 value of 1.7 A/m. The arithmetic mean calculated for all peridotite samples,

including harzburgite and dunite, is 3.8 A/m. Leaving out the dunite sample with high magnetization, the mean J_0 value becomes 3.0 A/m. This value is similar to previously reported mean values of 2.4–8.2 A/m (e.g., Dunlop and Prevot, 1982; Hamano et al., 1990), which suggests that the upper-mantle serpentinized peridotites have a strong enough magnetization to contribute to marine magnetic anomalies. Six gabbroic samples were measured and had relatively low J_0 values.

Table 11. Anisotropy of magnetic susceptibility.

Core, section, interval (cm)	k (10^{-6})	k_{\max}	Azi	Dip	k_{int}	Azi	Dip	k_{\min}	Azi	Dip	Error	P
147-895B-												
1R-1-64	7451	1.0480	133	4	1.0199	257	43	0.9320	43	6	± 0.0010	1.12
3R-1-13	23331	1.0670	265	18	0.9957	58	69	0.9373	172	9	± 0.0014	1.14
4R-1-83	23587	1.0812	331	18	0.970	236	16	0.9486	106	66	± 0.0005	1.14
4R-3-58	785	1.0080	8	62	1.0005	143	21	0.9915	241	18	± 0.0011	1.02
147-895D-												
2R-1-47	10346	1.0165	334	62	0.9992	230	8	0.9843	136	27	± 0.0009	1.03
2R-2-51	36541	1.0581	203	31	1.0173	348	54	0.9247	103	17	± 0.0006	1.14
3R-1-45	5819	1.0405	29	58	1.0289	129	6	0.9306	222	31	± 0.0006	1.12
4R-3-10	2472	1.0227	137	29	1.0025	339	59	0.9748	233	9	± 0.0005	1.05
4R-5-3	4844	1.0341	271	15	1.0050	178	11	0.9610	53	72	± 0.0006	1.08
5R-1-52	24691	1.0562	62	16	1.0093	158	19	0.9345	294	65	± 0.0007	1.13
5R-2-100	11454	1.0329	44	44	1.0101	312	2	0.9570	219	46	± 0.0004	1.08
6R-1-32	348	1.0181	192	56	0.9962	58	25	0.9857	317	21	± 0.0010	1.03
7R-2-92	32481	1.0675	97	2	1.0284	187	8	0.9040	350	82	± 0.0011	1.18
7R-1-11	27923	1.0335	197	13	1.0008	83	61	0.9657	293	26	± 0.0004	1.07
8R-1-45	28531	1.0268	203	63	1.0047	339	20	0.9685	75	17	± 0.0006	1.06
8R-2-4	313	1.0189	243	39	1.0083	84	49	0.9728	342	10	± 0.0007	1.05
9R-1-12	67232	1.0485	192	51	1.0228	327	30	0.9287	71	23	± 0.0018	1.13
147-895E-												
1R-1-47	321	1.0118	265	41	1.0063	167	10	0.9818	66	48	± 0.0022	1.03
1R-2-72	74485	1.0193	192	57	1.0021	321	22	0.9786	60	23	± 0.0004	1.04
1R-3-12	443	1.0241	98	42	1.0058	191	3	0.9701	284	48	± 0.0013	1.06
1R-3-49	113454	1.0632	185	4	1.0374	94	16	0.8994	289	73	± 0.0015	1.18
2R-2-10	59865	1.0888	171	15	0.9902	61	53	0.9211	271	33	± 0.0009	1.18
3R-2-55	115420	1.0657	152	3	1.0499	58	60	0.8843	244	30	± 0.0009	1.21
3R-3-14	125396	1.0739	89	15	1.0189	183	16	0.9072	318	68	± 0.0009	1.18
4R-1-10	58440	1.0327	153	12	1.0034	265	60	0.9639	56	27	± 0.0004	1.07
4R-3-6	278	1.0162	260	63	0.9953	142	13	0.9886	46	23	± 0.0025	1.03
5R-1-14	67451	1.0547	286	56	0.9886	111	34	0.9567	19	2	± 0.0005	1.10
5R-2-11	76307	1.0615	289	7	1.0390	196	19	0.8995	38	70	± 0.0008	1.18
6R-2-11	27223	1.0251	20	0	1.0171	290	57	0.9578	110	33	± 0.0006	1.07
6R-3-10	25470	1.0465	202	12	1.0141	88	62	0.9394	298	25	± 0.0005	1.11
6R-5-66	46474	1.0382	238	25	1.0017	82	63	0.9601	333	10	± 0.0003	1.08
7R-2-10	46447	1.0640	277	19	1.0048	7	1	0.9312	100	71	± 0.0008	1.14
7R-3-60	35640	1.0569	218	27	0.9953	109	33	0.9478	339	45	± 0.0004	1.12
7R-4-36	12740	1.0559	254	22	1.0006	6	42	0.9435	145	40	± 0.0004	1.12
8R-2-57	59209	1.0249	299	37	0.9950	172	39	0.9800	55	30	± 0.0003	1.05
8R-3-10	68411	1.0314	240	26	1.0155	345	27	0.9531	114	51	± 0.0007	1.08

Notes: Principal values are normalized (normalization factor: bulk susceptibility), principal directions (azimuth, dip) in core coordinates. The errors refer to the normalized principal values.

However, these gabbroic rocks were moderately to pervasively altered to calc-silicate minerals.

Natural remanent magnetization intensities measured from half cores were consistent with the results obtained for minicores (Fig. 37). The $254 J_0$ values varied over a range of about four orders of magnitude with an arithmetic mean of 2.5 A/m. This large variation was again directly related to the differences in rock types: the average intensity for 238 measurements from peridotites is 2.6 A/m, and the mean calculated for 16 measurements from gabbroic rocks is 0.007 A/m. Continuous half-core measurements also show substantial differences in magnetization between harzburgites (dominant in Hole 895D) and dunites (dominant in Hole 895E) (Figs. 37B and 37D).

Magnetic Susceptibility (k)

Results of magnetic susceptibility measurements are shown in Figures 39 and 40. Values for susceptibility for all samples lie between 0.0003 and 0.13, with an average of 0.037. As with natural remanent magnetization intensities, peridotites have a higher mean (0.045) than the altered gabbroic rocks, which average 0.0037. The mean value and range observed for peridotite samples are similar to previously reported values (e.g., Fox and Opdyke, 1973). Again, as in the case of natural remanent magnetization (NRM), dunite samples indicate higher values, with an average of 0.068, than those of harzburgite, which average 0.028 (Figs. 39 and 40).

Whole-core susceptibility values are in agreement with those made on minicores (Figs. 39 and 40). Measurements from peridotite samples (550) have values from 0.0027 to 0.1 (average 0.036), much higher than those of 37 values from gabbroic rocks (from 0.00014 to 0.0012, with an average of 0.00039). Susceptibility values from Hole 895D were somewhat lower than those from Hole 895E, indicating that harzburgites are somewhat less magnetic than dunites.

The positive correlation between susceptibilities and natural remanent magnetizations for Holes 895D and 895E suggests that the remanence is a function of the concentration of magnetic minerals.

Koenigsberger Ratio (Q)

The Koenigsberger ratio, Q , compares remanent magnetization to induced magnetization. It is used to determine whether in-situ magnetization of the crustal section is dominated by remanent magnetization ($Q > 1$) or an induced component parallel to the current field ($Q < 1$). As Figure 41 shows, Koenigsberger ratios are usually greater than unity except for four samples (Table 10), indicating that remanent magnetization is predominant in total magnetization.

Demagnetization Character

Both alternating field (AF) and thermal demagnetization were performed on minicores from Site 895. The results discussed here

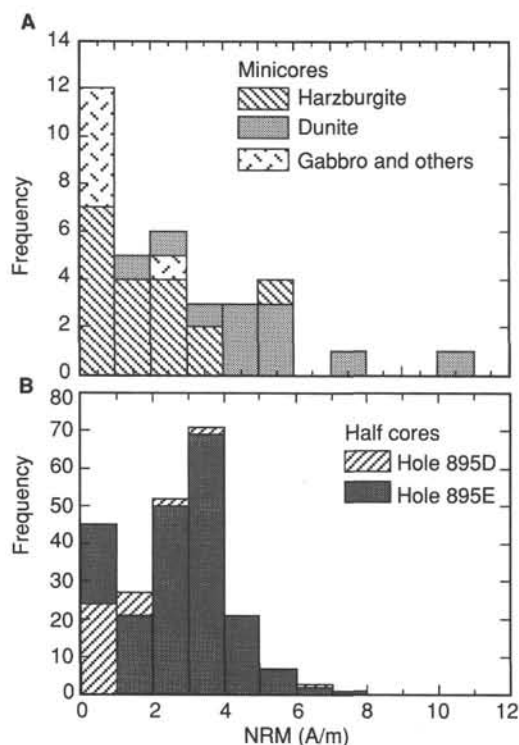


Figure 38. Histograms of NRM intensity. **A.** Minicores from different lithologies. **B.** Half core samples from Holes 895D and 895E.

concentrate on harzburgites and dunites, which make up most of the recovered cores at this site. Thermal demagnetization of a few selected samples showed a distributed unblocking temperature spectrum between room temperature and 600°C (Fig. 42). There was a near-linear decrease in the magnetization with temperature between room temperature and 400°–500°C, above which the demagnetization rate increased slightly. Such distributed unblocking temperatures, at which the magnetization goes to zero between 550° and 600°C, are typical for a sample that contains multidomain magnetite. No other sharp decrease in magnetization, which would suggest that another mineral is contributing to the NRM, occurs. Thus, it is likely that the dominant carrier of remanence in these peridotites is relatively pure magnetite, a finding that is consistent with previous studies of oceanic

peridotites (e.g., Dunlop and Prevot, 1982; Hamano et al., 1990). Thin section observations show that the magnetite present is predominantly a secondary mineral formed during serpentinization (see “Metamorphism” section, this chapter). A relatively pure magnetite in single and pseudosingle domain size that has a Curie temperature between 520° and 580°C was reported as a remanence carrier for a small amount of peridotite recovered during Leg 37 (Dunlop and Prevot, 1982). The Site 895 samples, however, showed a broader distribution for unblocking temperatures than expected, suggesting that a large portion of the NRM is carried by multidomain magnetite. Gabbroic rocks from Hole 894G showed much narrower distributions in the blocking temperatures, which revealed that most of the magnetization was lost between 500° and 600°C (Fig. 42). This indicates that the peridotites have a larger magnetic grain-size distribution than that observed in Hole 894G gabbroic rocks.

The peridotites were relatively easily demagnetized by AF techniques, as shown in Figure 43 for representative samples of dunite and harzburgite. The shapes for the demagnetization curves shown in this figure are also consistent with a multidomain-like magnetic character. The median destructive field (MDF), which is the AF field required to demagnetize half of the NRM, gives an indication of how resistant the sample is to AF demagnetization. A histogram of the MDF values for the peridotites is displayed in Figure 44, in which the samples are broken down into harzburgites and dunites. Actual values are listed in Table 10. The dunites are generally less resistant to AF demagnetization than are the peridotites, as can be seen in Figure 44, although their ranges overlap significantly. The somewhat higher stability against AF demagnetization is also evident from the MDF, which has a mean of 10.3 mT for the dunites and 12.1 mT for harzburgites. The mean MDF value of 11.4 for the peridotites is less than half that observed for the gabbroic rocks at Hole 894G, which had a mean MDF value of 28.6. Obviously the overall magnetic stability of the magnetization of the peridotites is substantially less than that of the gabbroic rocks from Hole 894G.

Direction of Remanent Magnetization

Individual components of magnetization were identified for each minicore using a least-squares fit of each component of magnetization identified on a Zijdeveld diagram (Fig. 45; Zijdeveld, 1967). Approximately half of the samples measured acquired a component of secondary magnetization. In most cases, this secondary magnetization is soft and close to vertical (Table 10 and Fig. 46). In previous studies of DSDP drill cores, near-vertical components of magnetization have been attributed to remanent magnetization acquired during

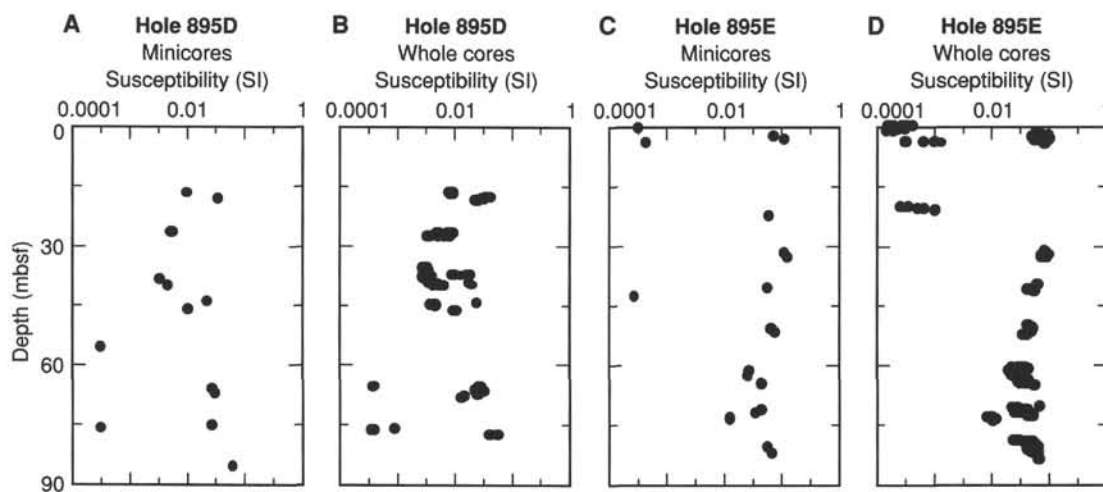


Figure 39. Plots of magnetic susceptibility vs. depth in Holes 895D and 895E.

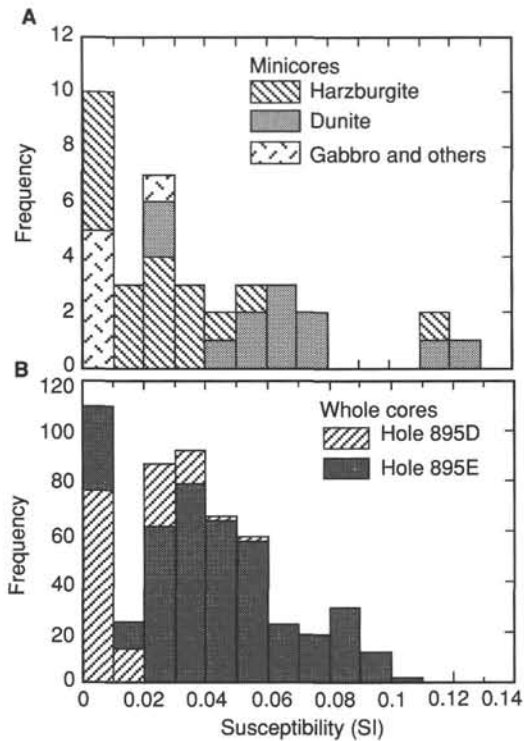


Figure 40. Histograms of magnetic susceptibilities. **A.** Minicores from different lithologies. **B.** Whole core samples from Holes 895D and 895E.

drilling (Ade-Hall and Johnson, 1976; Johnson, 1978; Lowrie and Kent, 1978). Because the magnetization is near vertical, it is unlikely that it was acquired parallel to the ambient geomagnetic field at the latitude of Site 895. Therefore, it seems probable that the secondary magnetization, which was generally small and soft, was indeed acquired during drilling.

Stable magnetic directions were determined for all but four samples. Figure 47 shows the distribution of stable inclination (I_{stable}) values. The median I_{stable} is 36° , similar to the mean I_{stable} value determined for Hole 894G samples. Figure 48 shows the variation of I_{stable} with depth for each hole drilled at Site 895. Although most Site 895 samples have values between 10° and 60° , several samples from Hole 895D have low or negative inclination values. The range of variation for Hole 895D samples (-59° to $+59^\circ$) is much greater than that observed for Holes 895E or 894G (see "Paleomagnetism" section, "Site 894" chapter, this volume). Because the confidence in individual I_{stable} values for Hole 895D minicores samples is high, the wide range of values likely results from penetration into large boulders, or blocks of crust (roughly 10–20 m in scale) that experienced different amounts of tectonic rotation. Upon examination of these data as a function of lithology (Fig. 49), it is apparent that no relationship exists between the lithologic type and the value of I_{stable} . Rather, the scatter in I_{stable} values is more dependent on which hole the sample is from.

Despite the large scatter in I_{stable} values for Hole 895D, most stable inclination values from Site 895 fall within a fairly narrow range. As discussed in the "Paleomagnetism" section of the "Site 894" chapter, the expected magnetic inclination for this latitude is near zero. Minicores from both Sites 894 and 895 have I_{stable} values that are substantially higher than the expected value. It is thus probable that the two crustal sections experienced significant tectonic rotation about a horizontal axis subsequent to acquisition of remanent magnetization. Because the values from both sites are similar (a median I_{stable} value of 36° for Site 895 compared with a mean I_{stable} value of 40° from Hole 894G), both sections probably experienced a similar amount of tectonic rotation. The oxide petrography and magnetic properties

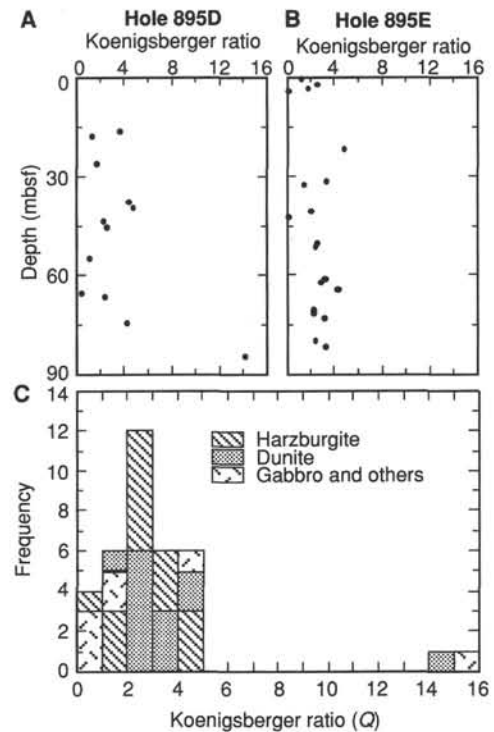


Figure 41. Plot of the Koenigsberger ratio (Q) vs. depth using a value of 33×10^{-6} T for the geomagnetic field intensity at Site 895. **A.** Hole 895D. **B.** Hole 895E. **C.** Histogram of Q for different lithologies.

measurements indicate that the remanent magnetization of both the gabbroic rocks (Hole 894G samples) and harzburgites and dunites (Holes 895D and 895E) is carried by magnetite formed by alteration of silicate minerals (olivine and pyroxene for the gabbroic rocks and olivine for the upper-mantle peridotites). The alteration events that formed the magnetic minerals in these two sections could either be related to hydrothermal alteration that occurred near the ridge axis, or to fracturing that occurred during the opening of Hess Deep.

Anisotropy of Magnetic Susceptibility

The sources of magnetic susceptibility were investigated with the low-temperature magnetic susceptibility method on one harzburgite (Sample 147-895D-3R-1, 45–47 cm) that has a comparatively low room-temperature susceptibility (5.81×10^{-3}). The reciprocal susceptibility vs. temperature curve (Fig. 50) shows a pronounced jump due to the transition from an orthorhombic to a cubic lattice in magnetite at approximately 118 K (Verwey transition). The slightly convex shape of the curve above the transition is typical for a combination of the physical properties of both paramagnetic and ferromagnetic minerals. Quantitative analysis of the curve shows a ferromagnetic contribution of about 70% to the total susceptibility.

The anisotropy of magnetic susceptibility (AMS) results on minicores from Holes 895B to 895E are summarized in Table 11. The samples have a relatively weak anisotropy with a degree of anisotropy ($P = k_{\text{max}}/k_{\text{min}}$) that varies between 1.02 and 1.21 (arithmetic mean: $P = 1.09$). A plot of the principal susceptibility values vs. the bulk susceptibility shows that the regression lines through k_{max} , k_{int} , and k_{min} meet close to the origin of the diagram, suggesting a simple mixture between paramagnetic and ferromagnetic minerals (Fig. 51; Henry and Daly, 1983). The shapes of the susceptibility ellipsoids of all samples are shown in a Flinn-type diagram in Figure 52. The shape of the ellipsoids varies from nearly isotropic (close to the origin of the diagram) to strongly oblate. A few samples have a prolate suscep-

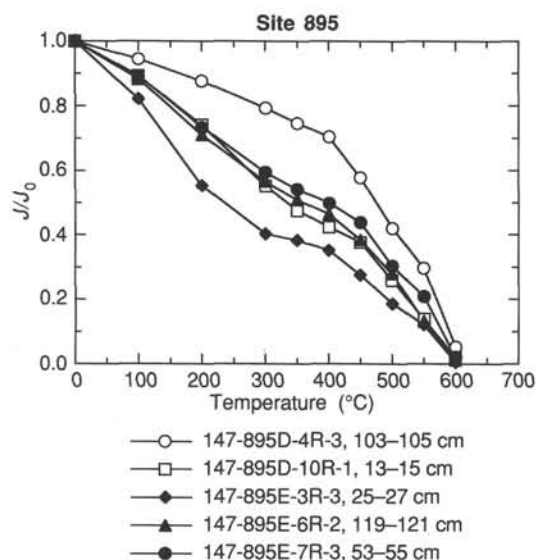


Figure 42. Thermal demagnetization curves of representative samples of dunites (solid symbols) and harzburgites (open symbols). J is the remaining magnetization and J_0 is the initial NRM. The quasilinear decrease in magnetization between room temperature and 600°C suggests that multidomain magnetite is the significant magnetic carrier.

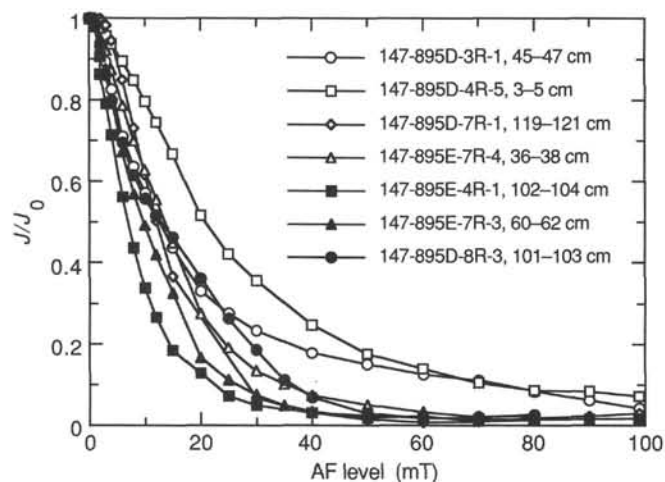


Figure 43. AF demagnetization curves of NRM representing typical dunites (solid symbols) and harzburgites (open symbols). The dunites are generally less resistant to AF demagnetization than the harzburgites, but the ranges overlap significantly.

tibility ellipsoid, but most ellipsoids are triaxial. Because magnetite is the major source of magnetic susceptibility, the AMS ellipsoid represents the overall shape and preferred orientation of magnetite grains. The predominantly triaxial to oblate shapes indicate a planar petrofabric. Figure 53 shows the variation of the degree of anisotropy as a function of depth below seafloor for Holes 895B, 895C, 895D, and 895E. Though some zones of higher and weaker anisotropy exist, the limited number of samples does not permit a conclusive interpretation. The basalt Sample 147-895C-4R-3, 58–60 cm, is basically isotropic. Low anisotropies are found in the altered samples from shallow depths of Hole 895E and a highly altered gabbro (Sample 147-895E-4R-3, 6–8 cm), indicating that alteration has a major effect on the AMS. The principal AMS directions of all minicores with stable paleomagnetic directions are presented in Figure 54A in lower-hemi-

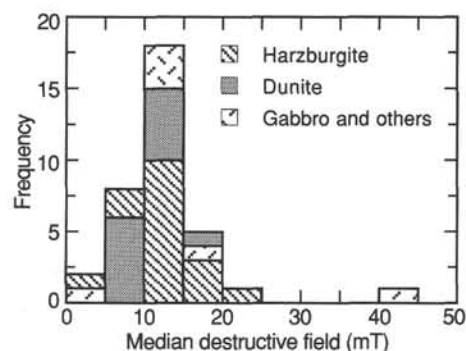


Figure 44. A histogram of the median destructive field (MDF) for all samples for which it could be calculated. The lower mean MDF for the dunites compared with the harzburgites confirms the general observation from Figure 43 that the dunites have a softer remanent magnetization than the harzburgites.

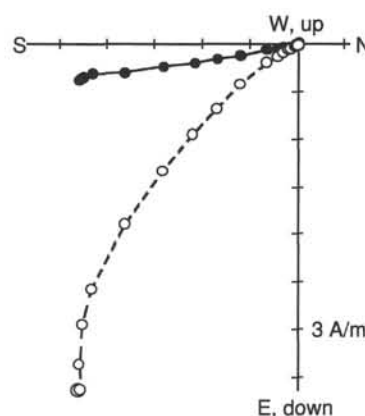


Figure 45. Zijderveld plot for Sample 147-895E-8R-2, 57–59 cm. This sample is typical of many dunites and harzburgites sampled from Site 895D in having a soft secondary component of magnetization. The stable component of magnetization decays to the origin of the Zijderveld plot, but overlaps with the secondary magnetization. Filled circles = projection into the horizontal plane; open circles = vertical plane.

sphere equal-area stereograms. The data are rotated under the assumption that the stable direction points to north. Corrections for the inclination of the stable direction were not performed. A clustering of the axes is not obvious, due to the small number of samples, the weak anisotropy, and uncertainties in the paleomagnetic reorientation. Figures 54B–E show, as examples, the distribution of the principal directions of samples from Hole 895E in more detail. The great circles represent the plane of k_{\max} and k_{\min} (magnetic foliation) with the direction of k_{\max} (magnetic lineation) shown with a short line. Samples from Core 147-895E-1R have northwest-plunging lineations. This core is altered, has low anisotropies (Fig. 54B), and comes from shallow depths. Samples from Cores 147-895E-3R and -4R have shallow plunging north–south striking lineations (Fig. 54C). Samples from Cores 147-895E-5R and -6R have both north–south and east–west-oriented magnetic lineations (Fig. 54A–D). Samples from Cores 147-895E-7R and -8R have south-plunging magnetic lineations (Fig. 54E). Though the fabrics are weak and a macroscopic lineation cannot be determined, the AMS results suggest a north–south-oriented mineral-preferred orientation.

Conclusions

1. The magnetization values obtained from 29 peridotite samples have an arithmetic mean of 3.8 A/m. This average is reduced to 3.0

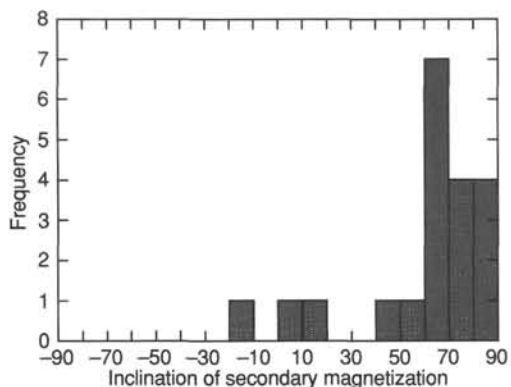


Figure 46. Histogram of the inclination of secondary components of magnetization shows that the majority of secondary components are very steep and positive. It is likely that this near-vertical component is a drilling-induced remanent magnetization.

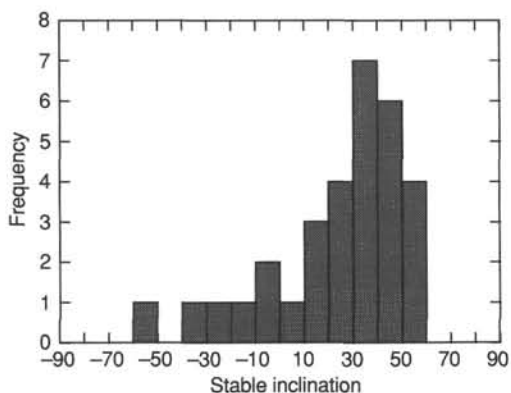


Figure 47. Histogram of the stable magnetic inclination values for Site 895 micrites. The median value is 36° and is similar to that observed for micrites sampled from Hole 894G.

A/m by leaving out a sample with an anomalously high value. This average is similar to previously reported values for DSDP/ODP peridotites. Although the magnetic intensity suggests that peridotites could contribute significantly to marine magnetic anomalies, it is not clear when the peridotites acquired their remanent magnetization (i.e., at the ridge crest or in relation to the opening of Hess Deep).

2. Thermal demagnetization showed that the samples studied have distributed unblocking spectra between room temperature and 600°C, suggesting that a large portion of remanence is carried by relatively pure multidomain magnetite. The samples were soft against AF demagnetization. The peridotites indicated an average MDF value of 11.4 mT. The dunites were in general more easily demagnetized by AF than the harzburgites.

3. Stable magnetic inclination values from Hole 895D samples are widely scattered, suggesting that drilling may have penetrated several large blocks of crust that experienced different degrees of tectonic rotation. In general, however, the stable inclinations from Site 895 fall within a fairly narrow range and have a similar mean value (+36°) to those obtained for Site 894G (+40°). These data suggest that both sites experienced a similar amount of tectonic rotation about a horizontal axis.

4. Low-temperature magnetic susceptibility measurements showed that the major source of magnetic susceptibility is magnetite, which is consistent with the thermal and AF demagnetization observations. The anisotropy of magnetic susceptibility (AMS) represents the overall shape and preferred shape orientation of magnetite. The anisotropy is

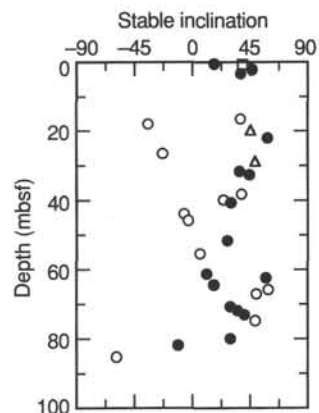


Figure 48. Stable inclination (I_{stable}) values for Holes 895B (square), 895C (triangles), 895D (open circles), and 895E (filled circles) are plotted vs. depth. Although most samples have I_{stable} values between +10° and +60°, many samples from Hole 895D have near horizontal, or negative, inclination values. Because of the high degree of scatter within the Hole 895D samples, it seems likely that drilling penetrated large boulders, or blocks of crust (roughly 10–20 m in scale) that experienced different amounts of tectonic rotation.

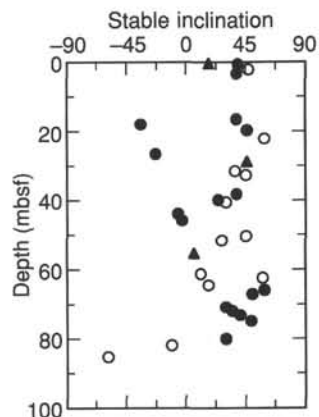


Figure 49. Stable inclination (I_{stable}) values are separated according to lithology and plotted vs. depth. Solid circles = harzburgite samples, open circles = dunite samples, and solid triangles = gabbroic samples. This figure shows that shallow and negative I_{stable} values are not related to a specific lithology.

weak, especially in altered samples and basalts. The ellipsoid shape is mainly triaxial to oblate. Hole 895E has a consistent north-south striking magnetic lineation caused by the preferred orientation of long magnetite axes. This suggests a north-south-oriented extension or flow direction.

PHYSICAL PROPERTIES

The measurements of physical properties of harzburgites, dunites, olivine gabbros, and troctolites recovered from Site 895 are described in the following section. In an attempt to correlate the mineralogical composition of these lower-oceanic-crust and upper-mantle rocks to the physical properties, 47 samples from Holes 895B through 895E were analyzed.

Index Properties

Index property measurements of wet and dry weights and volumes were performed at an approximate frequency of one every other section (1.5 m). Occasionally, where the recovery was good, three or four samples per core were obtained. The measurements were then

Table 12. Index properties of the crystalline rocks recovered from Site 895.

Core, section, interval (cm)	Piece	Depth (mbsf)	Bulk density (g/cm ³)	Grain density (g/cm ³)	Porosity (%)	Water content (%)	Comments
147-895B-1R-1, 64-66	9B	0.64	2.677	2.75	3.99	1.53	Harzburgite (altered 80%)
147-895C-3R-1, 139-141	22	19.69	2.698	2.72	1.36	0.52	Harzburgite (altered 50%)
4R-1, 77-81	12	28.67	2.722	2.75	1.40	0.53	Olivine gabbro (altered 75%)
4R-1, 83-85	12	28.73	2.743	2.77	1.23	0.46	Olivine gabbro (altered 75%)
4R-3, 58-60	6	31.06	2.982	2.98	0.10	0.03	Meta-basalt (amphibolite)
147-895D-2R-1, 47-49	6B	16.47	2.722	2.76	1.96	0.74	Harzburgite (altered 80%-100%)
2R-2, 47-49	3A	17.89	2.616	2.69	4.51	1.77	Harzburgite (altered 85%-100%)
2R-2, 51-55	3A	17.93	2.588	2.68	5.44	2.15	Harzburgite (altered 85%-100%)
3R-1, 45-47	6D	26.45	2.731	2.76	1.65	0.62	Harzburgite (altered 60%)
4R-3, 104-108	12	38.03	2.857	2.87	0.47	0.17	Harzburgite (altered 65%-75%)
4R-3, 110-112	12	38.09	2.833	2.84	0.61	0.22	Harzburgite (altered 65%-75%)
4R-5, 3-5	1	39.76	2.842	2.86	0.74	0.27	Harzburgite (altered 70%)
5R-1, 52-54	8	43.82	2.783	2.80	0.90	0.33	Harzburgite (altered 55%)
5R-2, 100-102	14	45.74	2.669	2.71	2.27	0.87	Harzburgite (altered 60%-70%)
6R-1, 32-34	6	55.32	2.899	2.91	0.39	0.14	Gabbroite
7R-1, 119-121	20A	65.79	2.647	2.68	1.94	0.75	Harzburgite (altered 80%-85%)
7R-1, 123-128	20A	65.83	2.635	2.66	1.72	0.67	Harzburgite (altered 80%-85%)
7R-2, 92-94	12A	66.99	2.504	2.57	4.20	1.72	Harzburgite (altered 85%-100%)
8R-1, 45-47	7	74.75	2.605	2.64	2.38	0.94	Harzburgite (altered 75%-90%)
8R-2, 4-6	1	75.72	2.900	2.90	0.21	0.07	Gabbroite
9R-1, 120-122	18	85.20	2.533	2.58	3.22	1.30	Dunite (altered 90%-100%)
10W-1, 13-15	2		2.534	2.61	4.86	1.97	Dunite (altered >95%)
147-895E-1R-1, 36-41	5A	0.36	2.781	2.79	0.44	0.16	Olivine gabbro (altered 85%)
1R-1, 47-49	5B	0.47	2.781	2.79	0.63	0.23	Olivine gabbro (altered 85%)
1R-2, 72-74	15	2.16	2.517	2.57	3.64	1.48	Dunite (altered 95%)
1R-3, 49-51	4A	3.35	2.550	2.60	3.22	1.29	Harzburgite (altered 85%-90%)
1R-3, 122-124	9	4.08	2.749	2.79	2.01	0.75	Troctolite (altered > 85%)
2R-2, 107-109	15	22.03	2.467	2.56	5.94	2.47	Dunite (altered 95%)
3R-2, 55-57	5	31.52	2.530	2.59	3.61	1.46	Dunite (altered 90%-100%)
3R-3, 14-16	3	32.61	2.535	2.60	4.05	1.64	Dunite (altered 100%)
3R-3, 20-25	3	32.67	2.538	2.60	3.90	1.57	Dunite (altered 100%)
4R-1, 102-104	15B	40.52	2.527	2.60	4.27	1.73	Dunite (altered 100%)
4R-1, 106-110	15C	40.56	2.540	2.62	5.11	2.06	Dunite (altered 100%)
4R-3, 6-9	1	42.47	2.867	2.87	0.29	0.10	Olivine gabbro (altered 70%)
5R-1, 145-147	21	50.35	2.540	2.60	3.42	1.38	Dunite (altered >95%)
5R-2, 115-117	18	51.55	2.527	2.60	4.50	1.83	Dunite (altered >95%)
6R-2, 111-113	7	61.21	2.581	2.61	1.72	0.68	Dunite (altered 95%)
6R-2, 115-120	7	61.25	2.597	2.62	1.56	0.61	Dunite (altered 95%)
6R-3, 101-103	5B	62.32	2.591	2.62	1.73	0.68	Dunite (altered 95%)
6R-5, 66-68	5	64.41	2.560	2.60	2.61	1.04	Dunite (altered 95%-100%)
7R-2, 102-104	11C	70.72	2.573	2.61	2.22	0.88	Harzburgite (altered 95%-100%)
7R-3, 53-58	4B	71.73	2.578	2.62	2.62	1.04	Harzburgite (altered 95%-100%)
7R-3, 60-62	4B	71.80	2.592	2.63	2.19	0.86	Harzburgite (altered 95%-100%)
7R-4, 36-38	4	73.06	2.659	2.68	1.11	0.43	Harzburgite (altered 80%-90%)
8R-2, 57-59	5B	79.96	2.542	2.59	3.05	1.23	Harzburgite (altered 90%)
8R-3, 101-103	6	81.83	2.555	2.60	2.90	1.16	Dunite (altered 100%)
8R-3, 107-111	6	81.89	2.543	2.59	3.11	1.25	Dunite (altered 100%)

Note: Alteration percentages were obtained from visual core descriptions.

used to determine the parameters of wet-bulk density, grain density, porosity, and water content. Results are given in Table 12.

A total of six holes at this site recovered mostly ultramafic rocks (harzburgite and dunite) and a minor quantity of mafic rocks (basaltic dike, olivine gabbro, and troctolite). The mean bulk-density value for the harzburgites is 2.66 g/cm³ with a standard deviation of 0.10 g/cm³, whereas the dunites have a mean of 2.54 g/cm³ and a standard deviation of 0.03 g/cm³. These low values are attributed to the extensive serpentinization observed throughout the rocks recovered from Site 895. The average bulk density of the gabbroic samples (including troctolites) is 2.81 g/cm³ with a standard deviation of 0.07 g/cm³. This value is significantly lower than that obtained for the gabbros from Site 894G. A pervasive style of alteration containing tremolite and prehnite appears to be the main reason for the difference in bulk density between these two sites. Tremolite has been described (see "Metamorphism" section, this chapter) as the main amphibole replacing the pre-existing pyroxenes in these rocks; it has a reported density of 2.86 g/cm³ (Christensen, 1982). Porosity values for the harzburgites have a mean value of 2.31% with a standard deviation of 1.35%; the dunites have a mean of 3.54% and a standard deviation

of 1.22%, whereas the gabbroic rocks have a mean value of 0.82% with a standard deviation of 0.65%. The water content for all the rocks from Site 895 has a mean value of 0.95% with a standard deviation of 0.65%. The range in porosity and water content values corresponds to the amount of alteration, with the dunites being the most altered rocks and having the highest porosity values.

Density-porosity systematics (Fig. 55) show a trend of decreasing density with increasing porosity. This diagram also compares the different rock types. The harzburgites show the widest range in densities and porosities, whereas the dunites have the lowest densities and highest porosities. The most striking feature of the diagram is the apparent change of slope with a change in lithology from harzburgites to dunites. This change might be related to the presence or absence of pyroxene and to different weathering, as well as fracturing patterns between both rock types. A metamorphosed basalt (Sample 147-895C-4R-3, 58-60 cm) has the highest density and lowest porosity values. This sample contains a large percentage of hornblende (60% brown-green amphiboles in thin-section Sample 147-895C-4R-3, 60-64 cm), which has replaced all or most of the clinopyroxenes and destroyed any pre-existing porosity. The average reported density

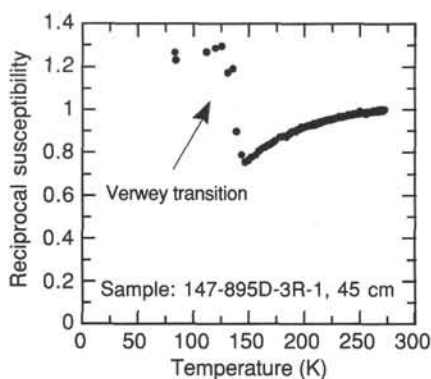


Figure 50. Temperature dependence of the magnetic susceptibility between 77 and 273 K. The transition from orthorhombic to cubic lattice symmetry in magnetite is marked by a susceptibility jump (Verwey transition). Quantification of the curve yields a contribution of 70% ferromagnetic susceptibility (magnetite) to the total susceptibility.

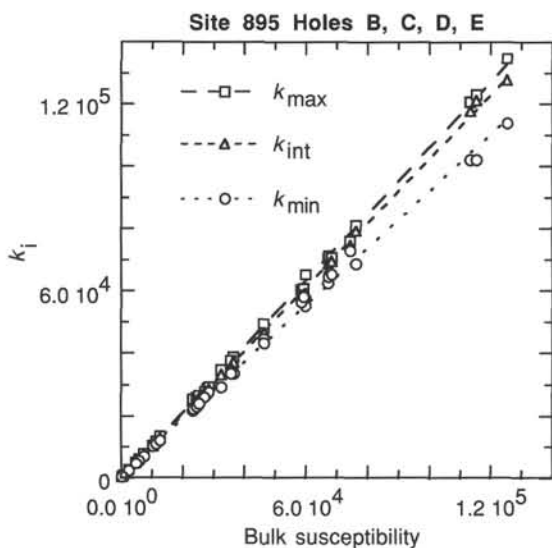


Figure 51. Plot of the principal susceptibility axes vs. the bulk susceptibility shows that the regression lines meet in the origin of the diagram, suggesting a simple mixture between the paramagnetic and the ferromagnetic susceptibilities.

value for hornblende is 3.14 g/cm^3 (Christensen, 1982). The gabbroic rocks show a decreasing trend in density with increasing porosity that can also be attributed to the amount of alteration within these samples.

A comparison of density-porosity relationships with depth for Holes 895D and 895E (Fig. 56) shows a marked difference in rock types and alteration. The main rock type recovered from Hole 895D is harzburgite, with a mean density of 2.70 g/cm^3 with a standard deviation of 0.11 g/cm^3 , whereas Hole 895E is characterized by a predominance of dunite with an average density of 2.54 g/cm^3 and a standard deviation of 0.03 g/cm^3 . The density-porosity profiles show a higher porosity curve and lower density values for the dunites, suggesting a higher tendency to microfracture for the rocks of Hole 895E. Again, the reason for this behavior might be associated with the occurrence of orthopyroxene in the harzburgites, but at this point further studies are needed.

Densities were also determined at 147 points on the Site 895 core using the 2-min discrete GRAPE measurement technique to supplement the minicore determined density information. Figure 57 compares

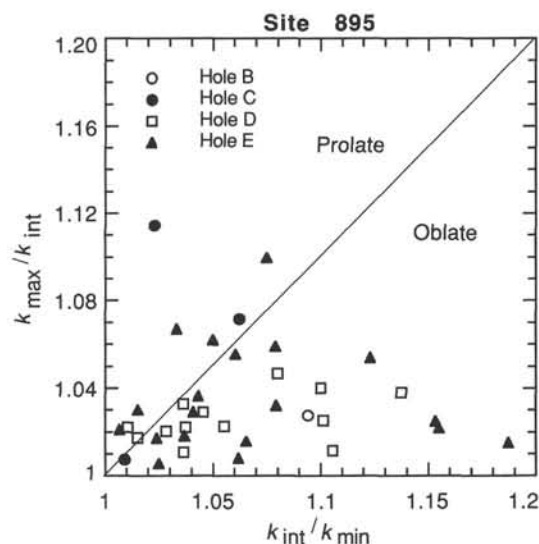


Figure 52. Flinn-type diagram of the AMS ellipsoid shapes of the samples from all holes. The anisotropy is comparatively weak, the shape scatters between spherical and oblate forms, and most ellipsoids are triaxial.

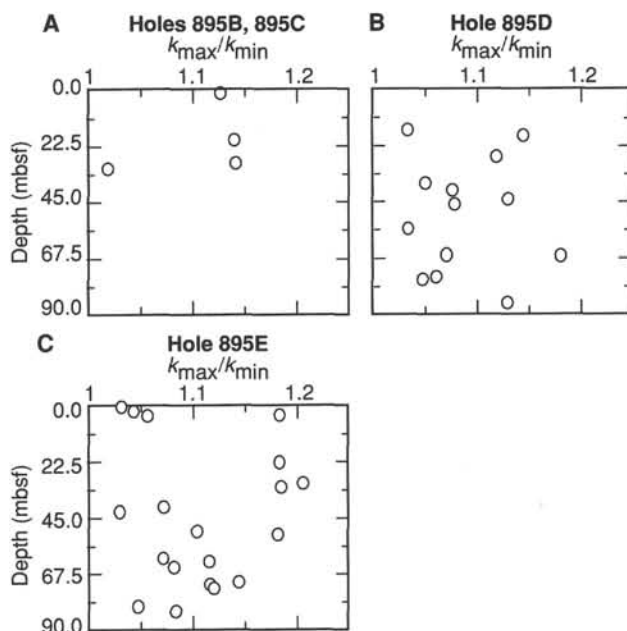


Figure 53. The degree of anisotropy ($P = k_{\text{max}}/k_{\text{min}}$) as a function of depth for Holes 895B through 895E. Isotropic samples with a P ratio close to 1 are a basalt in Hole 895C, the altered samples from shallow depth of Hole 895E, and a highly altered gabbro of Hole 895E.

the density determined in this manner to the pycnometer-determined densities for the 15 measurements from Site 895 in which a minicore was taken within 5 cm of a discrete GRAPE measurement. A shift needs to be applied to the GRAPE-determined densities to account for the gamma-ray beam passing through the core some distance above the core center line. This is necessary because the core tray was aligned for larger-diameter sediment cores. The minicore wet-bulk densities in the Site 895 data set are higher by a mean shift of 0.09 g/cm^3 and a median shift of 0.10 g/cm^3 . This compares with a mean shift of 0.11 g/cm^3 and a median shift of 0.09 g/cm^3 for the 12

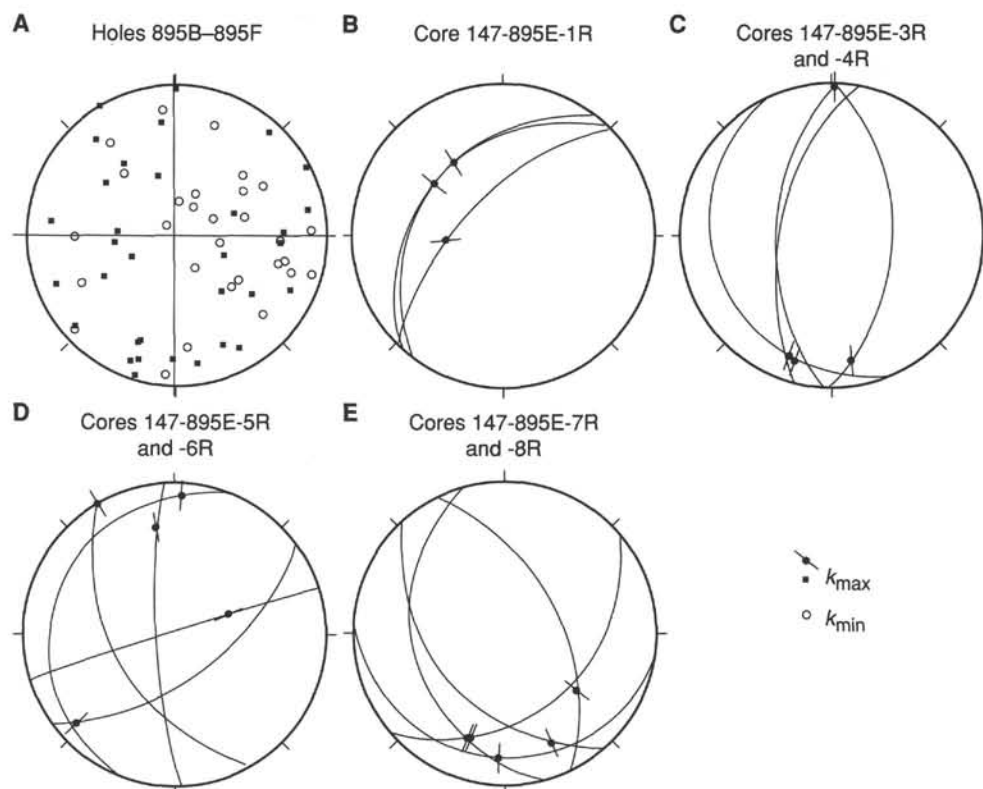


Figure 54. Orientation of the principal susceptibility directions in lower hemisphere equal area stereograms. **A.** Maximum and minimum axes rotated under the assumption that the stable paleomagnetic direction pointed to the N. Maximum axes have an intermediate to shallow plunge. **B–E.** The magnetic foliations (k_{\max} - k_{\min} planes) of the susceptibility ellipsoids from samples from Hole 895E rotated into magnetic N; circles are magnetic lineations (k_{\max}). The lineations are shallow with a predominantly north-south strike.

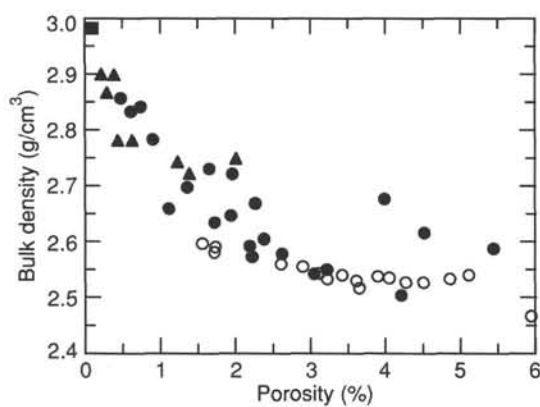


Figure 55. Density-positivity relationships for the crystalline rocks from Site 895. Open circles = dunite; filled circles = harzburgite; triangles = gabbro; square = metamorphosed basalt.

comparison samples from Site 894. A constant shift of 0.10 g/cm^3 has been applied to the tabulated GRAPE data (Table 13 and Fig. 58) as was done with the Site 894 GRAPE data. The quartz and air calibrations, as discussed in the “Explanatory Notes” chapter of this volume, were consistent throughout, giving a Compton attenuation coefficient (Qtz_p) of 0.0782. The quartz calibration sample thickness of 50.15 mm is considered sufficiently close to the 55-mm typical core thickness such that no sample diameter correction is needed, and porosities were low enough that no apparent water density correction is needed.

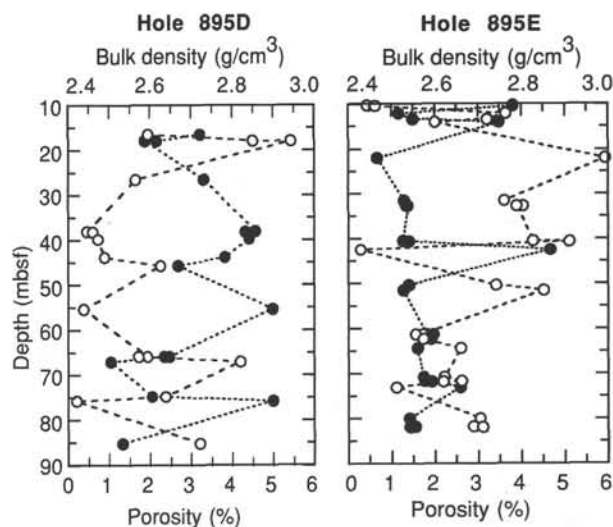


Figure 56. Density and porosity values as a function of depth for minicore data from Holes 895D and 895E. Solid symbols = bulk density; open symbols = porosity measurements on the same minicore samples.

Compressional-wave Velocities

Compressional-wave velocity measurements at atmospheric pressure and ambient temperature were performed on minicore samples with an approximate diameter of 25 mm and lengths varying from 17 mm to 35 mm. Individual velocity determinations were attempted in a

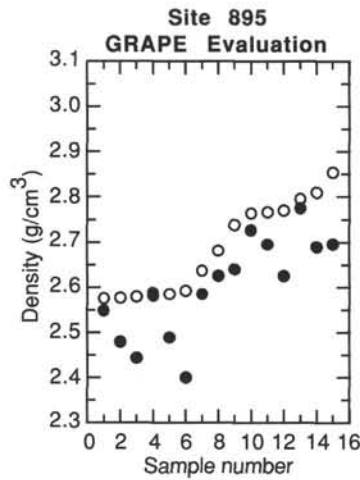


Figure 57. GRAPE density (solid symbols) evaluation diagram showing a comparison with minicore bulk density data (open symbols) for similar depth intervals.

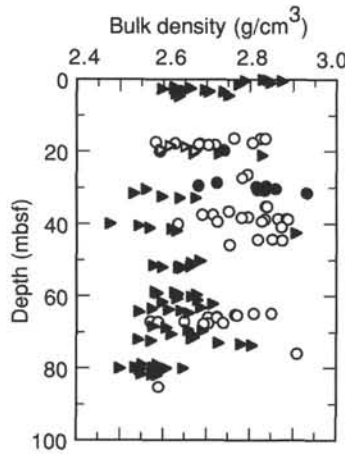


Figure 58. Corrected GRAPE density as a function of depth for all the holes at Site 895. Solid circles = Hole C; open circles = Hole D data; solid triangles = Hole E; and open triangles = Hole F.

vertical direction or parallel to the core and a horizontal orientation or orthogonal to the core split plane (see the "Physical Properties" section, "Explanatory Notes" chapter, this volume). The results of directional velocity measurements for discrete samples are given in Table 14.

The mean horizontal velocity value for harzburgite is 5558 m/s with a standard deviation of 535 m/s, whereas dunite has a mean of 4946 m/s with a standard deviation of 298 m/s. The mean horizontal velocity for the gabbroic rocks from Site 895 is 6488 m/s with a standard deviation of 574 m/s and with values ranging from 7000 m/s to 5588 m/s. This mean value is somewhat lower than the value obtained for the gabbroic rocks from Hole 894G, implying a higher degree of alteration for the rocks of Site 895, although the range of values falls well within previously reported measurements for oceanic gabbros (Christensen, 1982; Robinson, Von Herzen, et al., 1989; Iturrino et al., 1991).

The low mean values for both the harzburgites and dunites reflect the high degree of serpentinization observed in these samples. A velocity-density plot (Fig. 59) shows a cluster of points representing the dunite samples with velocities ranging from approximately 5500 m/s to 4500 m/s, whereas harzburgite displays a much wider velocity range. The gabbroic samples and the metamorphosed basalt define the higher end in a fairly linear trend that shows a significant decrease in velocities with an increase in alteration. A velocity-porosity plot

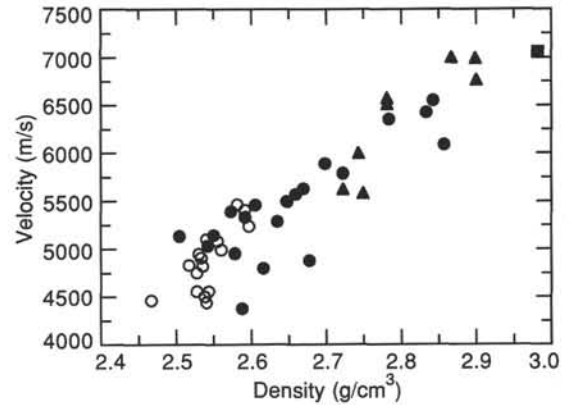


Figure 59. Velocity-density relationship for the crystalline rocks from Site 895. Open circles = dunite; filled circles = harzburgite; triangles = gabbro; square = metamorphosed basalt.

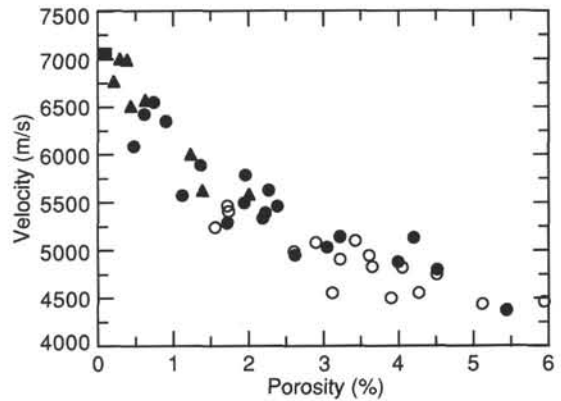


Figure 60. Velocity-porosity systematics for the crystalline rocks from Site 895. Open circles = dunite; filled circles = harzburgites; triangles = gabbro; square = metamorphosed basalt.

(Fig. 60) shows a similar linear trend of decreasing velocity with increasing porosity. This relationship also shows that the most altered dunite samples have the highest porosity and lowest velocity values.

A basic assessment of velocity anisotropy is possible using the values from adjacent and mutually orthogonal samples (Fig. 61). The velocity-density systematics for the adjacent perpendicular minicores from Site 895 show a consistent trend of lower vertical velocities with respect to their corresponding horizontal pair. At this point, we can only suggest that these variations might be caused by either subhorizontal to horizontal preferred microcrack orientation or due to preferred mineral orientation within the observed foliation and serpentine fabric (see "Structure" section, this chapter).

Electrical Resistivity

Measurements of the electrical resistivity of oceanic rocks are useful for the interpretation of oceanic electromagnetic induction data and borehole resistivity logs, as well as for providing a measure of the type of porosity in the rock. During Leg 147, the resistivities of a series of the most altered samples were obtained at atmospheric pressure and temperature.

Electrical resistivity measurements performed in water-saturated minicores (Table 14) show a strong inverse correlation with porosity, suggesting that ionic pore-fluid conduction dominates in these samples with the dunites having the lowest resistivity. The values range from 4013 Ωm to 13 Ωm ; most of the measurements fall within the

Table 13. Minicore bulk density and 2-minute GRAPE data obtained for rocks drilled at Site 895.

Core, section, interval (cm)	Depth (mbsf)	Quartz counts	Core counts	Density (g/cm ³)	Diameter (cm)	Air counts	Core, section, interval (cm)	Depth (mbsf)	Quartz counts	Core counts	Density (g/cm ³)	Diameter (cm)	Air counts
147-895C-							1R-4, 7	4.57		1.412E+05	2.65	5.650	
3R-1, 141	19.69	1.603E+05	1.491E+05	2.64	5.412	4.538E+05	1R-4, 24	4.74	1.605E+05	1.528E+05	2.54	5.505	4.546E+05
3R-2, 18	19.96	1.612E+05	1.568E+05	2.49	5.475	4.536E+05	2R-1, 99	20.59		1.463E+05	2.57	5.650	4.534E+05
4R-1, 84	28.72		1.465E+05	2.63	5.529		2R-1, 106	20.66		1.457E+05	2.63	5.545	
4R-2, 8	29.46		1.478E+05	2.58	5.578		2R-2, 6	21.16	1.607E+05	1.384E+05	2.73	5.585	
4R-2, 28	29.66		1.386E+05	2.74	5.558		3R-1, 90	30.50		1.530E+05	2.46	5.670	
4R-2, 43	29.81		1.374E+05	2.72	5.645		3R-2, 54	31.64		1.559E+05	2.43	5.640	
4R-2, 66	30.04		1.368E+05	2.74	5.621		3R-2, 135	32.45		1.509E+05	2.50	5.660	
4R-2, 100	30.38		1.372E+05	2.76	5.560		3R-3, 25	32.85		1.481E+05	2.58	5.580	
4R-2, 112	30.50		1.361E+05	2.72	5.681		3R-3, 30	32.90	1.609E+05	1.478E+05	2.54	5.670	4.536E+05
4R-2, 129	30.67		1.364E+05	2.73	5.640		4R-1, 46	39.96		1.604E+05	2.38	5.615	4.531E+05
4R-3, 58	31.46		1.316E+05	2.83	5.608		4R-1, 101	40.51		1.576E+05	2.44	5.556	
							4R-2, 13	41.13		1.529E+05	2.47	5.655	
147-895D-							4R-2, 44	41.44		1.540E+05	2.52	5.505	
2R-1, 41	16.41		1.376E+05	2.66	5.750		4R-2, 93	41.93		1.489E+05	2.53	5.650	
2R-1, 51	16.51		1.318E+05	2.73	5.819		4R-3, 4	42.54	1.603E+05	1.347E+05	2.81	5.550	4.540E+05
2R-1, 59	16.59		1.311E+05	2.74	5.821		5R-1, 143	50.33		1.453E+05	2.59	5.650	
2R-2, 5	17.55		1.523E+05	2.48	5.643		5R-1, 136	50.26		1.466E+05	2.59	5.610	
2R-2, 12	17.62		1.374E+05	2.71	5.666		5R-2, 47	50.87		1.462E+05	2.57	5.665	
2R-2, 28	17.78		1.473E+05	2.53	5.715		5R-2, 115	51.55		1.556E+05	2.48	5.545	
2R-2, 44	17.94		1.399E+05	2.59	5.840		5R-2, 136	51.76		1.514E+05	2.54	5.550	
2R-2, 51	18.01		1.411E+05	2.58	5.803		5R-2, 139	51.79		1.489E+05	2.56	5.580	
2R-2, 69	18.19		1.410E+05	2.62	5.725		5R-3, 12	52.02		1.550E+05	2.50	5.520	
2R-2, 80	18.30	1.606E+05	1.397E+05	2.60	5.805	4.534E+05	5R-3, 23	52.13		1.508E+05	2.54	5.575	
3R-1, 44	26.45		1.334E+05	2.69	5.830	4.538E+05	5R-3, 35	52.25	1.600E+05	1.518E+05	2.54	5.530	4.532E+05
3R-1, 131	27.31	1.609E+05	1.339E+05	2.68	5.834	4.533E+05	6R-2, 22	58.82		1.560E+05	2.48	5.525	
4R-1, 43	35.13		1.316E+05	2.74	5.803		6R-2, 35	58.95		1.529E+05	2.53	5.525	
4R-1, 48	35.18		1.317E+05	2.74	5.790		6R-2, 61	59.21		1.553E+05	2.49	5.535	
4R-2, 25	36.45		1.348E+05	2.65	5.870		6R-2, 85	59.45		1.520E+05	2.53	5.540	
4R-2, 125	37.45		1.395E+05	2.59	5.842		6R-2, 110	59.70		1.472E+05	2.58	5.605	
4R-2, 129	37.49		1.386E+05	2.62	5.820		6R-2, 116	59.76		1.516E+05	2.53	5.560	
4R-3, 44	38.14		1.341E+05	2.70	5.801		6R-3, 10	60.20		1.478E+05	2.57	5.610	
4R-3, 56	38.26		1.342E+05	2.68	5.830		6R-3, 57	60.67		1.500E+05	2.53	5.610	
4R-3, 81	38.51		1.294E+05	2.77	5.820		6R-3, 104	61.14		1.483E+05	2.58	5.565	
4R-3, 95	38.65		1.298E+05	2.79	5.764		6R-4, 7	61.67		1.563E+05	2.50	5.480	
4R-3, 105	38.75		1.291E+05	2.79	5.783		6R-4, 57	62.17		1.461E+05	2.62	5.560	
4R-3, 111	38.81		1.304E+05	2.74	5.850		6R-5, 11	63.21		1.459E+05	2.59	5.630	
4R-4, 11	39.31		1.322E+05	2.73	5.800		6R-5, 41	63.51		1.532E+05	2.47	5.635	
4R-4, 18	39.38		1.379E+05	2.63	5.820		6R-5, 71	63.81		1.513E+05	2.51	5.610	
4R-4, 86	40.05		1.432E+05	2.53	5.840		6R-5, 93	64.03		1.528E+05	2.54	5.500	
4R-5, 8	40.78	1.606E+05	1.309E+05	2.77	5.750	4.541E+05	6R-5, 100	64.28		1.547E+05	2.44	5.650	
5R-1, 93	44.24		1.280E+05	2.75	5.900		6R-6, 7	64.67	1.600E+05	1.468E+05	2.56	5.660	4.541E+05
5R-1, 99	44.29		1.351E+05	2.72	5.720		7R-1, 15	68.35		1.569E+05	2.48	5.505	
5R-1, 120	44.50		1.295E+05	2.77	5.800		7R-1, 58	68.78		1.516E+05	2.51	5.615	
5R-2, 103	45.83	1.610E+05	1.368E+05	2.65	5.800	4.542E+05	7R-1, 118	69.38		1.466E+05	2.56	5.670	
7R-1, 18	64.78		1.311E+05	2.75	5.790		7R-1, 138	69.58		1.433E+05	2.59	5.710	
7R-1, 24	64.84		1.319E+05	2.71	5.850		7R-2, 86	70.56		1.494E+05	2.52	5.660	
7R-1, 50	65.10		1.371E+05	2.67	5.759		7R-2, 108	70.78		1.465E+05	2.57	5.650	
7R-1, 66	65.26		1.342E+05	2.67	5.852		7R-3, 28	71.48		1.468E+05	2.57	5.630	
7R-1, 123	65.83		1.395E+05	2.62	5.765		7R-3, 66	71.86		1.464E+05	2.57	5.660	
7R-1, 127	65.87		1.398E+05	2.60	5.800		7R-3, 83	72.03		1.563E+05	2.44	5.600	
7R-1, 134	65.94		1.382E+05	2.62	5.815		7R-3, 123	72.43		1.555E+05	2.47	5.560	
7R-2, 96	67.06		1.497E+05	2.47	5.760		7R-4, 27	72.97		1.459E+05	2.63	5.540	
7R-2, 93	67.03		1.447E+05	2.55	5.755		7R-4, 56	73.26		1.412E+05	2.68	5.590	
7R-2, 111	67.21		1.491E+05	2.49	5.740		7R-4, 89	73.59	1.601E+05	1.408E+05	2.71	5.550	4.541E+05
7R-2, 132	67.42		1.370E+05	2.64	5.825		8R-1, 102	78.92		1.596E+05	2.45	5.475	4.541E+05
7R-2, 141	67.51		1.404E+05	2.60	5.780		8R-1, 116	79.05	1.611E+05	1.527E+05	2.49	5.622	4.551E+05
7R-3, 12	67.72	1.618E+05	1.407E+05	2.59	5.795	4.546E+05	8R-2, 36	79.76		1.568E+05	2.48	5.508	
8R-2, 7	75.87	1.607E+05	1.280E+05	2.81	5.780	4.544E+05	8R-2, 41	79.81		1.605E+05	2.44	5.478	
9R-1, 119	85.19	1.607E+05	1.517E+05	2.49	5.650	4.539E+05	8R-2, 52	79.92		1.561E+05	2.50	5.479	
							8R-2, 57	79.97		1.617E+05	2.40	5.520	
147-895E-							8R-2, 61	80.01		1.593E+05	2.45	5.495	
1R-1, 16	0.16		1.334E+05	2.73	5.750		8R-2, 65	80.05		1.503E+05	2.55	5.570	
1R-1, 24	0.24		1.353E+05	2.74	5.665		8R-2, 69	80.09		1.529E+05	2.51	5.571	
1R-1, 40	0.40		1.420E+05	2.69	5.545		8R-2, 96	80.36		1.559E+05	2.45	5.609	
1R-1, 50	0.50		1.338E+05	2.77	5.645		8R-3, 25	81.15		1.554E+05	2.47	5.560	
1R-1, 105	1.05		1.366E+05	2.75	5.605		8R-3, 45	81.35		1.527E+05	2.48	5.630	
1R-1, 139	1.39		1.442E+05	2.67	5.500		8R-3, 73	81.63		1.568E+05	2.45	5.570	
1R-2, 77	2.27		1.495E+05	2.53	5.640		8R-3, 86	81.76		1.579E+05	2.48	5.475	
1R-2, 109	2.59		1.480E+05	2.56	5.610		8R-3, 106	81.96		1.548E+05	2.49	5.554	
1R-2, 116	2.66		1.503E+05	2.53	5.615								
1R-2, 126	2.76		1.512E+05	2.50	5.650		147-895F-						
1R-3, 10	3.10		1.458E+05	2.60	5.610		2R-1, 35	18.55		1.494E+05	2.52	5.665	
1R-3, 24	3.24		1.480E+05	2.55	5.640		2R-1, 62	18.82		1.451E+05	2.55	5.735	
1R-3, 48	3.48		1.446E+05	2.61	5.630		2R-1, 144	19.64		1.479E+05	2.50	5.765	
1R-3, 54	3.54		1.427E+05	2.64	5.625		2R-2, 28	19.98	1.605E+05	1.461E+05	2.57	5.650	4.522E+05
1R-3, 99	3.99		1.510E+05	2.53	5.585								

Table 14. Directional compressional-wave velocity and resistivity measurements of the crystalline rocks from Site 895.

Core, section, interval (cm)	Piece number	Depth (mbsf)	V _p (h) (m/s)	V _p (v) (m/s)	Resistivity (ohm-m)	Comments
147-895B-1R-1, 64-66	9B	0.64	4884		36.98	Harzburgite (altered 80%)
147-895C-3R-1, 139-141	22	19.69	5895		136.64	Harzburgite (altered 50%)
4R-1, 77-81	12	28.67		5627		Olivine gabbro (altered 75%)
4R-1, 83-85	12	28.73	6003		129.37	Olivine gabbro (altered 75%)
4R-3, 58-60	6	31.06	7056		248.05	Meta-basalt (amphibolite)
147-895D-2R-1, 47-49	6B	16.47	5793		116.99	Harzburgite (altered 80%-100%)
2R-2, 47-49	3A	17.89	4802		0.19	Harzburgite (altered 85%-100%)
2R-2, 51-55	3A	17.93		4379		Harzburgite (altered 85%-100%)
3R-1, 45-47	6D	26.45				Harzburgite (altered 60%)
4R-3, 104-108	12	38.03		6090		Harzburgite (altered 65%-75%)
4R-3, 110-112	12	38.09	6428		229.88	Harzburgite (altered 65%-75%)
4R-5, 3-5	1	39.76	6555		620.29	Harzburgite (altered 70%)
5R-1, 52-54	8	43.82	6355		345.19	Harzburgite (altered 55%)
5R-2, 100-102	14	45.74	5632		193.36	Harzburgite (altered 60%-70%)
6R-1, 32-34	6	55.32	6992		4012.51	Gabbro
7R-1, 119-121	20A	65.79	5499		129.64	Harzburgite (altered 80%-85%)
7R-1, 123-128	20A	65.83		5290		Harzburgite (altered 80%-85%)
7R-2, 92-94	12A	66.99	5136		38.35	Harzburgite (altered 85%-100%)
8R-1, 45-47	7	74.75	5463		75.79	Harzburgite (altered 75%-90%)
8R-2, 4-6	1	75.72	6768		2321.50	Gabbro
9R-1, 120-122	18	85.20	4909		49.33	Dunite (altered 90%-100%)
147-895E-1R-1, 36-41	5A	0.36		6513		Olivine gabbro (altered 85%)
1R-1, 47-49	5B	0.47	6574		194.96	Olivine gabbro (altered 85%)
1R-2, 72-74	15	2.16	4834		26.35	Dunite (altered 95%)
1R-3, 49-51	4A	3.35	5147		32.28	Harzburgite (altered 85%-90%)
1R-3, 122-124	9	4.08	5588		56.34	Troctolite (altered > 85%)
2R-2, 107-109	15	22.03	4464		35.21	Dunite (altered 95%)
3R-2, 55-57	5	31.52	4949		13.75	Dunite (altered 90%-100%)
3R-3, 14-16	3	32.61	4823		19.29	Dunite (altered 100%)
3R-3, 20-25	3	32.67		4505		Dunite (altered 100%)
4R-1, 102-104	15B	40.52	4560		24.84	Dunite (altered 100%)
4R-1, 106-110	15C	40.56		4442		Dunite (altered 100%)
4R-3, 6-9	1	42.47	7000		279.10	Olivine gabbro (altered 70%)
5R-1, 145-147	21	50.35	5103			Dunite (altered >95%)
5R-2, 115-117	18	51.55	4753		13.22	Dunite (altered >95%)
6R-2, 111-113	7	61.21	5467		107.88	Dunite (altered 95%)
6R-2, 115-120	7	61.25		5243		Dunite (altered 95%)
6R-3, 101-103	5B	62.32	5407		112.53	Dunite (altered 95%)
6R-5, 66-68	5	64.41	4927		66.14	Dunite (altered 95%-100%)
7R-2, 102-104	11C	70.72	5393		49.96	Harzburgite (altered 95%-100%)
7R-3, 53-58	4B	71.73		4957		Harzburgite (altered 95%-100%)
7R-3, 60-62	4B	71.80	5336		61.86	Harzburgite (altered 95%-100%)
7R-4, 36-38	4	73.06	5574		191.69	Harzburgite (altered 80%-90%)
8R-2, 57-59	5B	79.96	5035		21.63	Harzburgite (altered 90%)
8R-3, 101-103	6	81.83	5087			Dunite (altered 100%)
8R-3, 107-111	6	81.89		4560		Dunite (altered 100%)

Note: Alteration percentages were obtained from visual core descriptions.

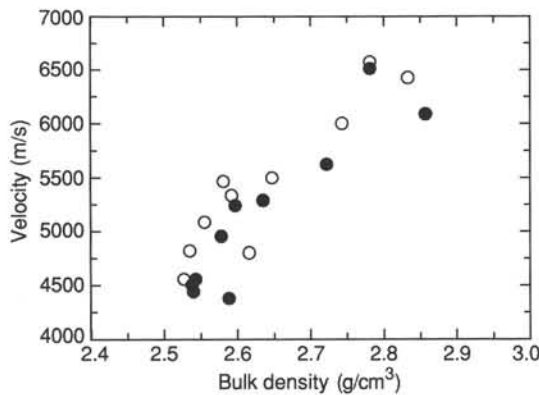


Figure 61. Velocity-density systematics for horizontal and adjacent vertical minicores. Open circles = horizontal velocities; solid circles = vertical velocities.

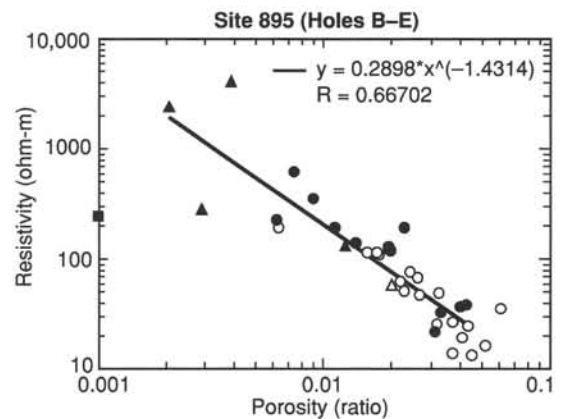


Figure 62. Resistivity-porosity relationship for the crystalline rocks from Site 895. Open circles = dunite; filled circles = harzburgites; closed triangles = gabbro; open triangles = troctolite; square = metamorphosed basalt. Line represents best fit to the data points.

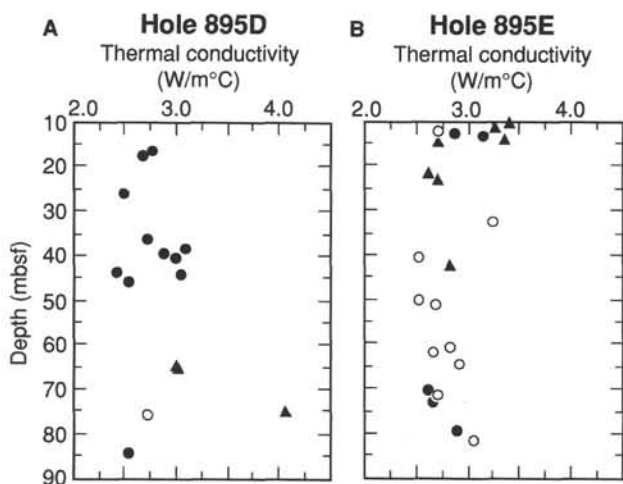


Figure 63. Thermal conductivity as a function of depth for samples from Holes 895D and 895E. Open circles = dunite; filled circles = harzburgite; triangles = gabbro.

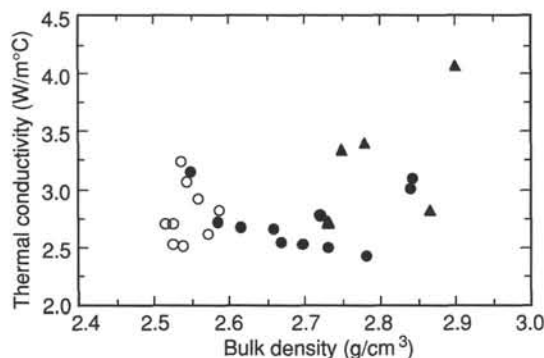


Figure 64. Thermal conductivity–bulk density systematics for samples with minicore density information. Open circles = dunite; filled circles = harzburgite; triangles = gabbro.

low end of the range of values previously measured at Site 894G. These data provide some of the first such measurements on serpentinized oceanic peridotites. Only one other such measurement was found in the ocean drilling literature (Hyndman and Drury, 1977).

Previous workers (Hyndman and Drury, 1977; Kirkpatrick, 1979; Cann and Von Herzen, 1983; Hyndman et al., 1984; Smith and Vine, 1987; Broglia and Moos, 1988; Pezard et al., 1991) have examined the relationship between porosity and resistivity in oceanic basalts, gabbros, and one peridotite using Archie's Law:

$$R_0 = (a R_w) / (\phi^m),$$

where R_0 is the measured resistivity of the saturated sample, R_w is the resistivity of the pore fluid, ϕ is the porosity expressed as a ratio of the rock volume, a is an empirical constant and m is the cementation exponent. To compare our results with those of previous workers, we plot the formation factor (R_0/R_w) vs. porosity as a ratio where $R_w = 0.20 \Omega\text{m}$, the resistivity of seawater at laboratory temperature (Fig. 62). Rearranging Archie's Law:

$$m = \log(a R_w/R_0) / \log(\phi),$$

where we can see that m is the slope on a log-log plot and that a is a shift of the line, which is allowed to vary to best fit the data. The most

recent studies (Broglia and Moos, 1988; Pezard et al., 1991) attach no significance to the value of a , whereas earlier studies (Hyndman et al., 1984; Smith and Vine, 1987) held a fixed at 1, a common value for sedimentary rocks. The best-fit line, after two anomalous points were thrown out, gives an m of 1.43 and an a of 1.4. The determination of m may be useful in that theoretical modelling using arrays of resistors (Shankland and Waff, 1974) suggests that m should be 1 for conduction through narrow fluid-filled cracks, whereas m should be 2 for conduction through spherical, randomly connected pores. Problems with this type of analysis include the effects of more highly conductive "bound water" or highly conductive minerals lining porosity. Such problems have been addressed with more complex models in sedimentary rocks (Serra, 1984) and in oceanic gabbros from Site 735B (Pezard et al., 1991). There is no apparent trend in either the measured resistivity values or the parameter m with depth at Site 895 or any significant shift in the data by hole. Variability by rock type can also be seen in Figure 62.

Thermal Conductivity

Thermal conductivity measurements, made on 45 samples from Site 895 (Table 15), have a mean value of 2.83 W/m°C. The harzburgites have a mean value of 2.73 W/m°C with a standard deviation of 0.22 W/m°C, whereas the dunites have an average value of 2.78 W/m°C with a standard deviation of 0.22 W/m°C. The mean value for the gabbroic samples (including troctolites) is 3.02 W/m°C with a standard deviation of 0.40 W/m°C. This value is significantly higher than the values recorded for samples from Hole 894G. In this case, the increase in thermal conductivity values might be attributed to increased olivine content in the samples from Site 895. A plot of thermal conductivity as a function of depth for Holes 895D and 895E (Figs. 63A and 63B) clearly shows the variability in conductivity between the gabbros, harzburgites, and dunites.

Previous measurements on serpentinites (Detrick, Honnorez, Bryan, Juteau, et al., 1988) show relatively high variations. Therefore, the distinctive high thermal conductivity values and variations for the harzburgites and dunites of Site 895 can be attributed to the range of serpentinization observed in these rocks. However, a plot of thermal conductivity as a function of minicore measured densities (Fig. 64) shows a cluster of points representing the dunite samples, which display variations in thermal conductivity without any significant changes in density. This indicates that the variations in thermal conductivity are not solely caused by the amount of serpentine but are perhaps also due to other product characteristics related to the serpentinization process. Thermal conductivity measurements from Site 735B (Robinson, Von Herzen et al., 1989) show a decrease in conductivity with an increase in Fe-Ti oxides; hence, the variations might be due to the presence of secondary oxides, although this has not been confirmed. The variations displayed by the gabbros from Site 895 follow a trend of decreasing thermal conductivity with decreasing density, as do those from Hole 894G. Finally, the harzburgites have the widest range in densities but do not show any apparent correlation with thermal conductivity.

REFERENCES*

- Ade-Hall, J.M., and Johnson, H.P., 1976. Paleomagnetism of basalts, Leg 34. In Yeats, R.S., Hart, S.R., et al., *Init. Repts. DSDP*, 34: Washington (U.S. Govt. Printing Office), 513–532.
- Allan, J.F., Batiza, R., Perfit, M.R., Fornari, D.J., and Sack, R.O., 1989. Petrology of lavas from the Lamont seamount chain and adjacent East Pacific Rise, 10°N. *J. Petrol.*, 30:1245–1298.

* Abbreviations for names of organizations and publication titles in ODP reference lists follow the style given in *Chemical Abstracts Service Source Index* (published by American Chemical Society).

- Bideau, D., Hébert, R., Hekinian, R., and Cannat, M., 1991. Metamorphism of deep-seated rocks from the Garret Ultrafast Transform (East Pacific Rise near 13°25'S). *J. Geophys. Res.*, 96:10079–10099.
- Bloomer, S.H., Natland, J.H., and Fisher, R.L., 1989. Mineral relationships in gabbroic rocks from fracture zones of Indian Ocean Ridges: evidence for extensive fractionation, parental diversity, and boundary-layer recrystallization. In Saunders, A.D., and Norry, M.J. (Eds.), *Magma-tism in the Oceanic Basins*. Geol. Soc. Spec. Publ. London, 42:107–124.
- Bonatti, E., Peyve, A., Kepezhinskas, P., Kurentsova, N., Seyler, M., Skolotnev, S., and Udintsev, E., 1992. Upper mantle heterogeneity below the Mid-Atlantic Ridge, 0°–15°N. *J. Geophys. Res.*, 97:4461–4476.
- Brogliola, C., and Moos, D., 1988. *In-situ* structure and properties of 110-Ma crust from geophysical logs in DSDP Hole 418A. In Salisbury, M.H., Scott, J.H., et al., *Proc. ODP, Sci. Results*, 102: College Station, TX (Ocean Drilling Program), 29–47.
- Cann, J.R., and Von Herzen, R.P., 1983. Downhole logging at Deep Sea Drilling Program Sites 501, 504, and 505, near the Costa Rica Rift. In Cann, J.R., Langseth, M.G., Honnorez, J., Von Herzen, R.P., White, S.M., et al., *Init. Repts. DSDP*, 69: Washington (U.S. Govt. Printing Office), 281–300.
- Cannat, M., Bideau, D., and Bougault, H., 1992. Serpentinized peridotites and gabbros in the Mid-Atlantic Ridge axial valley at 15°37'N and 16°52'N. *Earth Planet. Sci. Lett.*, 109:87–106.
- Cannat, M., Bideau, D., and Hébert, R., 1990. Plastic deformation and magmatic impregnation in serpentinized ultramafic rocks from the Garrett transform fault (East Pacific Rise). *Earth Planet. Sci. Lett.*, 101:216–232.
- Christensen, N.I., 1982. Seismic velocities. In Carmichael, R.S. (Ed.), *Handbook of Physical Properties of Rocks*: Boca Raton, FL (CRC Press), 2:1–228.
- Detrick, R., Honnorez, J., Bryan, W.B., Juteau, T., et al., 1988. *Proc. ODP, Init. Repts.*, 106/109: College Station, TX (Ocean Drilling Program).
- Dick, H.J.B., 1989. Abyssal peridotites, very slow spreading ridges and ocean ridge magmatism. In Saunders, A.D., and Norry, M.J. (Eds.), *Magma-tism in the Oceanic Basins*. Geol. Soc. Spec. Publ. London, 42:71–105.
- Dick, H.J.B., and Fisher, R.L., 1984. Mineralogical studies of the residues of mantle melting: abyssal and alpine-type peridotites. In Kornprobst, J. (Ed.), *Kimberlites II: The Mantle and Crust-Mantle Relationships*: Amsterdam (Elsevier), 295–308.
- Dick, H.J.B., and Kelemen, P.B., 1992. Light rare earth element enriched clinopyroxene in harzburgites from 15°05'N on the Mid-Atlantic Ridge. *Eos*, 73:584.
- Dick, H.J.B., Robinson, P.T., and Meyer, P.S., 1992. The plutonic foundation of a slow-spreading ridge. In Duncan, R.A., Rea, D.K., Weissel, J.K., Von Rad, U., and Kidd, R.B. (Eds.), *The Indian Ocean: A Synthesis of Results from the Ocean Drilling Program*. Am. Geophys. Union, Geophys. Monogr., 70:1–50.
- Dunlop, D.J., and Prevot, M., 1982. Magnetic properties and opaque mineralogy of drilled submarine intrusive rocks. *Geophys. J. R. Astron. Soc.*, 69:763–802.
- Fox, P.J., and Opydyke, N.D., 1973. Geology of the oceanic crust: magnetic properties of oceanic rocks. *J. Geophys. Res.*, 78:5139–5154.
- Francheteau, J., Armijo, R., Cheminee, J.L., Hekinian, R., Lonsdale, P., and Blum, N., 1990. 1 Ma East Pacific Rise oceanic crust and uppermost mantle exposed by rifting in Hess Deep (equatorial Pacific Ocean). *Earth Planet. Sci. Lett.*, 101:281–295.
- Girardeau, J., and Francheteau, J., 1993. Plagioclase-wehrlites and peridotites on the East Pacific Rise (Hess Deep) and the Mid-Atlantic Ridge (DSDP Site 339) evidence for magma percolation in the oceanic upper mantle. *Earth Planet. Sci. Lett.*, 115:137–149.
- Hamano, Y., Mansour Bina, M., and Krammer, K., 1990. Paleomagnetism of the serpentinized peridotite from ODP Hole 670A. In Detrick, R., Honnorez, J., Bryan, W.B., Juteau, T., et al. *Proc. ODP, Sci. Results*, 106/109: College Station, TX (Ocean Drilling Program), 257–262.
- Hébert, R., Adamson, A.C., and Komor, S.C., 1990. Metamorphic petrology of ODP Leg 109, Hole 670A serpentinized peridotites: serpentinization processes at a slow spreading ridge environment. In Detrick, R., Honnorez, J., Bryan, W.B., Juteau, T., et al. *Proc. ODP, Sci. Results*, 106/109: College Station, TX (Ocean Drilling Program), 103–115.
- Hekinian, R., Bideau, D., Francheteau, J., Lonsdale, P., and Blum, N., 1993. Petrology of the East Pacific Rise crust and upper mantle exposed in the Hess Deep (eastern equatorial Pacific). *J. Geophys. Res.*, 98:8069–8094.
- Henry, B., and Daly, L., 1983. From qualitative to quantitative magnetic anisotropy analysis: the prospect of finite strain calibration. *Tectonophysics*, 98:327–336.
- Honnorez, J., and Kirst, P., 1975. Petrology of rodingites from the Equatorial Mid-Atlantic fracture zones and their geotectonic significance. *Contrib. Mineral. Petrol.*, 49:233–257.
- Hyndman, R.D., Christensen, N.I., and Drury, M.J., 1984. The physical properties of basalt core samples from Deep Sea Drilling Project Leg 78B Hole 395A. In Hyndman, R.D., Salisbury, M.H., et al., *Init. Repts. DSDP*, 78 (Pt. 2): Washington (U.S. Govt. Printing Office), 801–810.
- Hyndman, R.D., and Drury, M.J., 1977. Physical properties of basalts, gabbros, and ultramafic rocks from DSDP Leg 37. In Aumento, F., Melson, W.G., et al., *Init. Repts. DSDP*, 37: Washington (U.S. Govt. Printing Office), 395–402.
- Iturrino, G.J., Christensen, N.I., Kirby, S., and Salisbury, M.H., 1991. Seismic velocities and elastic properties of oceanic gabbroic rocks from Hole 735B. In Von Herzen, R.P., Robinson, P.T., et al., *Proc. ODP, Sci. Results*, 118: College Station, TX (Ocean Drilling Program), 227–244.
- Jaques, A.L., and Green, D.H., 1980. Anhydrous melting of peridotite at 0–15 kb pressure and the genesis of the tholeiitic basalts. *Contrib. Mineral. Petrol.*, 73:287–310.
- Johnson, H.P., 1978. Paleomagnetism of igneous rock samples—DSDP Leg 45. In Melson, W.G., Rabinowitz, P.D., et al., *Init. Repts. DSDP*, 45: Washington (U.S. Govt. Printing Office), 387–396.
- Kirkpatrick, R.J., 1979. Results of downhole geophysical logging Hole 396B, DSDP Leg 46. In Dmitriev, L., Heirtzler, J.R., et al., *Init. Repts. DSDP*, 46: Washington (U.S. Govt. Printing Office), 401–407.
- Lowrie, W., and Kent, D.V., 1978. Characteristics of VRM in ocean basalts. *J. Geophys.*, 44:297–315.
- Mével, C., Cannat, M., Gente, P., Marion, E., Auzende, J.-M., and Karson, J.A., 1991. Emplacement of deep crustal and mantle rocks on the west median valley wall of the MARK area (MAR 23°N). *Tectonophysics*, 190:31–53.
- Nicolas, A., 1989. *Structure of Ophiolites and Dynamics of the Oceanic Lithosphere*: Dordrecht (Kluwer).
- Nicolas, A., Boudier, F., and Boullier, A.M., 1973. Mechanisms of flow in naturally and experimentally deformed peridotites. *Am. J. Sci.*, 273:853–876.
- Pezard, P.A., Howard, J.J., and Goldberg, D., 1991. Electrical conduction in oceanic gabbros, Hole 735B, Southwest Indian Ridge. In Von Herzen, R.P., Robinson, P.T., et al., *Proc. ODP, Sci. Results*, 118: College Station, TX (Ocean Drilling Program), 323–332.
- Ramsay, J.G., 1980. The crack-seal mechanism of rock deformation. *Nature*, 284:135–139.
- Robinson, P.T., Von Herzen, R., et al., 1989. *Proc. ODP, Init. Repts.*, 118: College Station, TX (Ocean Drilling Program).
- Rose, N.M., 1989. Calcium metasomatism in layered gabbros and dikes in central East Greenland [Ph.D. thesis]. Stanford Univ., Stanford, CA.
- Rose, N.M., and Bird, D.K., 1987. Prehnite-epidote phase relations in the Nordre Aputiteq and Kruuse Fjord layered gabbros. *J. Petrol.*, 28:1193–1218.
- Serra, O., 1984. *Fundamentals of Well Log Interpretation* (Vol. 1): *The Acquisition of Logging Data*: Amsterdam (Elsevier).
- Shankland, T.J., and Waff, H.S., 1974. Conductivity in fluid-bearing rocks. *J. Geophys. Res.*, 79:4863–4868.
- Shibata, T., and Thompson, G., 1986. Peridotites from the Mid-Atlantic Ridge at 43°N and their petrogenetic relation to abyssal tholeiites. *Contrib. Mineral. Petrol.*, 93:144–159.
- Smith, G.C., and Vine, F.J., 1987. Electrical conductivity of basalts from CCSP Drill Holes CY-2 and CY-2A at Agrokopia Mines, Cyprus. In Robinson, P.T., Gibson, I.L., and Panayiotou, A. (Eds.), *Cyprus Crustal Study Project: Initial Report, Holes CY-2 and CY-2A*. Geol. Surv. Can., Pap. 85-29:339–346.
- Zijderveld, J.D.A., 1967. AC demagnetization of rocks: analysis of results. In Collinson, D.W., Creer, K.M., and Runcorn, S.K. (Eds.), *Methods in Palaeomagnetism*: New York (Elsevier), 254–286.

Ms 147IR-104

NOTE: For all sites drilled, core-description forms (barrel sheets) and core photographs have been reproduced on coated paper and can be found in Section 3, beginning on page 163. Thin-section data are given in Section 4, beginning on page 309. Conventional-log and FMS data can be found in CD-ROM form (back pocket).

Table 15. Summary of thermal conductivity data from Site 895.

Core, section, interval (cm)	Piece number	Depth (mbsf)	TC (W/m°C)	Comments
147-895C-				
1R-1, 53-69	9	0.53	2.481	Harzburgite (75% altered)
3R-1, 87-99	15	19.17	2.652	Harzburgite (75% altered)
3R-1, 131-144	22	19.61	2.521	Harzburgite (75% altered)
3R-2, 13-24	2	19.93	2.651	Harzburgite (75% altered)
4R-1, 82-91	12	28.72	2.718	Olivine gabbro (75% altered)
4R-2, 93-107	6A	30.33	3.094	Olivine gabbro (75% altered)
4R-2, 107-120	6B	30.47	2.616	Olivine gabbro with large plagioclase patch (75% altered)
4R-2, 120-134	6C	30.60	2.943	Olivine gabbro (75% altered)
147-895D-				
2R-1, 45-55	6B	16.45	2.764	Harzburgite (80%-100% altered)
2R-2, 33-49	3	17.83	2.671	Harzburgite (85%-100% altered)
3R-1, 37-50	6	26.37	2.494	Harzburgite (60% altered)
4R-2, 19-30	4	36.39	2.712	Harzburgite (75% altered)
4R-3, 102-117	12	38.78	3.097	Harzburgite (70%-80% altered)
4R-4, 15-24	2	39.35	2.876	Harzburgite (70%-80% altered)
4R-5, 1-19	1	40.71	2.998	Harzburgite (70% altered)
5R-1, 42-56	8	43.72	2.428	Harzburgite (75%-90% altered)
5R-1, 114-122	18	44.44	3.037	Harzburgite (75%-90% altered)
5R-2, 97-110	14	45.77	2.540	Harzburgite (60%-70% altered)
7R-1, 14-28	4	64.74	2.987	Gabbronorite (70% altered)
7R-1, 45-55	8	65.05	3.013	Troctolite (90% altered)
8R-2, 1-12	1	74.99	4.070	Gabbronorite (50% altered)
8R-2, 115-125	16	76.14	2.723	Dunite (95%-100% altered)
9R-1, 35-45	6	84.35	2.528	Harzburgite (90%-100% altered)
147-895E-				
1R-1, 46-57	5B	0.46	3.398	Olivine gabbro (85% altered)
1R-1, 132-143	16	1.32	3.255	Olivine gabbro (85% altered)
1R-2, 67-82	15	2.17	2.701	Dunite (95% altered)
1R-3, 1-18	1	3.01	2.859	Harzburgite (85%-90% altered)
1R-3, 41-62	4	3.41	3.147	Harzburgite (85%-90% altered)
1R-3, 120-128	9	4.20	3.343	Troctolite (85% altered)
1R-4, 1-12	1	4.51	2.717	Troctolite (85% altered)
2R-1, 91-102	14	21.29	2.623	Olivine gabbro (80% altered)
2R-2, 1-15	1	22.95	2.718	Olivine gabbro (80% altered)
3R-3, 24-33	3B	32.71	3.242	Dunite (90%-100% altered)
4R-1, 94-104	15B	40.44	2.530	Dunite (100% altered)
4R-3, 1-10	1	42.42	2.818	Olivine gabbro (70% altered)
5R-1, 128-147	21	50.18	2.514	Dunite (95%-100% altered)
5R-2, 105-119	18	51.45	2.691	Dunite (95%-100% altered)
6R-2, 104-115	7	61.14	2.817	Dunite (95% altered)
6R-3, 59-70	2B	61.90	2.667	Dunite (95% altered)
6R-5, 63-80	5	64.38	2.920	Dunite (95%-100% altered)
7R-2, 90-106	11C	70.60	2.612	Harzburgite (95%-100% altered)
7R-3, 58-71	4B	71.78	2.708	Harzburgite (80%-90% altered)
7R-4, 31-48	4	73.01	2.650	Harzburgite (80%-90% altered)
8R-2, 28-42	5B	79.67	2.895	Harzburgite (90% altered)
8R-3, 98-107	6	81.80	3.061	Dunite (100% altered)